

Droplet epitaxy of GaAs studied  
by *in situ* surface electron  
microscopy

Zhenyu Zhou



School of Physics, Monash University

November 7, 2012



## Insertion of Changes

### Amendments

Page 9: Add in the middle of para 2:

For example, if only one non-centred spot in a diffraction pattern is allowed to contribute to the image through an aperture, only areas consisting of phases which contribute to the specific diffraction spot will give rise to bright contrast.

Page 13: Add para 2:

The Arsenic cracker cell can be used to deposit  $As_4$  or  $As_2$  . . . . . A water cooling shroud is also integrated into the design.

Page 14: Add para 2:

In LEEM it is customary to heat the specimen by electron beam bombardment of the specimen wafer surface. . . . . This design significantly improves the temperature uniformity across the sample which is essential for dynamic studies.

Page 21 line 2 and line 5: “ $As_2$  “ for “As”

Page 22 Change in para 3 line 4:

The Ga droplets move forward or backward along the [110] direction with the same probability, ruling out thermal gradient effects.

Page 27 Add in para 3 line 3:

(and we assume step density),

Page 46 Change in line 16:

Below  $T_c$ ,  $\mu_{Ga} < \mu_{Ga,0}$ , so a Ga droplet will lose Ga to the surrounding surface. The Ga atoms diffuse away from Ga droplets as surface adatoms until all Ga droplets eventually disappear.

Page 65: Change in line 1:

At high temperatures Ga is released too rapidly during evaporation to diffuse far because of increased nucleation. This is modeled by large  $F$ .

Page 72: Change in the mid of para 2 line 3:

A skirt or disk-like structure ( $S_{II}$ ) is visible outside of the droplet perimeter after a few seconds and gradually increases in thickness (Figure 1b) .

Page 72: Change in the mid of para 2 line 10:

(see also section 2.1.2)

Page 76: Add in the last line:  
light (blue)

Page 77: Add in the caption of Fig. 3:  
Light (blue) and dark (brown)

Page 94: Change in line 1:

Noting that the droplet etching rate  $\frac{dh}{dt}$  is proportional to  $J_e$ , then from (2) we can write,

Page 96: Change in line 2:

Let us assume this only occurs at the collar giving,

Page 96: Rewrite equation (9)

$$J_{Ga,D} = 2\pi D_{Ga} \left. \frac{dC_{Ga}(r)}{dr} \right|_{r=r_D} = 2\pi\beta [C_{Ga}(r_D) - C_{Ga}^0]$$

Page 96: Change in line 6:

Based on the boundary conditions (7) and (9), for  $r \ll L$  one finds the solution of Eq. (6) consists of a modified bessel function, which can be written as,

Page 98: Change in para 2:

The final etching depth of a given point is the integral of the etching rate  $\frac{dh}{dt}$  with respect to the overall etching time. Combining Eqs. (4) and (14), the final etching profile is,

---

# Contents

<b>Contents</b>	<b>iii</b>
<b>Abstract</b>	<b>vii</b>
<b>General Declaration</b>	<b>ix</b>
<b>Acknowledgements</b>	<b>xi</b>
<b>1 Introduction to droplet epitaxy</b>	<b>1</b>
<b>2 Development of a III-V low energy electron microscope</b>	<b>7</b>
2.1 Introduction to surface electron microscopy	7
2.1.1 Low energy electron microscopy (LEEM)	7
2.1.2 Mirror electron microscopy (MEM)	10
2.1.3 Photoemission electron microscopy (PEEM)	11
2.2 Development of a III-V LEEM system	12
<b>3 Ga droplet surface dynamics during Langmuir evaporation of GaAs</b>	<b>15</b>
<b>4 Introduction to the thermodynamics of Ga droplet formation during Langmuir evaporation</b>	<b>35</b>
<b>5 Congruent evaporation temperature of GaAs(001) controlled by As flux</b>	<b>39</b>
<b>6 Introduction to the evolution of Ga droplet size distributions</b>	<b>51</b>

<b>7</b>	<b>Time evolution of the Ga droplet size distribution during Langmuir evaporation of GaAs(001)</b>	<b>55</b>
<b>8</b>	<b>Dynamic observation and modelling of nanoscale ring formation during droplet epitaxy</b>	<b>67</b>
<b>9</b>	<b>Real-time imaging and modelling of local droplet etching</b>	<b>87</b>
<b>10</b>	<b>Conclusions and future work</b>	<b>103</b>
	<b>Bibliography</b>	<b>105</b>

**Notice 1**

Under the Copyright Act 1968, this thesis must be used only under the normal conditions of scholarly fair dealing. In particular no results or conditions should be extracted from it, nor should it be copied or closely paraphrased in whole or in part without the written consent of the author. Proper written acknowledgement should be made for any assistance obtained from this thesis.

**Notice 2**

I certify that I have made all reasonable efforts to secure copyright permissions for third-party content included in this thesis and have not knowingly added copyright content to my work without the owner's permission.



---

# Abstract

Droplet epitaxy is a recently developed variant of molecular beam epitaxy (MBE) which is used to form compound semiconductor quantum structures. This usually involves the deposition of group III material liquid droplets on a substrate followed by crystallisation of the droplets under As flux. The electronic properties of quantum structures depend sensitively on the size and shape of nanoscale rings formed in the crystallisation process and so it is important to understand how to control the formation of these features for potential device applications.

A significant difficulty in studying quantum structure formation is the presence of the large As flux which limits real-time studies using conventional techniques such as scanning tunnelling microscopy (STM). The first aim of this thesis is therefore to develop a III-V low energy electron microscope (LEEM) system for *in situ*, real time imaging of droplet epitaxy.

The thesis begins with the development of the III-V LEEM system and its application to study Langmuir evaporation of GaAs (Chapters 2 and 3). We find the III-V LEEM can achieve *in situ*, real time observation of droplet nucleation, evolution, motion and coalescence. This establishes the feasibility of studying droplet epitaxy using III-V LEEM.

As a prelude to studying droplet epitaxy, in Chapter 4 we consider the thermodynamics of Ga droplet formation during Langmuir evaporation of GaAs (001). The congruent evaporation temperature  $T_c$  plays a critical role in this process. Below  $T_c$ , Ga and As evaporate from the surface at equal rates, preserving substrate stoichiometry. However, above  $T_c$ , As evaporates more rapidly than Ga leaving behind Ga-rich droplets on the surface. At  $T_c$ , the droplets are stable and neither shrink nor grow, which provides an accurate measure of  $T_c$ . In Chapter 5 we apply this condition for droplet stability to experimentally measure  $T_c$  in the presence of As flux using III-V LEEM.

This dependence is explained by modifying the thermodynamic model for evaporation to incorporate As flux. This work provides a method of controlling congruent evaporation which is important for MBE growth, droplet epitaxy, surface preparation and modifying droplet motion.

The creation of droplets above  $T_c$  during Langmuir evaporation provides a potential means of self-assembling droplet arrays for subsequent crystallisation under As flux. It is therefore important to understand how the droplet size distribution evolves with time during this process. This is considered in Chapters 6 and 7 where we apply real-time surface electron microscopy to make movies of how droplet arrays evolve. Surprisingly, new Ga droplets are seen to form in regions cleared by the coalescence of larger droplets. A simple Monte Carlo model incorporating daughter droplet generation by coalescence is used to reproduce and explain the major features of our experimental droplet size distributions.

In Chapter 8 we study droplet epitaxy of GaAs in real-time using surface electron microscopy which provides new insights into the dynamics of Ga droplet crystallisation under As flux. The resulting movies are used as the basis of a theoretical model for quantum ring formation which can qualitatively explain the origin of quantum features observed under a variety of experimental conditions. The model predicts that Ga adatom diffusion, under differing conditions of temperature and As flux, chiefly controls the quantum structure morphology.

Local droplet etching (LDE) has received significant attention over recent years as a means of fabricating nanoscale holes in semiconductor surfaces. The technique offers the significant advantage that it avoids the need for lithographic processes and can be applied to a wide range of materials. In Chapter 9 we utilise III-V LEEM to study the time-evolution of Ga droplet etching of GaAs under As flux. A theoretical model of the etching process is developed from the movies which requires a minimum number of assumptions and is simply based on the liquid droplet maintaining a composition close to its equilibrium liquidus value. Conclusions and further work is considered in Chapter 10.

---

# General Declaration

## Declaration for thesis based or partially based on conjointly published or unpublished work

In accordance with Monash University Doctorate Regulation 17 / Doctor of Philosophy and Master of Philosophy (MPhil) regulations the following declarations are made:

I hereby declare that this thesis contains no material which has been accepted for the award of any other degree or diploma at any university or equivalent institution and that, to the best of my knowledge and belief, this thesis contains no material previously published or written by another person, except where due reference is made in the text of the thesis.

This thesis includes three original papers published in peer reviewed journals and two manuscripts which are about to be submitted. The core theme of the thesis is droplet epitaxy of GaAs studied by *in situ* surface electron microscopy. The ideas, development and writing up of all the papers in the thesis were the principal responsibility of myself, the candidate, my supervisors David Jesson and Wen-Xin Tang, and the co-authors of the respective papers. The inclusion of co-authors reflects the fact that the work came from active collaboration between researchers and acknowledges input into team-based research. Each paper includes a specific declaration describing the relative contribution of each author.

In the case of chapters 3,5,7,8,9 my contribution to the work involved the following:

Thesis chapter	Publication title	Publication status	Nature and extent of candidate's contribution
3	Ga droplet surface dynamics during Langmuir evaporation	Published	Co-development of the III-V LEEM, co-performed the experiments to position nanostructures using spatial variations in $T_c$ , co-wrote the paper
5	Congruent evaporation temperature of GaAs(001) controlled by As flux	Published	Designed the experiments, co-performed the experiments, co-developed the model used in the paper, co-wrote the paper
7	Time evolution of the Ga droplet size distribution during Langmuir evaporation of GaAs(001)	Published	Developed the model used in the paper, performed the Monte Carlo simulations and analysis, co-wrote the paper

## GENERAL DECLARATION

8	Dynamic Observation and Modelling of Nanoscale Ring Formation during Droplet Epitaxy	In preparation	Designed the experiments, co-performed the experiments, co-developed the model used in the paper, designed and ran the simulation, co-wrote the paper
9	Real-time Imaging and Modelling of Local Droplet Etching	In preparation	Designed the experiments, co-performed the experiments, co-developed the model used in the paper, designed and ran the simulation, co-wrote the paper

Signed: .....  .....

Date: ..... 11/08/2012 .....

---

# Acknowledgements

I would like to express my sincere acknowledgement in the support and assistance of my supervisors David Jesson and Wen-Xin Tang, whose wide knowledge, patience, wisdom and inspiration have guided me throughout my PhD project.

I acknowledge the insights of Jerry Tersoff in much of the theoretical modeling work.

I acknowledge the assistance of Changxi Zheng for his excellent experimental support, cooperation and numerous useful discussions.

I acknowledge the assistance of Rod Mackie who contributed invaluable technical support for the laboratory work.

I acknowledge the very kind and patient help of Jean Pettigrew with regard to assistance with paperwork connected with this thesis.

I acknowledge the electronic technical support provided by Nino Benci and David Zuidema.

I acknowledge the support of administrative staff in the School of Physics, Faculty of Science and the Monash Research Graduate School.

I acknowledge financial assistance from the J. L. William Bequest, Endeavor International Postgraduate Research Scholarship from the Australian Government and the Monash Graduate Scholarship from Monash University.



---

# Introduction to droplet epitaxy

Droplet epitaxy is a special growth technique variant of molecular beam epitaxy (MBE) which allows the control of the size, shape and distribution of self-assembled three-dimensional nanostructures on the surfaces of III-V compounds (Koguchi et al., 1991; Koguchi and Ishige, 1993; Lee et al., 2009). Controlling nanostructure properties allows the tailoring of electronic properties for novel device applications such as quantum-dot lasers (Huffaker et al., 1998; Cao et al., 2010; Fedorova et al., 2010), infrared photodetectors (Pan et al., 1998; Wu et al., 2010; Chakrabarti et al., 2011), high electron mobility transistors (HEMTs) in microwave monolithic integrated circuits (MMIC) (Muller et al., 1997; Baumann et al., 1995), electron amplifiers (Heiblum et al., 1985; Chiu et al., 2009; Chang et al., 2011), and single-photon devices (Michler et al., 2000; Claudon et al., 2010; Ikezawa et al., 2012). Droplet epitaxy was invented by N. Koguchi and his co-workers in the early 1990s (Koguchi et al., 1991; Koguchi and Ishige, 1993; N.Koguchi et al., 1993) and it has been widely used for III-V nano-structure growth (Watanabe et al., 2000; Mano and Koguchi, 2005; Gong et al., 2005; Huang et al., 2006; Mano et al., 2000).

Typical III-V droplet epitaxy consists of two main stages. In the first stage, liquid droplets of group-III metal, such as Ga, In, and Al, are created on the surface of a substrate by depositing the metal via an atomic beam (Koguchi

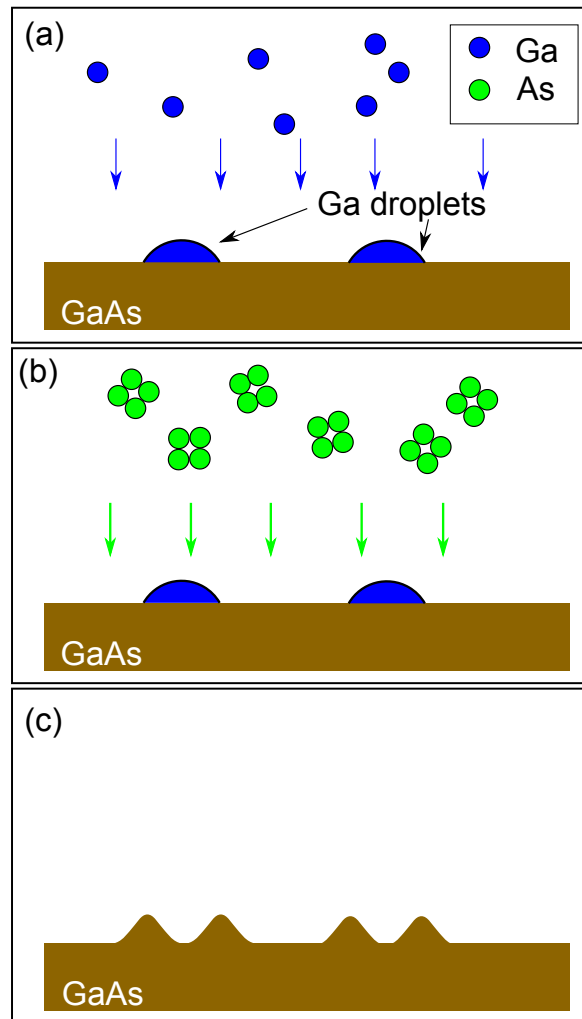


Figure 1.1: Schematic of GaAs droplet epitaxy. (a) Ga droplets are created on the surface of GaAs substrate by depositing Ga flux. (b) As<sub>4</sub> flux is deposited onto the Ga droplets. The Ga droplets react with the As<sub>4</sub> flux. (c) The Ga droplets eventually crystallise into GaAs nanostructures (here a ring shape is shown as an example).

et al., 1991; Koguchi and Ishige, 1993; Lee et al., 2009) or high temperature annealing of the substrate (Tersoff et al., 2009; Tang et al., 2011). In the second stage, a group-V molecular beam (typically As flux) is introduced to react with the metal droplets. The droplets eventually crystallise into high-quality nanostructures (Koguchi and Ishige, 1993; Lee et al., 2009). The size, shape and distribution of the nanostructures can be tuned by varying the substrate temperature and flux intensities. Fig. 1.1 contains a schematic illustrating the

main stages of GaAs droplet epitaxy.

Compared with the widely used strain-driven Stranski-Krastanov growth method for lattice-mismatched systems (Lay and Kern, 1978; Venables et al., 1984; Joyce and Vvedensky, 2004), droplet epitaxy is applicable for both lattice-matched and lattice-mismatched systems (Koguchi and Ishige, 1993; Watanabe et al., 2000; Gong et al., 2005; Huang et al., 2006; Mano et al., 2000). It also allows greater flexibility in quantum dot material selection and improved uniformity of quantum dot size (Watanabe et al., 2000). Furthermore, droplet epitaxy can fabricate more complex structures such as quantum single rings (Mano and Koguchi, 2005), double rings (Huang et al., 2006; Mano et al., 2005), quantum dot molecules (Yamagiwa et al., 2006), quantum dot pairs (Wang et al., 2006; Wu et al., 2010) and nanoholes (local droplet etching) (Wang et al., 2007). Particular nanostructure features can be tuned by the fine control of temperature and flux, thereby generating designer shapes and complex morphology.

Fig. 1.2 contains atomic force microscopy (AFM) images of some typical GaAs nanostructures fabricated using droplet epitaxy. Fig. 1.2 (a) shows GaAs quantum dots on an AlGaAs substrate. The Ga droplets crystallised into quantum dots at  $T = 250\text{ }^{\circ}\text{C}$  under As flux (Heyn et al., 2010). With different growth temperature, As flux intensity and substrate composition, Ga droplets can crystallise into more complex structures such as single rings (Huang et al., 2006) and double rings (Mano et al., 2005) (see Fig. 1.2 (b) and (c)). At high temperatures (typically  $T = 500\text{ }^{\circ}\text{C}$ ), Ga droplets will etch the substrate and eventually form nanoholes surrounded by single ring structures (Wang et al., 2007) (see Fig. 1.2 (d)).

Currently, however, the formation mechanisms of ring structures and local droplet etching are still poorly understood. One of the significant obstacles is the lack of *in situ*, real-time imaging methods to record the key growth processes. In general, the shape of fabricated nanostructures is characterised

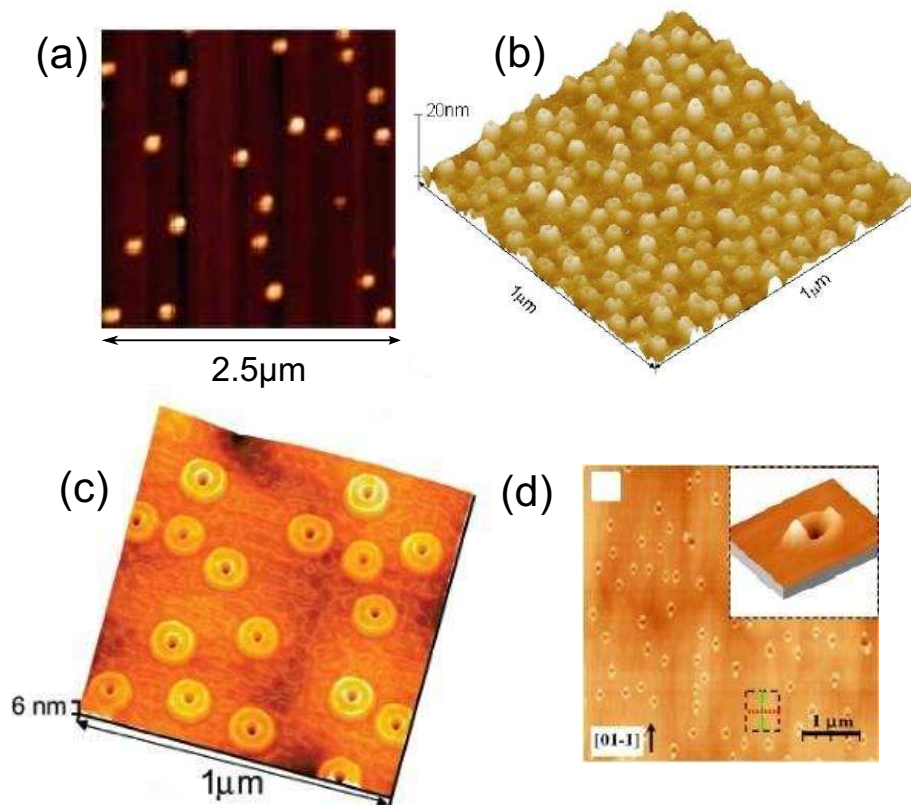


Figure 1.2: AFM images of various nanostructures fabricated by droplet epitaxy. (a) GaAs quantum dots on an AlGaAs substrate at  $T = 250\text{ }^{\circ}\text{C}$  with finite As flux (Heyn et al., 2010) (b) GaAs single ring structures on a GaAs (001) surface at  $T = 200\text{ }^{\circ}\text{C}$  with As flux  $F = 1 \times 10^{-6}\text{ torr}$  (Huang et al., 2006) (c) GaAs double ring structures on an  $\text{Al}_{0.3}\text{Ga}_{0.7}\text{As}$  surface at  $T = 200\text{ }^{\circ}\text{C}$  with As flux  $F = 2 \times 10^{-6}\text{ torr}$  (Mano et al., 2005). (d) Local droplet etching on a GaAs (001) surface at  $T = 500\text{ }^{\circ}\text{C}$  with As flux  $F = 1.1 \times 10^{-6}\text{ torr}$  (Wang et al., 2007)

by techniques such as AFM or scanning electron microscopy (SEM) following quenching to room temperature and exposure to air. Such processes may lead to changes in surface morphology so that the measured features may not be characteristic of as-grown shapes. In addition, the crystallisation of ring structures, local droplet etching and the nucleation, growth and coalescence of droplets are all dynamic processes. However, the reported images and measurements of these processes are limited to static snapshots which do not reveal the dynamic details of the fabrication process. These disadvantages

impede a deep understanding of the physical mechanism underlying droplet epitaxy.

To resolve these problems, we have developed a III-V low energy electron microscope (LEEM). LEEM is a powerful real-space image technique that can obtain real-time, *in situ* movies of semiconductor surface dynamics. We have combined conventional LEEM with a III-V MBE system so that the entire dynamic processes of droplet epitaxy can be imaged *in situ* and real time. Chapter 2 provides a review of conventional LEEM and then discusses the development of our III-V LEEM system, which lays the foundation of the main experiments in this thesis.



---

# Development of a III-V low energy electron microscope

## 2.1 Introduction to surface electron microscopy

### 2.1.1 Low energy electron microscopy (LEEM)

Low energy electron microscopy (LEEM) is a powerful real-space imaging technique used to obtain real-time, *in situ* movies of semiconductor, metal and metal oxide surface dynamics using low energy elastically back scattered electrons. The technique was invented by E. Bauer in the early 1960s (Bauer, 1962; Turner and Bauer, 1966), which was 35 years after Davisson and Germer pointed out the theoretical feasibility of surface imaging by backscattering of low energy electrons in their electron diffraction experiments (Davisson and Germer, 1927).

Fig. 2.1 contains a schematic representation of a LEEM system. An electron beam is accelerated to high energy (usually 20 keV), following emission from the electron gun, and passes through a series of condensor lenses. The beam is then deflected by the magnetic prism onto the optical axis of the objective lens which is normal to sample surface. After entering the objective lens, the electrons are decelerated to very low energy, usually 1 - 10 eV, by a uniform electric field between the objective lens and the sample surface

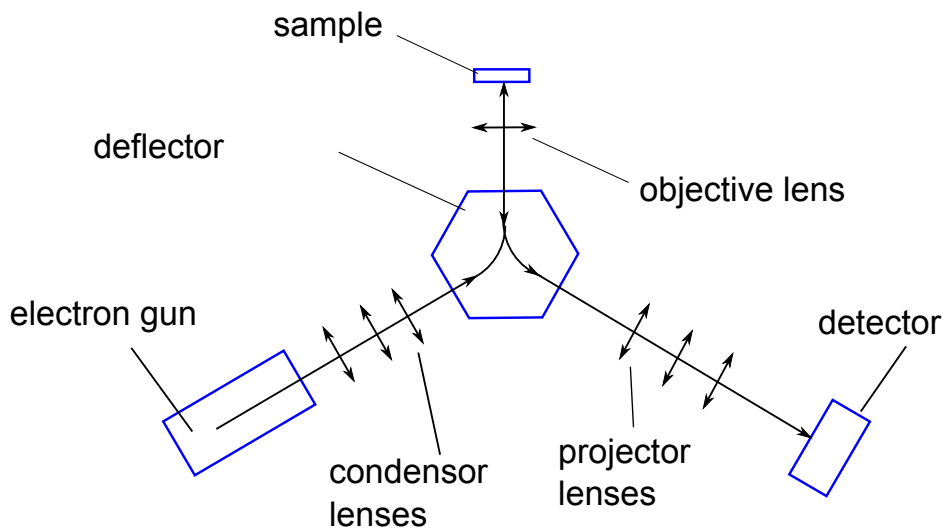


Figure 2.1: Schematic of low energy electron microscopy

before impacting the sample surface. The low energy electrons are highly sensitive to surface morphology and near-surface structure, and are elastically backscattered and re-accelerated to 20 keV by the uniform electric field before passing through the objective lens in the opposite direction. The deflector then directs the electron beam into the imaging column. The electrons are finally focused on the channel plate by the projector lens system where the image is recorded by a charge coupled device (CCD) detector which is optically connected to an image intensifier.

In a LEEM instrument, the objective lens is a cathode lens and the sample serves as an electrode that emits or reflects low energy electrons into the objective lens (Bauer, 1994; Altman, 2010). Electrons of energies less than 10 eV are very sensitive to the surface structure and composition with a penetration depth 0.5-5 nm (Tromp et al., 1998). Elastically backscattered electrons have a large cross section allowing instantaneous surface imaging without scanning pixel by pixel. Therefore LEEM attains true "real-time" observation over large areas ( $\sim 100 \mu\text{m} \times 100 \mu\text{m}$ ) which is a significant advantage compared to serial scanning techniques such as STM, SEM and AFM. Low energy electron diffraction (LEED) is naturally integrated with

LEEM because electron diffraction occurs during the elastic scattering of electron by crystalline samples. By using the micro-scale apertures available in LEEM, LEEM-based  $\mu$ -LEED enables localised diffraction information to be obtained from small areas on a sample surface, which is important for the detailed study of surface phases.

The imaging modes of LEEM can be divided into three main categories: phase contrast, diffraction contrast and reflectivity contrast. Phase contrast usually arises from the interference of electron waves which are reflected from the opposite sides of a step (step contrast) (Altman et al., 1998; Chung and Altman, 1998; Kennedy et al., 2009), or from the top and bottom faces of a thin film (quantum size contrast) (Altman et al., 1998, 2001). Diffraction contrast is usually induced by the geometrical structured differences between different phases (Bauer et al., 1989). For example, if only one non-centred spot in a diffraction pattern is allowed to contribute to the image through an aperture, only areas consisting of phases which contribute to the specific diffraction spot will give rise to bright contrast. Thus the spatial distribution of coexisting phases can be identified. Reflectivity contrast occurs when different surface areas show a difference in electron reflectivity, which usually depends on surface composition and/or reconstruction (Teliëps and Bauer, 1985). The combination of these imaging modes with  $\mu$ -LEED diffraction is very powerful for identifying and imaging the dynamics of phase transformations on surfaces.

In the past two decades, a series of technical improvements have been reported to enhance LEEM resolution by reducing spherical and chromatic aberration (Tromp and Reuter, 1991; Veneklasen, 1991; Bauer, 1994; Tromp et al., 1998; Wan et al., 2004; Tromp et al., 2010). Instruments can now obtain  $\sim 2$  nm resolution as reported recently by Tromp et al. (2010).

### 2.1.2 Mirror electron microscopy (MEM)

Mirror Electron Microscopy (MEM) is an important complementary imaging mode to LEEM. In MEM, the sample is biased to be slightly more negative than the electron source. Therefore, the equipotential surface close to the sample surface forms an "electron mirror". The electrons are reflected by the electron mirror without interacting with the sample (Griffith and Engel, 1991). The ideal smooth sample surface forms a homogeneous electric field close to the surface. However, variations in surface morphology and/or local micro fields create perturbations in the homogeneous electric field, thereby giving image contrast (Świąch et al., 1993).

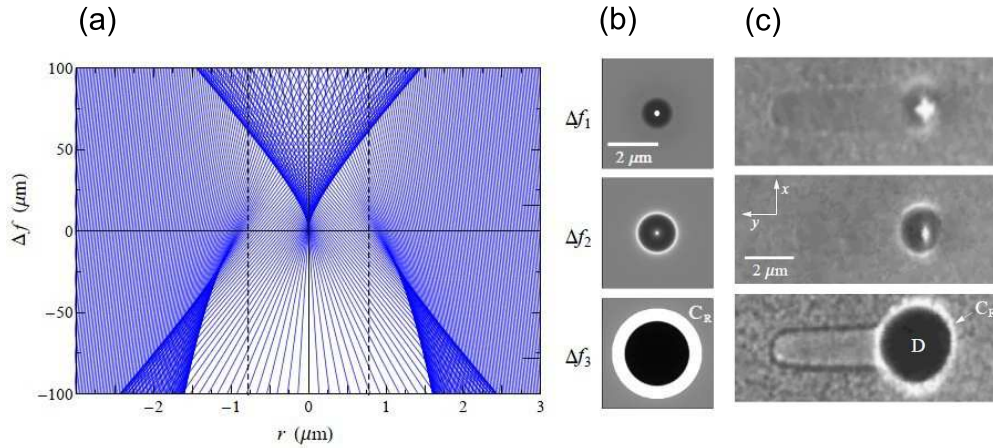


Figure 2.2: (a) Distribution of the envelope of electron ray trajectories in the virtual image plane of the LEEM objective lens after interaction with the electric field above a Ga droplet on a GaAs (001) surface. The projected radius of the droplet at  $R = 0.78 \mu\text{m}$  is indicated by vertical dashed lines. (b) Two dimensional image simulations are shown for three different defoci  $\Delta f_1 = 16 \mu\text{m}$ ,  $\Delta f_2 = 0 \mu\text{m}$ ,  $\Delta f_3 = -78 \mu\text{m}$ . (c) Corresponding experimental images of Ga droplets on GaAs (001). (Kennedy et al., 2011)

MEM is a convenient, non-invasive mode for imaging Ga droplet dynamics on GaAs (001) as discussed in chapters 3 and 5. The Ga droplets usually have large sizes ( $\sim 1 \mu\text{m}$ ) so the droplets deflect the electron trajectories dramatically

and create very strong image contrast, including caustic features. Kennedy et al. (2011) have developed a theoretical model of caustic imaging, which is able to directly derive surface topographical information from MEM images. Fig. 2.2 provides a comparison between caustic image simulations and MEM experimental images (Kennedy, 2010; Kennedy et al., 2011). It can be seen that negative defocus provides strong droplet contrast and a magnified image which is ideal for studying droplet dynamics. In this thesis, MEM has been applied to the dynamic observation of Ga droplet evolution (chapter 5), ring structure formation (chapter 8) and local droplet etching (chapter 9).

### 2.1.3 Photoemission electron microscopy (PEEM)

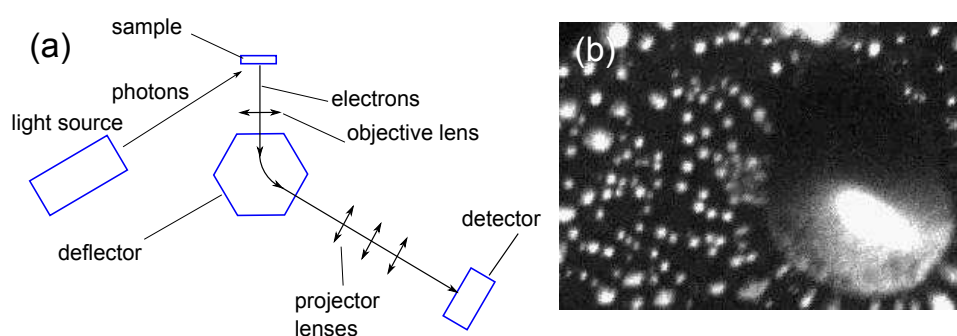


Figure 2.3: (a) Schematic of PEEM. (b) PEEM images of Ga droplets on a GaAs (001) surface during high temperature annealing.

Photoemission Electron Microscopy (PEEM) is a complementary imaging method utilising ultraviolet light to excite electrons from the sample surface (Bauer et al., 1989; Griffith and Engel, 1991; Rotermund, 1997; Günther et al., 2002). The excited electrons are focussed by the objective lens of the LEEM and are finally projected onto a channel plate detector (see Fig. 2.3 (a)). The light source is not limited to ultraviolet light (10 eV ~ 30 eV) but can also be extended to X-ray (Vogel et al., 2003; Świąch et al., 1997) and synchrotron radiation (Stasio et al., 1998; Świąch et al., 1997) (30 eV ~ 1 keV). The light source can be also polarised linearly or circularly to explore the magnetic and dichroism properties of samples (Świąch et al., 1997).

Ga droplets give rise to bright PEEM contrast on GaAs (001) because of their lower work function (Fig. 2.3 (b)) PEEM is therefore a convenient technique for studying the dynamic evolution of metal droplets over large areas (chapter 7). PEEM can be also integrated with other optical methods such as Lloyd's mirror (Jesson et al., 2007) to derive surface topographic information.

In chapter 7, PEEM, using a 100 W UV Hg arc-discharge lamp, has been used to measure the metallic Ga droplet size distribution during high temperature annealing of GaAs (001) surfaces, thereby providing *in-situ*, real-time experimental data for droplet size evolution modelling. Fig. 2.3 (b) shows a typical PEEM image of Ga droplets on GaAs (001) surface during high temperature annealing.

## 2.2 Development of a III-V LEEM system

In this section we describe the development of a III-V LEEM system, which combines conventional LEEM with a III-V molecular beam epitaxy (MBE) system for the *in situ* and real-time imaging of III-V surface dynamics. The electron optics is based on the standard Elmitec LEEM III configuration. To enhance brightness and beam coherence, this system incorporates a Schottky field emission electron source instead of the traditional LaB<sub>6</sub> electron gun. The optical system has the flexibility to allow the LEEM, PEEM and MEM imaging modes described earlier.

A number of significant modifications to the basic LEEM system have been made to incorporate III-V MBE. These modifications include the installation of multiple deposition sources, surface cleaning equipment and an internal cooling shroud to limit the build-up arsenic background pressure. An overview of the III-V LEEM is provided in Fig. 2.4.

The group III MBE sources consist of Ga and In effusion cells which are integrated with cooling shrouds and shutters. The effusion cells are mounted

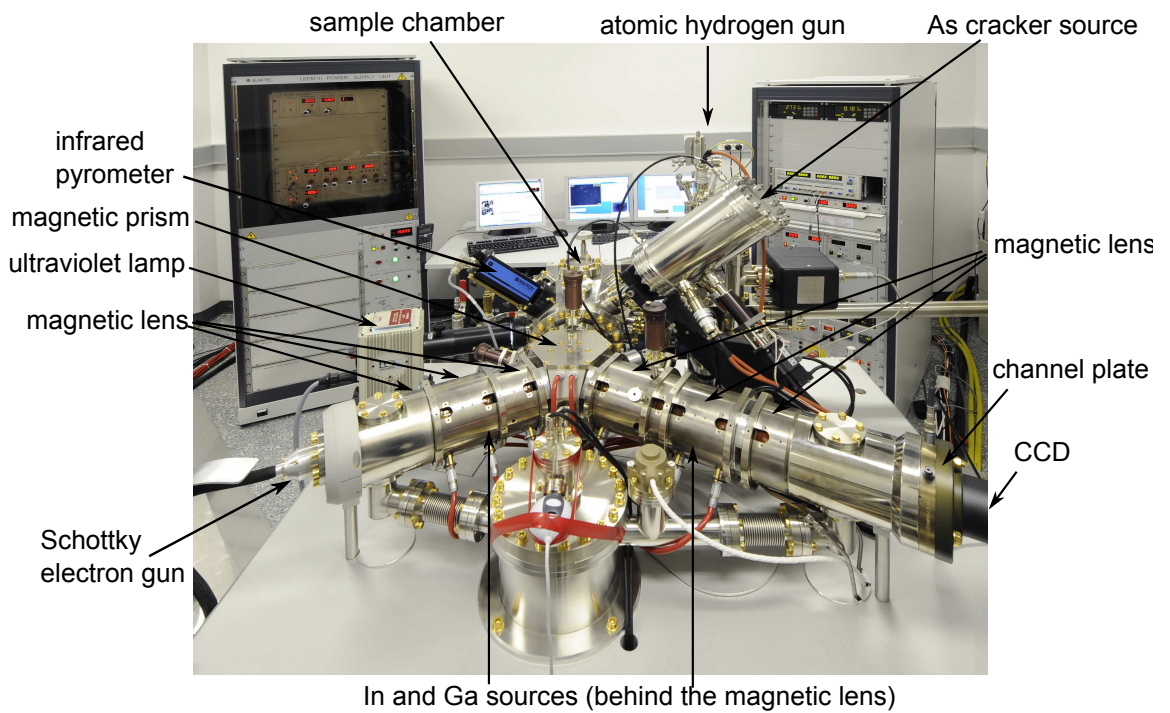


Figure 2.4: Overview of III-V LEEM system

in a face-up configuration because Ga and In are liquids at high temperature (underneath the sample chamber in Fig. 2.4). The evaporation beam is collimated through a PBN cap with a small orifice together with additional Ta shielding to reduce material deposition in the objective lens region.

The Arsenic cracker cell can be used to deposit  $As_4$  or  $As_2$ . It consists of 300 cc As crucible and a cracking zone. The crucible can be refilled without removing the cell from the chamber. As is evaporated by heating the crucible and the cracking zone allows control of the deposition species ( $As_4$  or  $As_2$ ) by varying the temperature. The integrated valve mechanism provides precise and fast flux control with a range of more than two orders of magnitude. The valve's position can be operated manually or by using external analogue voltage control. A water cooling shroud is also integrated into the design.

It is critical to prevent discharge between the specimen and the objective lens in surface electron microscopy because the voltage between specimen and the lens is typically 20 kV over a distance of 2 mm. The III-V LEEM

system therefore incorporates a liquid nitrogen cooling shroud to reduce the background As pressure which derives from high molecular  $\text{As}_4$  or  $\text{As}_2$  flux from the cracker source. Small apertures in the shroud allow Ga, In and  $\text{As}_4$  or  $\text{As}_2$  flux to impinge on the centre of the sample.

In LEEM it is customary to heat the specimen by electron beam bombardment of the specimen wafer surface. This can lead to significant temperature gradients across the sample since the central region of the wafer is closer to the bombardment filament than its edge. We employ a specially designed double plate sample holder consisting of two heating plates which are in contact with each other only at the outer edge. Heat transportation in the centre is therefore dominated by radiation while at the edge it chiefly occurs by conduction. This design significantly improves the temperature uniformity across the sample which is essential for dynamic studies.

The system uses an infrared pyrometer (MIKRON, MI-P 140) to measure the sample surface temperature which is cross-referenced with the thermocouple reading on the sample holder.

Our III-V LEEM system is run by our self-developed auto-control software based on the default software of Elmitec. The auto-control system is developed using Labview and C++ to implement various complex functions including data acquisition, sample heating, flashing, out-gassing and a continuous water cooling monitoring. The development of III-V LEEM allows complex experiments to study Ga droplet surface dynamics as described in chapter 3.

---

## Ga droplet surface dynamics during Langmuir evaporation of GaAs

This chapter is an author generated post print of the article

W.X. Tang, C.X. Zheng, Z.Y. Zhou, D.E. Jesson and J. Tersoff, 'Ga droplet surface dynamics during Langmuir evaporation of GaAs', *IBM Journal of Research and Development*, **Vol.5**, Issue 4, 10:1(2011), available electronically at

[http://ieeexplore.ieee.org/xpls/abs\\_all.jsp?arnumber=5985561](http://ieeexplore.ieee.org/xpls/abs_all.jsp?arnumber=5985561)

or via doi:10.1147/JRD.2011.2158762.

### Declaration for Thesis Chapter "Ga droplet surface dynamics during Langmuir evaporation of GaAs"

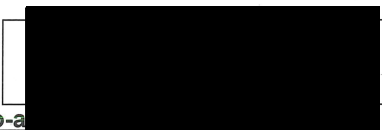
Declaration by candidate

For this chapter, the nature and extent of my contribution to the work was the following:

Nature of contribution	Extent of contribution(%)
Co-implementation and co-development of the III-V LEEM, co-performed the positioning nanostructures experiments, provided the technical expertise, co-wrote the paper.	20

The following co-authors contributed to the work. Co-authors who are students at Monash University must also indicate the extent of their contribution in percentage terms

Name	Extent of contribution(%)	Nature of contribution
Wen-XinTang (first author)		Co-implementation and co-development of the III-V LEEM, supervised the positioning nanostructures experiments, performed droplet velocity measurements, co-wrote the paper.
Changxi Zheng	20	Co-implementation and co-development of the III-V LEEM, co-performed the positioning nanostructures experiments, provided the technical expertise, co-wrote the paper.
David Jesson		Designed and developed the III-V LEEM system, performed droplet coalescence experiments, coordinated the experiment and theoretical studies, co-wrote the paper.
Jerry Tersoff		Helped develop the models.

Candidate's signature  Date 17/08/2012

Declaration by co-authors

The undersigned hereby certify that:

- (1) they meet the criteria for authorship in that they have participated in the conception, execution, or interpretation, of at least that part of the publication in their field of expertise;
- (2) they take public responsibility for their part of the publication, except for the responsible author who accepts overall responsibility for the publication;
- (3) there are no other authors of the publication according to these criteria;
- (4) potential conflicts of interest have been disclosed to (a) granting bodies, (b) the editor or publisher of journals or other publications, and (c) the head of the responsible academic unit; and
- (5) the original data are stored at the following location(s) and will be held for at least five years from the date indicated below:

Location(s)

School of Physics, Monash University, Clayton

Signature 1

Signature 2

Signature 3

Signature 4

	Date 16-08-12
	16-08-12
	16-08-12
	17/08/2012

# Ga droplet surface dynamics during Langmuir evaporation of GaAs

W. X. Tang, C. X. Zheng, Z. Y. Zhou, D. E. Jesson and J. Tersoff

**Abstract:** We describe the design and application of a low energy electron microscope (LEEM) dedicated to the study of III-V materials. Recent studies of Langmuir (free) evaporation of GaAs (001) have been reviewed. Running Ga droplets are observed and the motion is predicted and shown to slow and stop near a characteristic temperature. Striking bursts of “daughter” droplet nucleation accompany the coalescence of large “parent” droplets. These observations imply that evaporation and surface morphology are intimately connected, suggesting a new approach for the self-assembly and positioning of nanostructures on patterned surfaces.

## Introduction

GaAs based devices play a central role in radiofrequency communications technology and optoelectronics. Applications range from mobile phones and wireless networks to laser pointers and DVD players. GaAs high electron mobility transistors and III-V based laser diodes can be viewed as the major components underlying modern communications and optoelectronics. Such structures are composed of thin layers of III-V semiconductor materials, which are grown by molecular beam epitaxy (MBE) with atomic layer precision. Given the technological importance of III-V MBE growth, the real-space imaging of surface growth dynamics is highly desirable. However, this has remained elusive largely because any imaging method must be compatible with the incident As flux, which is a characteristic of III-V MBE.

In parallel with advancing current technologies, longer term objectives in III-V research are to move beyond the constraints of conventional

lithography and fabricate new quantum structures using variants of MBE. Quantum dots, double dots, rings, double rings, molecules and rods have now been assembled [1-4] with potential applications including novel lasers, electron-spin memory and quantum computing. However, a significant limitation in the realisation of new quantum structures is our inability to observe how they form in real time and hence understand how to tailor their characteristics. Just like interfaces grown by MBE, quantum structures are usually created under the As flux at elevated temperatures, and thus, imaging how they form under real growth conditions is highly desirable.

To facilitate imaging of technologically important interface and quantum structure formation under As flux, we have developed a surface electron microscope integrated with a III-V MBE system. In this paper, we describe the basic design of this III-V low energy electron microscope (LEEM). Applications of III-V LEEM to the study of Langmuir (free) evaporation of GaAs into a vacuum are then reviewed, revealing the unexpected and striking motion of Ga droplets [5] and how decomposition is controlled by surface morphology during evaporation [6].

### **III-V LEEM system**

The basic instrument consists of an Elmitec LEEM III configuration, which incorporates a Schottky field emission electron source for enhanced brightness and beam coherence compared with the conventional LaB<sub>6</sub> gun. Incorporation of III-V MBE required significant modifications, including installation of multiple deposition sources, dedicated equipment for surface cleaning, and an internal cooling shroud to limit the buildup of As background pressure [7]. Figure 1(a) contains an overview of our instrument. A cross-section of the basic LEEM system and the specimen region are shown in Figures 1(b) and (c), respectively.

The system is equipped with Ga and In effusion cells with integrated cooling shrouds and shutters and a metal valve As cracker source (MBE-

Komponenten). Since Ga and In are liquids at high temperature, it is necessary to mount the effusion cells in a face-up configuration [they are located underneath the instrument in Figure 1(a)]. Dual filaments are used to heat the crucibles to minimise droplet formation via condensation near the orifice to improve flux reproducibility. Both sources are equipped with automatic shutters. In order to reduce material deposition in the objective lens region, a pyrolytic boron nitride cap with a small orifice, together with additional Ta shielding, ensures a well-collimated evaporation beam. The Ga source is backed up by an uninterruptible power supply system to maintain the source temperature at 50 °C and prevent cracking of the crucible in the event of a power failure.

The As cracker source consists of a 300-mL As reservoir, which is heated to evaporate the As. A cracking zone on top of the reservoir can be used to convert naturally sublimated  $\text{As}_4$  into  $\text{As}_2$  if required. An integrated all-metal valve between the reservoir and cracking zone provides precise control of the As flux, which is important for dynamic imaging experiments. The reservoir and cracker temperature gradient is computer controlled during heating and cooling to reduce stress on the valve.

During III-V MBE, it is necessary to reduce the background As pressure resulting from high molecular  $\text{As}_4$  or  $\text{As}_2$  flux. Our III-V LEEM system therefore incorporates a cooling shroud for this purpose, which prevents discharge between the specimen and objective lens. The Cu shroud design is shown in Figure 1(c). Liquid nitrogen (LN) is supplied via a vacuum feed through to achieve thermal insulation. Small apertures in the shroud allow Ga, In and As fluxes to impinge on the centre of the sample. The background pressure is reduced by nearly 4 orders of magnitude when the shroud is in operation, which provides suitable conditions for imaging. However, following long time exposure to the As flux, the objective lens surface must be cleaned to reduce the probability of discharge. Magnetic shielding surrounds the cathode and anode regions in Figure 1(c) to screen

the electron beam from stray fields originating from the MBE sources. An atomic hydrogen source (AHS) [8] is used for *in situ* surface cleaning of GaAs wafers. The AHS is effective at removing the surface oxide layer and surface impurities such as carbon. Several imaging modes such as LEEM and photoemission electron microscopy (PEEM) are applied in this paper [9-11].

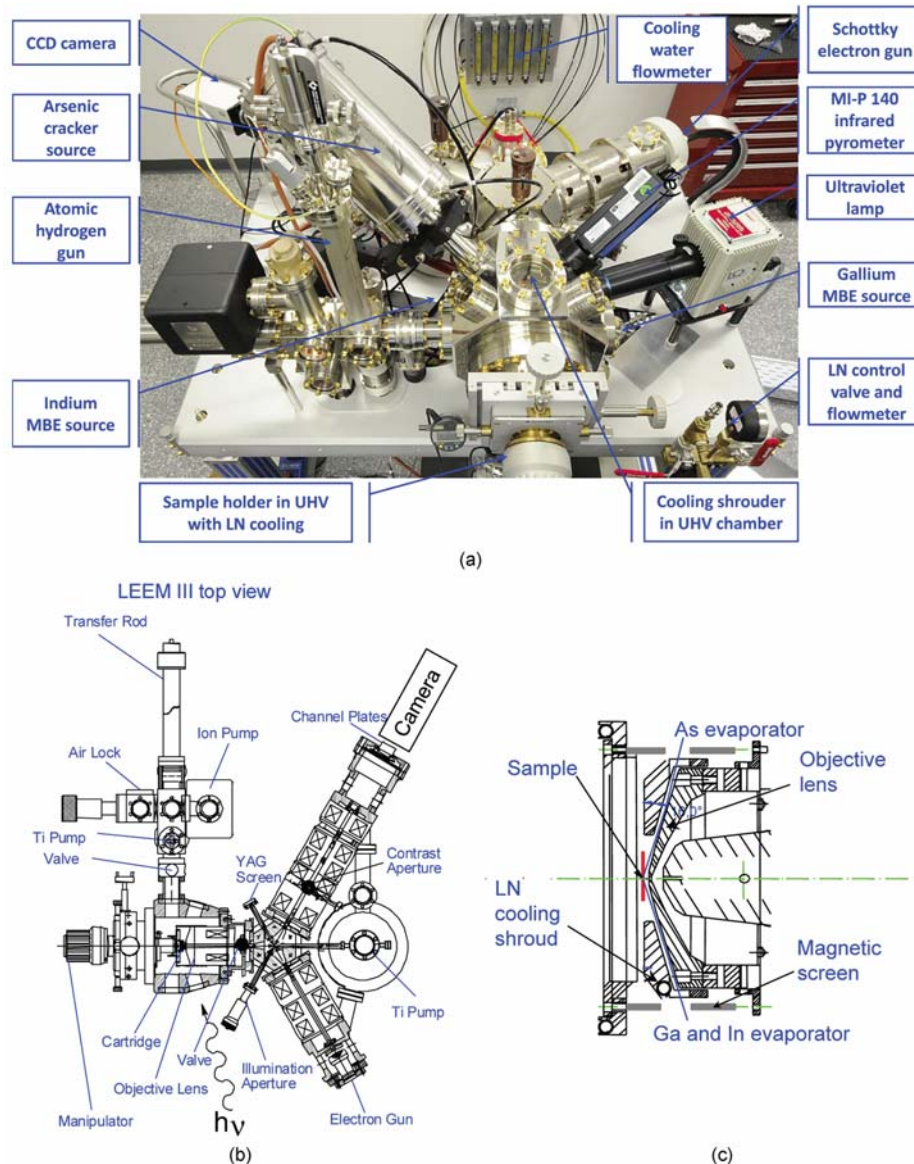


Figure 1 (a) Image of the III-V LEEM system [7]. (b) Cross section of the III-V LEEM instrument. (c) Enlarged view of the objective lens area showing the location of the cooling shroud and access for the MBE sources. (CCD: charge-coupled devices; YAG: yttrium-aluminium garnet.)

## Langmuir evaporation of GaAs

Langmuir (free) evaporation of GaAs (001) into a vacuum has been studied for many decades [12-15]. When heated, GaAs decomposes, and As<sub>2</sub> and Ga fluxes evaporate from the surface. Below congruent evaporation temperature  $T_c$ , the fluxes are equal, preserving the compound stoichiometry. However, above  $T_c$ , As<sub>2</sub> more readily evaporates, leaving behind Ga-rich droplets on the surface [16-19]. There has been a resurgence of interest in such droplets in the area of droplet epitaxy, where they are recrystallised under the As flux to generate GaAs quantum structures. Such structures can now be formed in different geometries, including dots, rings, and multirings with varied potential applications [20-22].

The formation and behaviour of Ga droplets can be imaged by heating an epitaxy-ready (epi-ready) GaAs substrate above  $T_c \sim 625$  °C [15] in the III-V LEEM. An undoped GaAs(001)  $\pm 0.1^\circ$  epi-ready wafer was initially degassed at 300 °C under ultrahigh vacuum for 24 hours in the LEEM system. This was followed by high-temperature flashing up to 600 °C and annealing at 580 °C for 2 hours to remove the surface oxide. Ga droplets were produced by annealing above  $T_c$ . The growth rate of the droplets is strongly dependent on annealing temperature, and this could be used to control their size. The base pressure of the system is below  $2 \times 10^{-10}$  torr, and typical pressures observed during imaging at the annealing temperature of 630 °C are approximately  $1 \times 10^{-9}$  torr with LN cooling of the internal shroud.

Mirror electron microscopy (MEM), in which the specimen potential is adjusted so that electrons turn around just before the surface, is an ideal imaging mode for studying droplets [5,6, 23-26]. A droplet distorts the uniform electric field between the planar sample surface and the objective anode, which significantly redistributes electron intensity. This can cause families of electron rays to overlap, creating strong caustic features in the

image. For a large negative defocus range of the objective lens, droplets appear as dark circles enclosed by a bright caustic ring [see Figure 2(a)]. It should be noted that the caustic ring diameter in Figure 2(a) is larger than the actual perimeter of the droplet so that the droplet size is enlarged in MEM. This contrast can be understood and quantified from a numerical evaluation of classical electron ray trajectories [25].

### Running Ga droplets

The most striking observation in the III-V LEEM is that Ga droplets spontaneously “run” across the surface during annealing. Even after evaporation of many hundreds of monolayers of the crystal, the motion continues. Despite many studies of GaAs Langmuir evaporation over the years [12-17], to our knowledge, Ga droplet dynamics had not been previously observed, illustrating the advantages of *in situ* real-time imaging.

MEM images taken from movies of Ga droplet motion at three different temperatures are shown in Figure 2(a). The epi-ready surface is associated with slight roughness, and as the droplets move, they leave behind a smooth trail. The motion has a stick-slip character. The Ga droplets move forward or backward along the [110] direction with the same probability, ruling out thermal gradient effects. It can be noted in Figure 2(a) that the size of the moving droplets decreases for  $T < T_c$  and increases for  $T > T_c$ . At  $T_c$  the droplet size remains stable, and surprisingly, there is a temperature range of approximately 20 °C about  $T_c$  in which the droplets do not move. To further explore the relationship between motion and temperature, we adjusted the temperature to the desired  $T$  and measured the droplet velocity averaged over many minutes. The results are shown in Figure 2(b). Away from  $T_c$ , the average droplet velocity increases with either increasing or decreasing temperature. This unusual temperature dependence suggest that the motion is intimately linked to  $T_c$ .

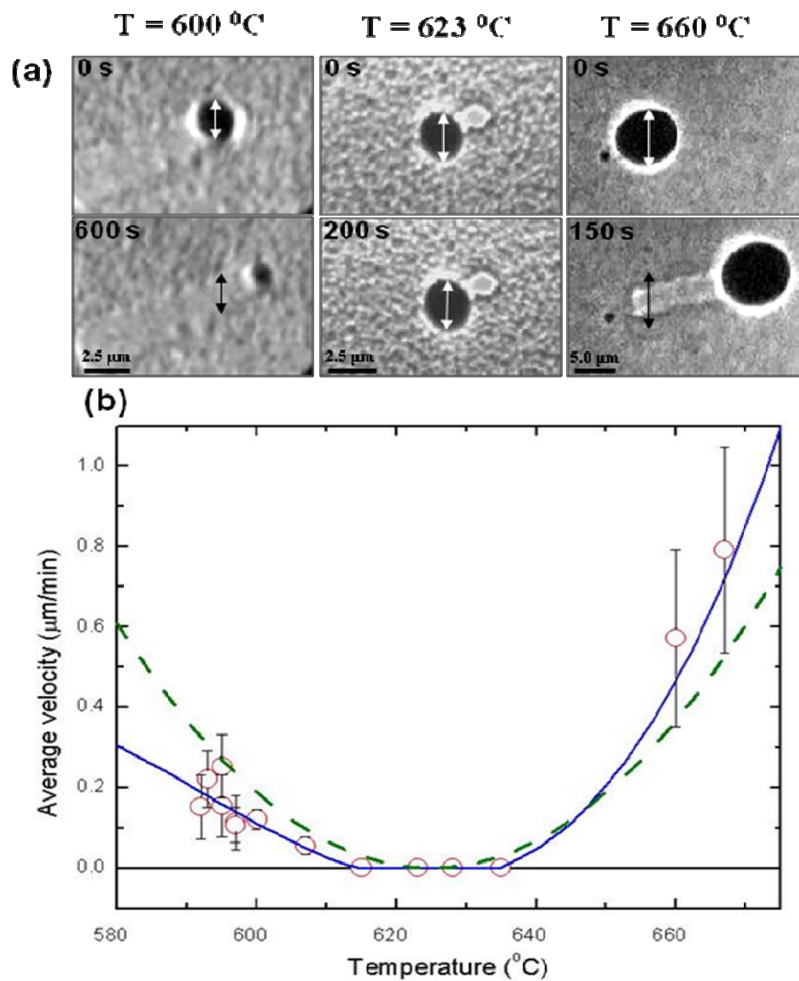


Figure 2 Droplet motion on epi-ready GaAs(001) [5]. (a) Image pairs are shown at successive times for three temperatures  $T$  as indicated; the centre image pair is near the congruent evaporation temperature. Arrows are reference markers for comparing position and diameter at two times. The droplets (left panel) move and shrink below  $T_c$  and (right panel) move and grow above  $T_c$ . Close to  $T_c$  (center panel), there is no visible motion or size change. (b) Average velocity versus temperature. Error bars show root-mean-square scatter of multiple measurements at the same  $T$ . The solid line is the truncated cubic fit described in the text, and the dashed line is the quadratic term alone, which is extracted from the fit.

Guided by the experimental results, it would seem natural to consider the net force on the droplet derived from the thermodynamics of the GaAs

surface during evaporation. The GaAs surface can be characterized by its surface Ga and As chemical potentials, i.e.,  $\mu_{Ga}$  and  $\mu_{As}$ , respectively, where the sum  $\mu_{Ga} + \mu_{As} = \mu_{GaAs}$  is fixed by equilibrium with the crystal, and  $\mu_{GaAs}$  is the bulk crystal free energy per atom pair. Congruent evaporation at a given temperature  $T$  occurs because  $\mu_{Ga}$  adjusts to a steady-state value where Ga and As evaporate at equal rates. Increasing  $T$  favours As evaporation, causing Ga to accumulate on the surface. Consequently,  $\mu_{Ga}$  increases until the Ga and As evaporation rates are equal and congruent evaporation is restored. However, with increasing  $T$ ,  $\mu_{Ga}$  will eventually rise beyond liquidus value  $\mu_L$ , and Ga can nucleate as liquid droplets rather than all evaporating. This defines the upper limit  $T_c$  for congruent evaporation. It is expected that the Ga droplets will stay close to equilibrium with the GaAs crystal at  $\mu_L$ , which gives rise to a disequilibrium between the droplet and surface for temperatures away from  $T_c$ , where  $\mu_{Ga} \neq \mu_L$ .

To see how the disequilibrium in chemical potential results in motion, it is necessary to consider the net force on a droplet when it is displaced (e.g. by a thermal fluctuation). Integrating the force vector around the periphery of the droplet, it can be shown that the total net force on a droplet is proportional to the difference in Gibbs free surface energy of the surfaces exposed and covered during the motion [5]. The newly exposed surface is created in equilibrium with the droplet at chemical potential  $\mu_L$ . However, before being covered by the droplet, the surface on the opposite side had a structure corresponding to  $\mu_{Ga}$ , whereas the reservoir for the excess Ga is now the droplet at  $\mu_L$ . Expanding to the lowest order in  $(T - T_c)$ , one finds that the difference in free surface energy is quadratic in  $(\mu_{Ga} - \mu_L)$  and that  $(\mu_{Ga} - \mu_L)$  is linear in  $(T - T_c)$ , giving the total net force on a droplet of diameter  $d$  at temperature  $T$  as

$$F = \alpha(T - T_c)^2 d, \quad (1)$$

where the coefficient  $\alpha$  embodies both thermodynamic and kinetic properties of the surface [5]. Modelling the time-averaged stick-slip motion as a damped response to  $F$  with an effective frictional force that is independent of velocity and opposite to the direction of motion, then from Equation (1), the velocity becomes

$$v \approx m\alpha(T - T_c)^2 - v_f, \quad (2)$$

where  $m$  is the mobility, and  $v_f$  is the friction term. For  $(T - T_c)^2 < v_f / m\alpha$ ,  $v = 0$ , which is consistent with the region of zero motion about  $T_c$ . When the range of  $T$  is large, it is necessary to include cubic and higher order terms in the expansion about  $T_c$ , and with Equation (2) extended to cubic order, it is possible to fit (solid blue line) the velocity data well, as shown in Figure 2(b). The basic prediction of  $v \propto (T - T_c)^2$  is, however, sufficient to capture the overall general behaviour.

We note that there have been a number of interesting studies of droplet dynamics on surfaces with different proposed mechanisms for motion [27-29]. The mechanism for running droplets described here should be applicable to other III-V semiconductors such as InAs, where the more slowly evaporating component forms droplets on the surface at temperatures where a liquidus exists. More broadly, the droplet motion may create new possibilities to position nanostructures in droplet epitaxy.

### **Droplet coalescence during Langmuir evaporation**

Above  $T_c$ , excess Ga is left behind during evaporation and diffuses to the droplets, which grow via adatom capture. Occasionally, however, droplets

also abruptly grow via coalescence [6,9] These events are particularly interesting, as illustrated by the sequence of PEEM images shown in Figure 3. Droplet 1 in Figure 3(a) is absorbed into droplet 2 (which remains stationary) in a coalescence event [see Figure 3(b)]. This leaves behind the etch pit framed in Figure 3(b) and magnified in Figure 3(c). Within 2 seconds, a rapid burst of daughter droplet nucleation occurs within this area. Following rapid growth, they begin to move at  $t = 51$  seconds. Eventually, the droplets move outside the etch pit arena, and there is no subsequent nucleation suggesting an unanticipated nucleation mechanism.

To elucidate the mechanism we employ MEM [5,6,23-26] to reveal information on surface morphology. In particular, MEM movies of coalescence events similar to Figure 3 reveal that the concave etch pit left behind by the coalescing droplet planarizes with time, and only then do the daughter droplets move away from the region. The time for significant planarization corresponds to the initial burst of nucleation and growth of the daughter droplets with no further nucleation occurring after the surface is planarized.

### **Simple model for Langmuir evaporation of GaAs**

The linkage between planarization and droplet formation suggests surface steps are important, and we develop a simple model of Langmuir evaporation from a miscut wafer of mean step spacing  $L_s$ . Our assumption is that Ga adatoms persist on the surface long enough to maintain approximate equilibrium between terrace and steps [30]. However, it is known that As readily evaporates, and a constant excess flux of As is required to prevent decomposition during MBE [15]. Consequently, we assume that, at our experimental temperatures, As surface species evaporate too rapidly to maintain a significant population across the terrace. Then, the rate of As evaporation is proportional to step density, whereas Ga evaporation is independent of step density. Formalizing this using a

standard transition-state model for As and Ga evaporation, the evaporation rates per unit area are

$$F_{Ga} = r_{Ga} \exp\left(\frac{\mu_{Ga} - E_{Ga}}{kT}\right), \quad (3)$$

$$F_{As} = r_{As,s} L_s^{-1} \exp\left(\frac{N(\mu_{GaAs} - \mu_{Ga}) - E_{AsN}}{kT}\right). \quad (4)$$

Here,  $E_{Ga}$  and  $E_{AsN}$  are the respective transition-state energy values for Ga and As evaporation, and it is assumed that the As transition state consists of  $N$  atoms. The rate constants  $r_{Ga}$  (per unit area) and  $r_{As,s}$  (per unit step length) include the transition-state entropy or degeneracy, for example, the density of sites for evaporation. As discussed earlier,  $\mu_{Ga}$  increases with increasing  $T$  until  $F_{Ga} = F_{As}$ . However, if  $\mu_{Ga}$  rises above the liquidus value, Ga can accumulate as droplets, which defines  $T_c$ . Inserting Equation (3) and (4) in the condition  $F_{Ga} = F_{As}$  for  $\mu_{Ga} = \mu_L$  then yields an expression for the congruent evaporation temperature, i.e.,

$$kT_c = \frac{(N+1)\mu_L - N\mu_{GaAs} - E_{Ga} + E_{AsN}}{\ln(r_{As,s} / L_s r_{Ga})}. \quad (5)$$

This simple model leads to several important predictions [6]. First, above  $T_c$ , if droplet coalescence suddenly exposes an etch pit of much higher local miscut (and we assume step density), then that region will experience much faster As evaporation and Ga release, explaining the burst of nucleation and subsequent growth of the daughter droplets. Second, the release of Ga increases  $\mu_{Ga}$  in the etch pit region. This drives the surface further from the liquidus composition, which enhances the force for the droplet motion [5] and accounts for the rapid daughter droplet dynamics. Finally, it can be observed in Equation (5) that  $T_c$  depends on the miscut via mean step

spacing  $L_S$ . This has potential implications for positioning nanostructures, which we consider in the next section.

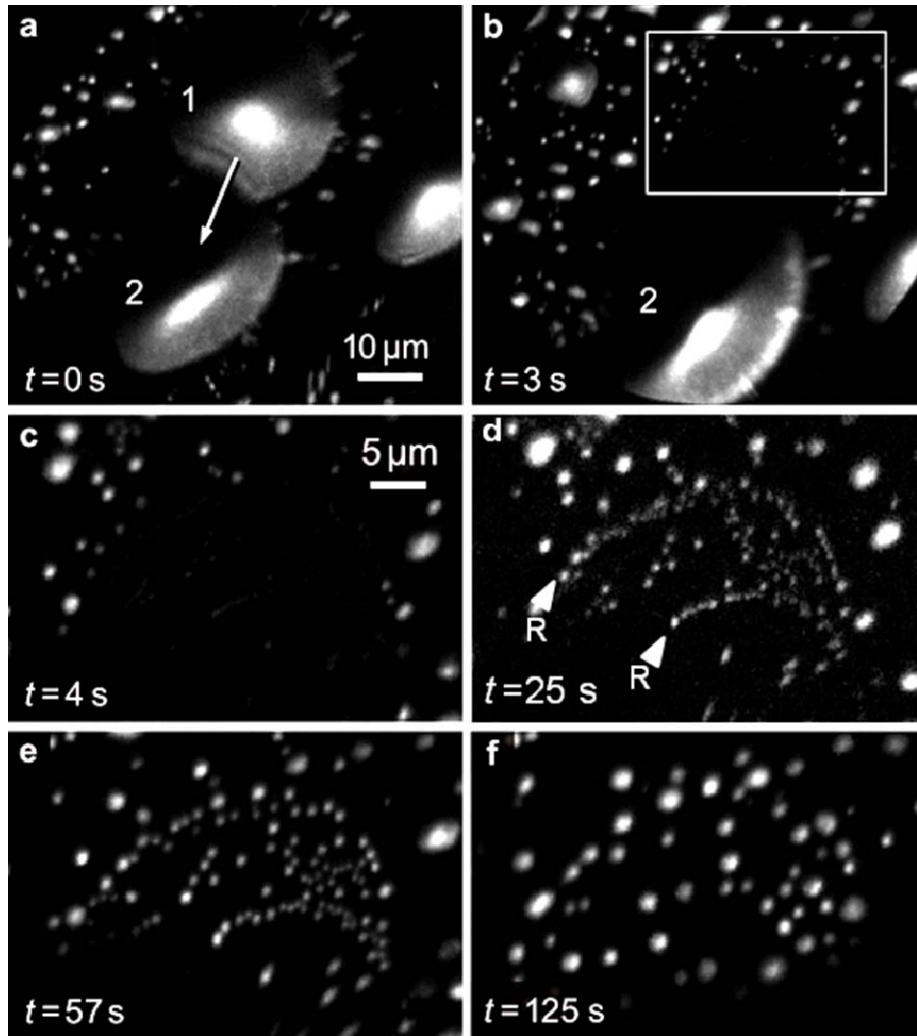


Figure 3 Images captured from a PEEM video of Ga droplet coalescence at 630 °C [6]. Liquid Ga appears bright against dark GaAs. (a) Droplets 1 and 2 are in close proximity at  $t=0$ . (b) At  $t=3$  seconds, droplet 1 translates across the substrate and coalesces with droplet 2, leaving an exposed shallow etch pit. This exposed etch pit, which is enclosed by the frame in (b), is magnified in (c-f). Daughter droplet formation and (d) growth are sometimes associated with surface ridges, R.

### **Positioning nanostructures using spatial variations in $T_c$**

Equation (5) indicates that regions of the surface possessing a higher local miscut will have a lower  $T_c$ , suggesting new possibilities for controlled nanostructure formation on lithographically patterned substrates. Evaporation should preferentially occur on the most highly sloped regions, allowing generation of droplets at predetermined locations. Annealing at temperatures above  $T_c$  for the sloped regions, but below  $T_c$  for the surrounding planar surface, should provide especially reliable Ga placement. The droplets could then be converted into quantum structures under an overpressure of a group V vapour as in standard droplet epitaxy methods [2, 20-22].

We have demonstrated droplet positioning at a proof-of-concept level. We first heated a GaAs(001) sample above  $T_c$  to form a number of well-separated Ga droplets [see Figure 4(a)] The sample was then cooled below  $T_c$  so that the Ga droplets shrink and eventually disappear [see Figure 4(b)]. This leaves a surface patterned with nanoscale depressions due to droplet etching. The largest droplet, which is designated 1 in Figure 4(a), is associated with the deepest etch pit and was the last to disappear. When we slowly increase the temperature to 620 °C, a new droplet appears at precisely the same position as droplet 1 [see Figure 4(c)]. We can control the stability of this single droplet over a significant time period (many minutes) and temperature range  $\pm 5$  °C [see Figure 4(d)]. On increasing the temperature to 635 °C, a new droplet is generated in the etch pit previously occupied by droplet 2 [see Figure 4(e)]. Even after 1 minute of annealing at 635 °C, approximately 90% of the new droplets generated in Figure 4(f) correspond to etch pit positions. This demonstrates that droplet positions can be controlled by surface patterning.

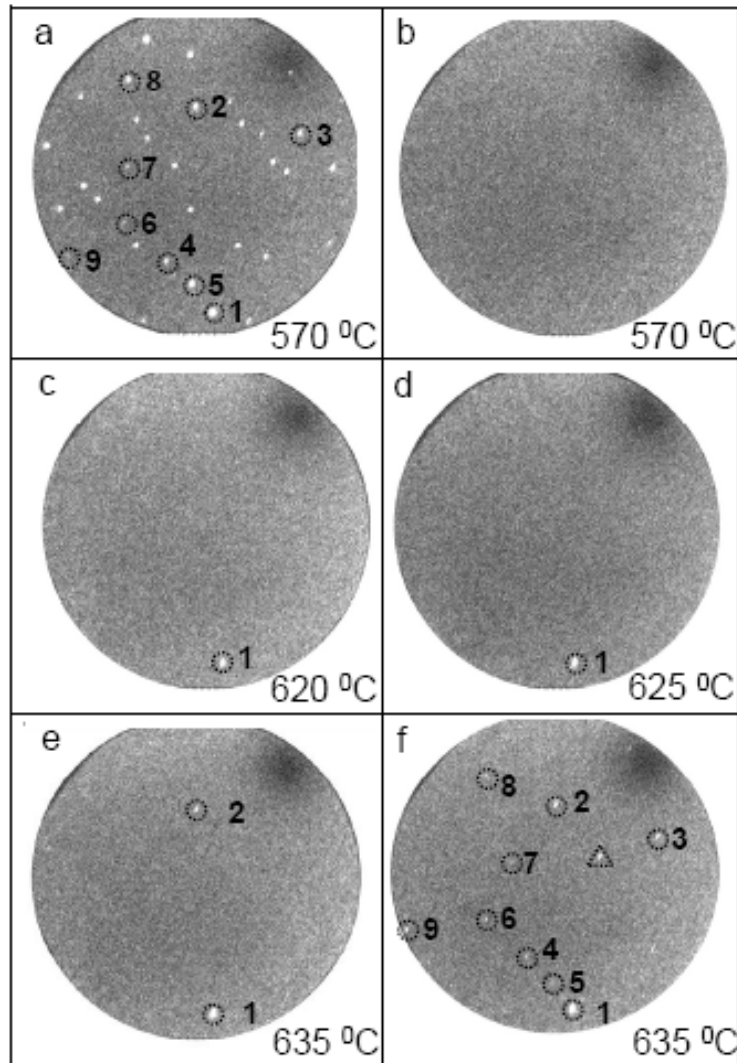


Figure 4 PEEM images of Ga droplet shrinkage and formation [6]. (a) The sample is cooled below  $T_c$  so that Ga droplets shrink and eventually disappear in (b). Circled droplet 1 in (a) is the largest droplet and the last to disappear. (c) On slowly heating the sample to 620 °C, a new droplet is generated in the original position of droplet 1. (d) This droplet was stable in the temperature range of 620–625 °C for several minutes. (e) Increasing the temperature to 635 °C results an additional droplet appearing at the original position of droplet 2 in (a). (f) After a further minute at 635 °C, 90% of the new droplets correspond to previous droplet positions in (a) (circled droplets). The droplet enclosed by a triangle has appeared at a new position.

## Conclusions

We have described the design of a III-V surface electron microscope and its application to study Langmuir evaporation of GaAs(001). Droplets move during evaporation, which is driven by disequilibrium with the surface, giving rise to an unusual temperature dependence. Coalescence events are associated with the nucleation and motion of numerous “daughter droplets”. These observations indicate a morphology-dependent congruent evaporation temperature, which has important implications for writing nanostructures.

## Acknowledgments

The work of D. E. Jesson and W. -X. Tang was supported by the Australian Research Council under grant DP0985290. We thank Rod Mackie for technical support.

## References

- [1] B. A. Joyce and D. D. Vvedensky, “Self-organized growth on GaAs surfaces,” *Mat. Sci. Eng. R.*, vol. 46, no. 6, pp. 127-176, Dec. 2004.
- [2] J. H. Lee, Z. M. Wan, Z. Y. AbuWaar, and G. J. Salamo, “Design of nanostructure complexes by droplet epitaxy,” *Cryst. Growth Des.*, vol. 9, no. 2, pp. 715-721, Jan. 2009.
- [3] S. Kiravittaya, A. Rastelli, and O. G. Schmidt, “Advanced quantum dot configurations,” *Rep. Prog. Phys.* vol. 72, no. 4, article no. 046502, Mar. 2009.
- [4] D. Spirkoska, C. Colombo, M. Heiss, G. Abstreiter, and A. F. I. Morral, “The use of molecular beam epitaxy for the synthesis of high purity III-V nanowires,” *J. Phys. Condens. Matter.* vol. 20, no.45, article no. 454255, Nov. 2008.
- [5] J. Tersoff, D. E. Jesson, and W. X. Tang, “Running droplets of Ga from evaporation of Ga arsenide,” *Science*, vol. 324, no. 5924, pp. 236-238. Apr. 2009.

- [6] J. Tersoff, D. E. Jesson, and W. X. Tang, “Decomposition controlled by surface morphology during Langmuir evaporation of GaAs,” *Phys. Rev. Lett.*, vol.105, no. 3, p. 035702, Jul. 2010.
- [7] D. E. Jesson and W. X. Tang, “Surface Electron Microscopy of Ga Droplet Dynamics on GaAs(001),” in *Microscopy: Science, Technology, Applications and Education*, A. Méndez-Vilas, J. Díaz, Eds. Badajoz, Spain: Formatex, 2010, pp. 1608-1619.
- [8] K. G. Tschersich and V. von Bonin, “Formation of an atomic hydrogen beam by a hot capillary,” *J. Appl. Phys.*, vol. 84, no. 8, pp.4065-4070, Oct. 1998.
- [9] E. Bauer, "Low energy electron microscopy". *Rep. Prog. Phys.* vol. 57, no. 9, pp. 895–938, sep. 1994
- [10] A. B. Pang, T. Müller, M. S. Altman, and E. Bauer, “Fourier optics of image formation in LEEM,” *J. Phys. Condens. Matter*, vol. 21, no. 31, article no. 314006, Jul. 2009.
- [11] S. Günther, B. Kaulich, L. Gregoratti, and M. Kiskinova, “Photoelectron microscopy and applications in surface and materials science,” *Prog. Surf. Sci.*, vol.70, no. 4-8, pp. 187-260, Jul. 2002.
- [12] C. T. Foxon, J. A. Harvey, and B. A. Joyce, “The evaporation of GaAs under equilibrium and non-equilibrium conditions using a modulated beam technique,” *J. Phys. Chem. Solids.*, vol. 34, no. 10, pp. 1693-1701, Oct. 1973.
- [13] J. R. Arthur, “Vapor pressures and phase equilibria in the Ga-As system,” *J. Phys. Chem. Solids.*, vol. 28, no. 11, pp. 2257-2267, Nov. 1967.
- [14] B. Goldstein, D. J. Szostak, and V. S. Ban, “Langmuir evaporation from the (100), (111A), and (111B) faces of GaAs,” *Surf. Sci.*, vol. 57, no. 2, pp.733-740, Jul. 1976.
- [15] J. Y. Tsao, *Materials Fundamentals of Molecular Beam Epitaxy*. 1st ed., San Diego, CA: Academic,1993.
- [16] M. Zinke-Allmang, L. C. Feldman, and W. van Saarloos, “Experimental study of self-similarity in the coalescence growth regime,” *Phys. Rev. Lett.* vol. 68, no. 15, pp. 2358-2361, Apr. 1992.

- [17] T. D. Lowes and M. Zinke-Allmang. “Microscopic study of cluster formation in the Ga on GaAs(001) system,” *J. Appl. Phys.*, vol. 73, no. 10, pp.4937-4941, May 1993.
- [18] Z. Y. Zhou, C. X. Zheng, W. X. Tang, D. E. Jesson and J. Tersoff, “Congruent Evaporation Temperature of GaAs(001) Controlled by As Flux,” *Appl. Phys. Lett.*, vol. 97, article no. 121912, Sep. 2010.
- [19] Z. Y. Zhou, W. X. Tang, D. E. Jesson and J. Tersoff, “Time-Evolution of the Ga Droplet Size-Distribution during Langmuir Evaporation of GaAs(001),” *Appl. Phys. Lett.*, vol. 97, no. 19, article no. 191914, Nov. 2010.
- [20] T. Mano, T. Kuroda, S. Sanguinetti, T. Ochiai, T. Tateno, J. Kim, T. Noda, M. Kawabe, K. Sakoda, G. Kido, and N. Koguchi “Self-assembly of concentric quantum double rings,” *Nano Lett.*, vol. 5, no. 3, pp.425-428, Mar. 2005.
- [21] M. Yamagiwa, T. Mano, T. Kuroda, T. Tateno, K. Sakoda, G. Kido, N. Koguchi, and F. Minami “Self-assembly of laterally aligned quantum dot pairs,”*Appl. Phys. Lett.*. vol. 89, no. 11, article no. 113115, Sep. 2006.
- [22] C. Somaschini, S. Bieti, N. Koguchi, S. Sanguinetti . Fabrication of multiple concentric nanoring structures. *Nano Lett.*, vol. 9, no. 10, pp. 3419-3424, Sep. 2009.
- [23] S. M. Kennedy, C. X. Zheng, W. X. Tang, D. M. Paganin, and D. E. Jesson, “Laplacian image contrast in mirror electron microscopy (addendum),” *Proc. Roy. Soc. A.*, published online, DOI: 10.1098/rspa.2011.9204.
- [24] S. M. Kennedy, C. X. Zheng, W. X. Tang, D. M. Paganin, and D. E. Jesson, “Laplacian image contrast in mirror electron microscopy,” *Proc. Roy. Soc. A*, vol. 466, no. 2122, pp. 2857–2874, Oct. 2010.
- [25] S. M. Kennedy, C. X. Zheng, W. X. Tang, D. M. Paganin, and D. E. Jesson, “Caustic Imaging of gallium droplets using mirror electron microscopy,” *Ultramicroscopy*, vol. 111, no. 5, pp. 356-363, Apr. 2011.

- [26] S. M. Kennedy, D. M. Paganin, and D. E. Jesson, "Laplacian and caustic imaging theories of MEM work-function contrast," *IBM J. Res. Dev.*, vol. 55, no. 4, paper 3, pp. 3:1-3:8, 2011.
- [27] E. Hilner, A.A. Zakharov, K. Schulte, P. Kratzer, J. N. Andersen, E. Lundgren, and A. Mikkelsen, " Ordering of the nanoscale step morphology as a mechanism for droplet self-propulsion," *Nano. Lett.*, vol. 9, no.7, pp. 2710-2714, Jun. 2009.
- [28] W.C. Yang, H. Ade, and R.J. Nemanich, "Stability and dynamics of Pt–Si liquid microdroplets on Si(001)," *Phys. Rev. B; Condens. Matter*, vol. 69, no. 4, article no. 045421, Jan. 2004.
- [29] P. Sutter, P.A. Bennett, J. I. Flege, and E. Sutter, "Steering liquid Pt–Si nanodroplets on Si(100) by interactions with surface steps," *Phys. Rev. Lett.*, vol. 99, no. 12, article no. 125504, Sep. 2007
- [30] J. Tersoff, M. D. Johnson, and B. G. Orr, "Adatom densities on GaAs: Evidence for near-Equilibrium growth", *Phys. Rev. Lett.*, vol. 78, no. 2, pp. 282-285, Jan. 1997.

---

## Introduction to the thermodynamics of Ga droplet formation during Langmuir evaporation

Langmuir evaporation has been studied for many decades (Foxon et al., 1973; Arthur, 1967; Goldstein et al., 1976; Tsao, 1993; Tang et al., 2011). During Langmuir evaporation, Ga and As species generated through the decomposition of GaAs evaporate into vacuum from the GaAs surface. An important characteristic of the GaAs (001) surface is the congruent evaporation temperature  $T_c$ . Fig. 4.1 illustrates the general concept of  $T_c$ . Fig. 4.1 (a) shows the ratio of the evaporation rates of As and Ga measured by mass spectrometer during Langmuir evaporation (Foxon et al., 1973). It can be seen that below  $T_c$ , the ratio of the evaporation rates of As and Ga is unity and no Ga droplets are generated on the surface because the overall substrate stoichiometry is preserved (Fig. 4.1 (c)); in contrast, above  $T_c$ , the As:Ga evaporation ratio becomes greater than unity and increases with temperature. The preferential evaporation of As therefore leaves behind Ga droplets on the surface (Fig. 4.1 (b)) (Zinke-Allmang, Feldman and van Saarloos, 1992; Lowes and Zinke-Allmang, 1993; Zhou et al., 2010).  $T_c$  is not only a major characteristic of GaAs surface, but also technologically important in defining the upper-bound in temperature for molecular beam epitaxy (MBE) growth (Tsao, 1993) and surface cleaning (Isomura et al., 2007). Therefore it is important to understand

the main factors governing  $T_c$ .

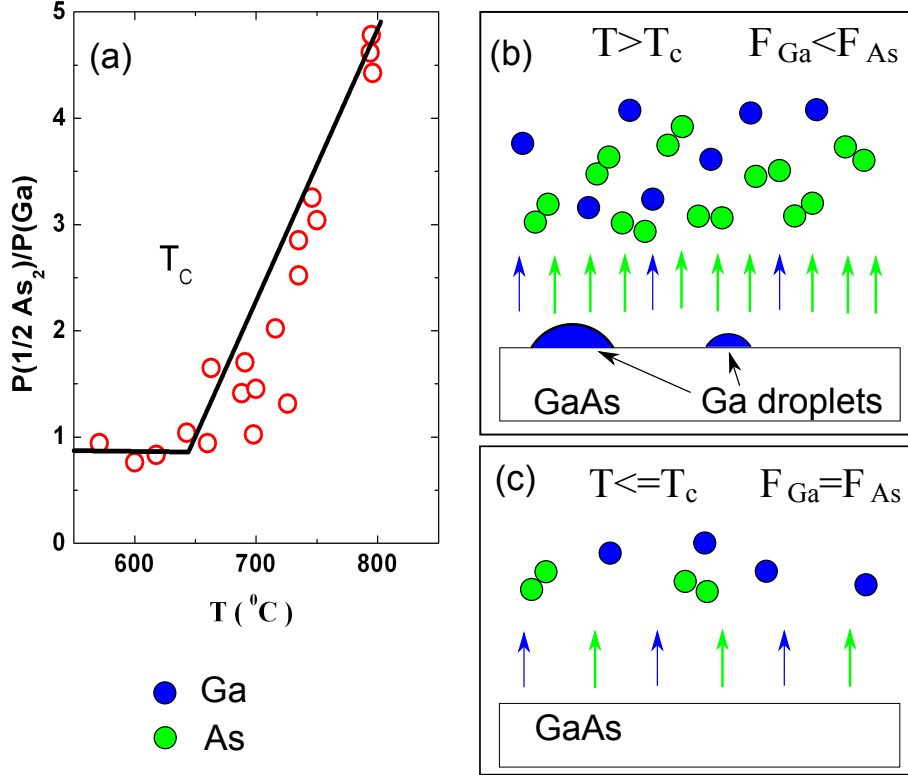


Figure 4.1: (a) As/Ga evaporation rate ratio of a GaAs surface during Langmuir evaporation (Foxon et al., 1973). (b) Above  $T_c$ , the evaporation rate  $F_{As} > F_{Ga}$ , leaving behind Ga droplets on the surface. (c) Below  $T_c$ , the evaporation rates are equal,  $F_{As} = F_{Ga}$ .

To formalise the concept of  $T_c$  discussed above we consider a simple thermodynamic model of GaAs Langmuir evaporation (Tersoff et al., 2009). Treating the surface as having Ga and As adatoms in equilibrium with the crystal, at any given temperature  $T$ , we define the chemical potential of Ga and As adatoms as  $\mu_{Ga}$  and  $\mu_{As}$ , respectively. We then have:

$$\mu_{Ga} + \mu_{As} = \mu_{GaAs}, \quad (4.1)$$

where  $\mu_{GaAs}$  is fixed by bulk GaAs.

The adatom densities are given by:

$$\begin{cases} \rho_{Ga} = \rho_0 \exp((\mu_{Ga} - E_{Ga})/(kT)), \\ \rho_{As} = \rho_0 \exp((\mu_{As} - E_{As})/(kT)), \end{cases} \quad (4.2)$$

where  $\rho_0$  is the surface site density, and  $E_{Ga}$  and  $E_{As}$  are adatom formation energies of Ga and As, respectively. Assuming Ga and As evaporation rates are proportional to the respective adatom densities with respective proportionality constants  $r_{Ga}$  and  $r_{As}$ , the evaporation rates are

$$\begin{cases} F_{Ga} = r_{Ga}\rho_0 \exp((\mu_{Ga} - E_{Ga})/(kT)), \\ F_{As} = r_{As}\rho_0 \exp((\mu_{As} - E_{As})/(kT)), \end{cases} \quad (4.3)$$

Congruent evaporation means  $F_{Ga} = F_{As}$ , and combining (4.3) with (4.1), gives,

$$\ln(F_{Ga}/F_{As}) = kT \ln(r_{Ga}/r_{As}) + 2\mu_{Ga} + E_{As} - E_{Ga} - \mu_{GaAs} = 0, \quad (4.4)$$

so that

$$2\mu_{Ga} = kT \ln(r_{As}/r_{Ga}) + E_{Ga} + \mu_{GaAs} - E_{As}. \quad (4.5)$$

The equilibrium limit for congruent evaporation is  $\mu_{Ga} \leq \mu_L$ , where  $\mu_L$  is the liquid Ga chemical potential. So that from (4.5) we obtain,

$$kT \leq kT_c = \frac{2\mu_L - E_{Ga} + E_{As} - \mu_{GaAs}}{\ln(r_{As}/r_{Ga})}. \quad (4.6)$$

Therefore for  $T > T_c$  As evaporates more rapidly than Ga, and Ga droplets can grow. Below  $T_c$ ,  $\mu_{Ga} < \mu_L$ , so a Ga droplet will lose Ga to the surrounding surface and eventually disappear. At  $T_c$ ,  $\mu_{Ga} = \mu_L$  and the droplet is stable, neither shrinking nor growing. This stability condition can therefore be used to measure  $T_c$  by observing droplets dynamically in the III-V low energy electron microscopy (LEEM).

According to our thermodynamic description of  $T_c$  described above, external As flux, which is commonly used during MBE growth, would be expected

to shift the value of  $T_c$  because the deposition of As flux partly compensates for its evaporation, thereby changing the As and Ga chemical potentials. However, the quantitative dependence of  $T_c$  on As flux has not previously been determined. In Chapter 5 we therefore apply the condition for droplet stability (neither shrinking or growing) to measure  $T_c$  in the presence of As flux. This dependence is explained by modifying our thermodynamic model for evaporation to incorporate As flux. This work provides a method of controlling congruent evaporation which is important for MBE growth, surface preparation and modifying droplet motion.

---

## Congruent evaporation temperature of GaAs(001) controlled by As flux

This chapter is an author generated post print of the article

Z. Y. Zhou, C. X. Zheng, W. X. Tang, D. E. Jesson, and J. Tersoff, 'Congruent Evaporation Temperature of GaAs(001) Controlled by As Flux', *Applied Physics Letters*, **97**, 121912(2010), available electronically at

<http://link.aip.org/link/doi/10.1063/1.3491552>

or via doi:10.1063/1.3491552.

### Declaration for Thesis Chapter "Congruent Evaporation Temperature of GaAs(001) Controlled by As Flux"

Declaration by candidate

For this chapter, the nature and extent of my contribution to the work was the following:

Nature of contribution	Extent of contribution(%)
Designed the experiments, co-performed the experiments, co-developed the model used in the paper, co-wrote the paper.	60

The following co-authors contributed to the work. Co-authors who are students at Monash University must also indicate the extent of their contribution in percentage terms

Name	Extent of contribution(%)	Nature of contribution
Changxi Zheng	25	Co-performed the experiments,co-wrote the paper
Wen-XinTang		Helped perform the experiments and provided technical expertise.
David Jesson		Co-wrote the paper, helped develop the model and provided technical expertise.
Jerry Tersoff		Co-wrote the paper, helped developed the model.

Candidate's  
signature



Date

17/08/2012

#### Declaration by co-authors

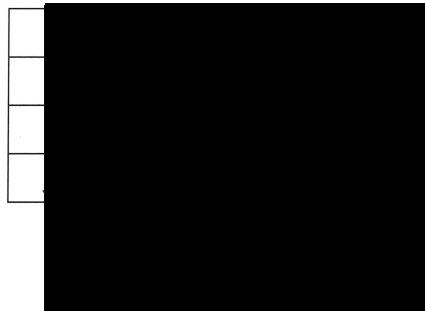
The undersigned hereby certify that:

- (1) they meet the criteria for authorship in that they have participated in the conception, execution, or interpretation, of at least that part of the publication in their field of expertise;
- (2) they take public responsibility for their part of the publication, except for the responsible author who accepts overall responsibility for the publication;
- (3) there are no other authors of the publication according to these criteria;
- (4) potential conflicts of interest have been disclosed to (a) granting bodies, (b) the editor or publisher of journals or other publications, and (c) the head of the responsible academic unit; and
- (5) the original data are stored at the following location(s) and will be held for at least five years from the date indicated below:

Location(s)

School of Physics, Monash University, Clayton

Signature 1



Date

16-08-12

Signature 2

16-08-12

Signature 3

16-08-12

Signature 4

17/08/2012

# Congruent Evaporation Temperature of GaAs(001) Controlled by As Flux

Z. Y. Zhou, C. X. Zheng, W. X. Tang, D. E. Jesson\*

*School of Physics, Monash University, Victoria 3800, Australia*

J. Tersoff

*IBM Research Division, Thomas J. Watson Research Center,*

*Yorktown, Heights, New York 10598, USA*

## Abstract

The congruent evaporation temperature  $T_c$  is a fundamental surface characteristic of GaAs and similar compounds. Above  $T_c$  the rate of As evaporation exceeds that of Ga during Langmuir (free) evaporation into a vacuum. However, during molecular beam epitaxy (MBE) there is generally an external As flux  $F$  incident on the surface. Here we show that this flux directly controls  $T_c$ . We introduce a sensitive approach to measure  $T_c$  based on Ga droplet stability, and determine the dependence of  $T_c$  on  $F$ . This dependence is explained by a simple model for evaporation in the presence of external flux. The capability of manipulating  $T_c$  via changing  $F$  offers a means of controlling congruent evaporation with relevance to MBE, surface preparation methods and droplet epitaxy.

---

\* [REDACTED]

Langmuir evaporation of GaAs (001), in which the surface freely evaporates into a vacuum, has been widely studied over the years [1–4]. Central to understanding the physics of Langmuir evaporation is the so-called congruent evaporation temperature  $T_c$ . Below  $T_c$ , Ga and As fluxes leaving the surface are equal which preserves compound stoichiometry. However, above  $T_c$ , As preferentially evaporates from the surface leaving behind Ga-rich liquid droplets [5, 6]. In addition to being a major characteristic of III-V surfaces[7],  $T_c$  is technologically important in defining the upper-bound in temperature for MBE growth[4] and surface cleaning[8]. Recently, it has also been shown that  $T_c$  plays a central role in the physics of Ga droplet dynamics on GaAs (001) (Refs. 9 and 10) which has implications for extending the droplet epitaxy technique [11]. It is therefore important to understand how  $T_c$  depends on experimental conditions.

In this paper we demonstrate that one can directly control  $T_c$  by varying As deposition flux. A sensitive approach is presented for the measurement of  $T_c$  based on the stability of Ga droplets. Our results are explained using a simple model for evaporation in the presence of external As flux. The ability to control  $T_c$  via an applied As flux provides a means of investigating the evaporation and decomposition of III-V materials, as well as elucidating the effect of As flux during surface preparation and MBE growth.

The measurement of  $T_c$  in the presence of external As flux presents a significant experimental challenge. Previous studies have measured  $T_c$  in the absence of flux using careful modulated beam measurements and evaporated species identification [1]. However, there is a barrier to the initial nucleation of Ga droplets. This could lead to hysteresis effect, which would explain the large scatter in earlier measurements of  $T_c$ [1, 3]. To avoid this, we focus on the stability of droplets that are already present, finding the temperature where they neither shrink nor grow. In this way we can determine  $T_c$  in the presence of an incident As flux  $F$ , as long as the As

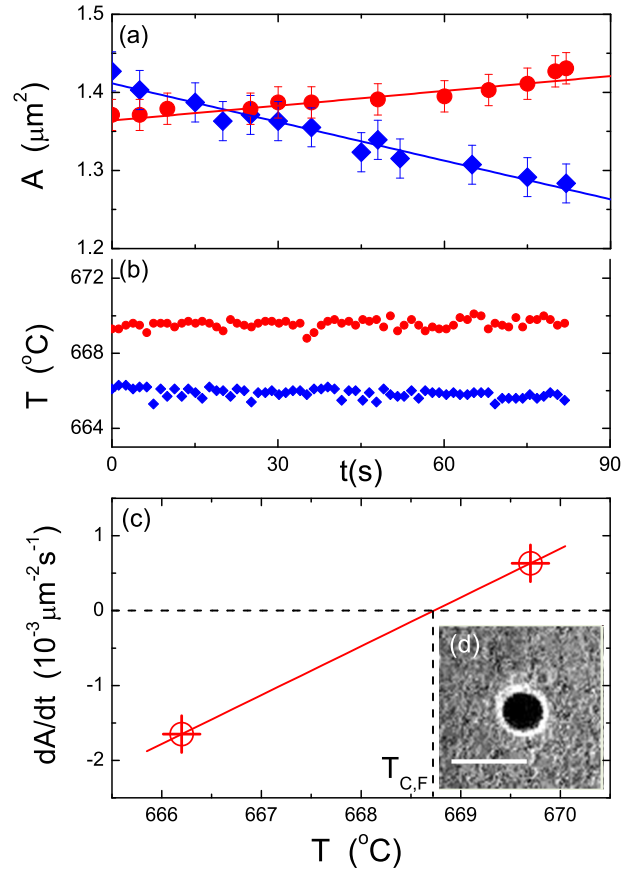


FIG. 1. (Color online)(a) Droplet area  $A$  as a function of time  $t$ . The area is defined as the dark region enclosed within the bright concentric ring in (d). Circles/diamonds in (a) correspond to the respective temperature variation indicated by the circles/diamonds in (b). Temperatures are measured to an accuracy of  $\pm 0.2^\circ\text{C}$ . (c)  $dA/dt$  as a function of temperature  $T$  obtained from the gradients of two lines in (a).  $T_{C,F}$  for the droplets is estimated to occur at the intersection of the straight-line connecting the points with  $dA/dt = 0$ . (d) MEM image of a Ga droplet with the area  $A$  defined as the dark region within the bright concentric ring (scale bar,  $1 \mu\text{m}$ ). For this series of measurements  $P_{As} = 4.6 \times 10^{-6}$  Torr.

pressure is not so high as to prevent electron imaging of the droplets.

To create Ga droplets we degassed an undoped GaAs (001)  $\pm 0.1^\circ$  epi-ready wafer at  $300^\circ\text{C}$  under ultra high vacuum for 24 h in an Elmitec low energy electron microscope (LEEM) III system. This was followed by high temperature flashing up to  $600^\circ\text{C}$  and annealing at  $580^\circ\text{C}$  for 2 hours to remove the surface oxide. Well-separated Ga droplets ( $\sim 5\mu\text{m}$ ) were prepared by annealing at  $650^\circ\text{C}$  and were imaged using mirror electron microscopy (MEM) [12–14], in which droplets appear as dark circles surrounded by a bright concentric ring (Fig. 1(d))[9, 14]. The droplets were brought into a stable condition by adjusting the temperature so that they neither shrink nor grow. This is the congruent evaporation temperature for zero flux,  $T_{c,0}$ , to which we assign the literature value [4] of  $625^\circ\text{C}$ . All temperatures were measured relative to this value and remained stable to within  $\pm 1^\circ\text{C}$ .

On opening the As shutter, there are transient effects due to changes in surface work function. This occurred over a period of 30 s and care was taken to allow the imaging and As deposition conditions to stabilise before droplet stability measurements commenced. The beam effective pressure (BEP) of the  $\text{As}_4$  molecular beam  $P_{\text{As}}$  was determined from the calibrated valve position of the cracker source. Following image stabilisation, we use pattern recognition software to measure and record the droplet area  $A$  as a function of time. The temperature was adjusted to slow the rate of change of droplet size below  $\sim 2 \times 10^{-3} \mu\text{ms}^{-1}$ . The area  $A$  is defined as the dark region enclosed within the bright concentric ring as shown in Fig. 1(d). Note that the droplets appear larger in MEM than their real size[9, 12] but, as we are only concerned with nulling the rate of change of droplet size, this does not influence our measurements.

Having obtained a condition where a droplet shrinks (or grows) with a rate  $\leq 2 \times 10^{-3} \mu\text{ms}^{-1}$  the temperature was recorded and then slightly in-

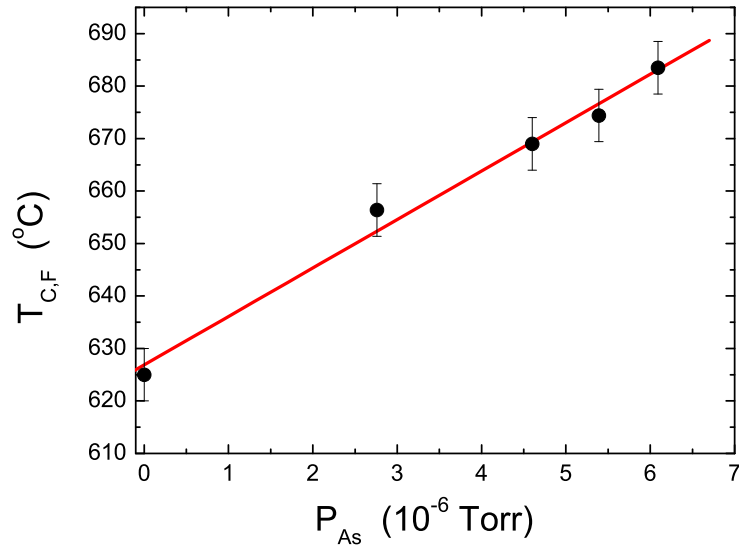


FIG. 2. (Color online) Congruent evaporation temperature  $T_{c,F}$  as a function of  $As_4$  BEP,  $P_{As}$ .

creased (decreased) to produce the opposite behaviour, growth (shrinkage). Such a pair of readings is displayed in Fig. 1(a) and (b) for  $P_{As} = 4.6 \times 10^{-6}$  Torr and yields two values of  $dA/dt$  of opposite sign which are plotted against  $T$  in Fig. 1(c). Note that all droplets were observed to shrink (or grow) simultaneously within the field of view ( $50 \mu\text{m}$ ). The method is very sensitive and allows the stability condition to be determined to within a few degrees centigrade. As shown in Fig. 1(c),  $T_{c,F}$  is determined within this narrow temperature range as the intersection point between a straight line connecting the data points and  $dA/dt = 0$ . This procedure was repeated for different values of  $P_{As}$  and the resulting plot of  $T_{c,F}$  versus  $P_{As}$  is shown in Fig. 2. Error bars were estimated as the temperature range spanning the pair of  $dA/dt$  measurements for each value of  $T_{c,F}$  (see, for example, Fig. 1(c)).

Figure 2 shows that  $T_{c,F}$  increases linearly with As flux. We explain this using a standard transition rate model for Ga and As evaporation. Consider a GaAs (001) surface at temperature  $T$  with zero external As flux. We assume that the surface is in equilibrium with the crystal so that

$$\mu_{Ga} + \mu_{As} = \mu_{GaAs}, \quad (1)$$

where  $\mu_{Ga}$  and  $\mu_{As}$  are the respective Ga and As surface chemical potentials and  $\mu_{GaAs}$  is the chemical potential of the bulk crystal. During congruent evaporation,  $\mu_{Ga}$  attains a steady-state value such that Ga and As evaporate at equal rates. As  $T$  increases,  $\mu_{Ga}$  will increase (thereby equalizing the evaporation rates) until it reaches the liquidus value  $\mu_{Ga,0}$  which defines the upper limit  $T = T_c$  for congruent evaporation. Above  $T_c$ ,  $\mu_{Ga} > \mu_{Ga,0}$  so excess Ga can collect as droplets. These are assumed to remain close to equilibrium with the GaAs substrate at the liquidus composition. The Ga droplets act as sinks for Ga adatoms, which restricts the increase in  $\mu_{Ga}$ . Therefore for  $T > T_c$  As evaporates more rapidly than Ga, and Ga droplets can grow[4]. Below  $T_c$ ,  $\mu_{Ga} < \mu_{Ga,0}$ , so a Ga droplet will lose Ga to the surrounding surface. The Ga atoms diffuse away from Ga droplets as surface adatoms until all Ga droplets eventually disappear. At  $T_c$ ,  $\mu_{Ga} = \mu_{Ga,0}$  and the droplet is stable, it neither shrinks nor grows. This stability condition can therefore be used as a sensitive test for measuring  $T_c$ .

Now consider the GaAs crystal under external As flux  $F$ , which changes the steady-state value of  $\mu_{Ga}$  during congruent evaporation. Consequently, the congruent evaporation temperature at which  $\mu_{Ga}$  is at the liquidus value will also change, making  $T_c$  dependent on  $F$ . For clarity, we denote the flux dependent congruent evaporation temperature as  $T_{c,F}$ , and  $T_{c,0}$  is the conventional congruent evaporation temperature in the absence of flux. The bulk liquidus values of the chemical potential are  $\mu_{Ga,F}$  and  $\mu_{Ga,0}$  at  $T_{c,F}$  and  $T_{c,0}$ , respectively. The  $T_{c,F}$  measured by the droplet stability

condition thus corresponds to the temperature at which  $\mu_{Ga} = \mu_{Ga,F}$  with the surface under an As flux  $F$ .

The net evaporation rates per unit area are

$$\Phi_{Ga} = r_{Ga} \exp\left(\frac{\mu_{Ga} - E_{Ga}}{kT}\right), \quad (2)$$

$$\Phi_{As} = Nr_{As} \exp\left(\frac{N\mu_{As} - E_{As,N}}{kT}\right) - \alpha F, \quad (3)$$

where  $\alpha$  is the sticking probability of the incident As species and it is assumed that As evaporates as an  $N$ -mer (probably a dimer).  $E_{Ga}$  and  $E_{As,N}$  are the respective transition state energies for Ga adatom and As  $N$ -mer evaporation, with associated rate constants  $r_{Ga}$  and  $r_{As}$  (including the transition state entropy or degeneracy, e.g. number of sites for evaporation per unit area). In Eq. (3),  $\Phi_{As}$  and  $F$  are defined per atom independent of  $N$ , while  $r_{As}$  refers to  $N$ -mer desorption events. For congruent evaporation we have  $\Phi_{Ga} = \Phi_{As}$  and so combining (1) - (3) gives

$$\begin{aligned} Nr_{As} \exp\left(\frac{N\mu_{GaAs} - N\mu_{Ga} - E_{As,N}}{kT}\right) - \alpha F \\ = r_{Ga} \exp\left(\frac{\mu_{Ga} - E_{Ga}}{kT}\right). \end{aligned} \quad (4)$$

$T_{c,F}$  is given by replacing  $\mu_{Ga}$  in Eq. (4) by its liquidus value  $\mu_{Ga,F}$  at  $T_{c,F}$ . Note that the bulk liquidus chemical potential is a basic thermodynamic material property, independent of evaporation. However, it does depend on  $T$ , so from Eq. (4) we obtain an implicit equation for  $T_{c,F}$ . To solve this we expand  $\mu_{Ga,F}$  to first order about  $T_{c,0}$ , the congruent temperature in the absence of flux, giving

$$\mu_{Ga,F} = \mu_{Ga,0} + \mu'_{Ga,0}(T_{c,F} - T_{c,0}). \quad (5)$$

$T_{c,F}$  is then obtained by substituting (5) into (4) for  $\mu_{Ga} = \mu_{Ga,F}$  at  $T = T_{c,F}$ , expanding to first order in  $(T_{c,F} - T_{c,0})$  and rearranging to give

$$T_{c,F} = T_{c,0} + \eta F, \quad (6)$$

where the constant  $\eta$  is given by

$$\eta^{-1} = \frac{r_{Ga}}{\alpha k T_{c,0}^2} \exp\left(\frac{\mu_{Ga,0} - E_{Ga}}{k T_{c,0}}\right) [E_{As,N} - E_{Ga} + (N + 1)(\mu_{Ga,0} - \mu'_{Ga,0} T_{c,0}) - N \mu_{GaAs}]. \quad (7)$$

We note  $P_{As} = \beta F/4$  where the factor of 4 arises because of the incident As<sub>4</sub> species and  $\beta = (2\pi m k T_s)^{1/2}$  with  $m$  the molecular mass and  $T_s$  the temperature of the As<sub>4</sub> gas. Eq. (6) predicts a linear dependence of  $T_{c,F}$  on  $P_{As}$ , as long as the As flux is not too large. This is precisely the behaviour observed in Fig. 2. Unfortunately, the slope  $4\eta/\beta$  is a mix of several unknown parameters, so we cannot compare our measurements with the quantitative value. However, the experimental results of Fig. 2 confirm the behaviour predicted by the theory.

Although it is well appreciated that an external As flux compensates for loss of As by evaporation, the control of  $T_{c,F}$  by varying  $F$  offers important complementary insight into this process. In particular, the results of Fig. 2 provide a quantitative basis for systematic interpolation and extrapolation to different growth conditions. This data also allows a quantitative understanding of the As flux required to avoid decomposition of GaAs during oxide desorption at elevated temperatures [15]. Finally, it is known that  $T_c$  controls the motion of Ga droplets on GaAs[9]. Changing  $T_{c,F}$  by varying As flux will therefore allow the manipulation of droplet motion which may have applications in the positioning of quantum structures formed via droplet epitaxy methods [11].

## ACKNOWLEDGMENTS

We are grateful to Rod Mackie for technical support and Bruce Joyce for helpful discussions. DEJ and WXT acknowledge support from the ARC,

Grant No. DP0985290.

---

- [1] C. T. Foxon, J. A. Harvey, and B. A. Joyce, *J. Phys. Chem. Solids* **34**, 1693 (1973).
- [2] J. R. Arthur, *J. Phys. Chem. Solids* **28**, 2257 (1967).
- [3] B. Goldstein, D. J. Szostak, and V. S. Ban, *Surf. Sci.* **57**, 733 (1976).
- [4] J. Y. Tsao, *Materials Fundamentals of Molecular Beam Epitaxy*(Academic, San Diego 1993) p. 733 (1993).
- [5] M. Zinke-Allmang, L. Feldman, and W. van Saarloos, *Phys. Rev. Lett.* **68**, 2358 (1992).
- [6] T. D. Lowes and M. Zinke-Allmang, *J. Appl. Phys.* **73**, 4937 (1993).
- [7] C. Chatillon and D. Chatain, *J. Cryst. Growth* **151**, 91 (1995).
- [8] N. Isomura, S. Tsukamoto, K. Iizuka, and Y. Arakawa, *J. Cryst. Growth* **301-302**, 26 (2007).
- [9] J. Tersoff, D. E. Jesson, and W. X. Tang, *Science* **324**, 236 (2009).
- [10] J. Tersoff, D. E. Jesson, and W. X. Tang, *Phys. Rev. Lett.* **105**, 035702 (2010).
- [11] See, for example, T. Mano, T. Kuroda, S. Sanguinetti, T. Ochiai, T. Tateno, J. Kim, T. Noda, M. Kawabe, K. Sakoda, G. Kido, and N. Koguchi, *Nano Lett.* **5**, 425 (2005); M. Yamagiwa, T. Mano, T. Kuroda, T. Tateno, K. Sakoda, G. Kido, N. Koguchi, and F. Minami, *Appl. Phys. Lett.* **89**, 113115 (2006); S. Huang, Z. Niu, Z. Fang, H. Ni, Z. Gong, and J. Xia, *Appl. Phys. Lett.* **89**, 031921 (2006); C. Somaschini, S. Bietti, N. Koguchi, and S. Sanguinetti, *Nano Lett.* **9**, 3419 (2009); J. H. Lee, Z. M. Wang, Z. Y. AbuWaar, and G. J. Salamo, *Cryst. Growth & Design* **9**, 715 (2009) .
- [12] S. A. Nepijko, N. N. Sedov, and G. Schönhense, *J. Microsc* **203**, 269 (2001).
- [13] S. M. Kennedy, D. E. Jesson, M. J. Morgan, A. E. Smith, and P. F. Barker,

Phys. Rev. A **74**, 044701 (2006).

- [14] S. M. Kennedy, C. X. Zheng, W. X. Tang, D. M. Paganin, and D. E. Jesson, Proc. Roy. Soc. A **466**, 2857 (2010).
- [15] T. Van. Buuren, M. K. Weilmeier, I. Athwal, K. M. Colbow, J. A. Mackenzie, T. Tiedje, P. C. Wong, and K. A. R. Mitchell, Appl. Phys. Lett. **59**, 464 (1991).

---

## Introduction to the evolution of Ga droplet size distributions

Size distribution of clusters on surfaces have been widely studied in surface physics over many decades (Family and Meakin, 1988, 1989; Zinke-Allmang, Feldman and Grabow, 1992; Amar and Family, 1995; Kelton, 2005; Slezov, 2009). Controlling the size distribution of clusters is of crucial relevance to the quality of heterostructures and devices grown by thin-film techniques such as molecular beam epitaxy (MBE) and droplet epitaxy (Zinke-Allmang, Feldman and Grabow, 1992; Watanabe et al., 2000). Studying clustering kinetics is also important for investigating fundamental aspects of surface physics such as surface diffusion, adsorption, desorption, and phase transitions (Zinke-Allmang, Feldman and Grabow, 1992; Family and Meakin, 1988; Hohenberg and Halperin, 1977).

The time evolution of cluster size distributions can be generally divided into three typical stages: nucleation, early stage growth and late stage growth (Zinke-Allmang, Feldman and Grabow, 1992). Schematics of these stages are shown in Fig. 6.1. Nucleation can be regarded as a phase transition process from an initial single phase, which could be a dense adatom phase, into a two-phase coexistence regime. The transition can be driven by a quench (isoconcentration) or deposition at a constant temperature (isothermal), both of which can lead to a non-equilibrium supersaturation in which the single dense adatom phase is no longer stable. The nucleation rate can be predicted

by various models based on classical thermodynamics (Frenkel, 1924; Becker and Döring, 1935), atomistic quantities (Walton, 1962; Binder and Stauffer, 1976) and kinetic rate equations (Zinsmeister, 1966). After the formation of the first stable nuclei, the clusters then grow by diffusively capturing adatoms from the supersaturated adatom phase (Zinke-Allmang, Feldman and Grabow, 1992), thereby reducing the initial supersaturation. This is termed as early stage growth.

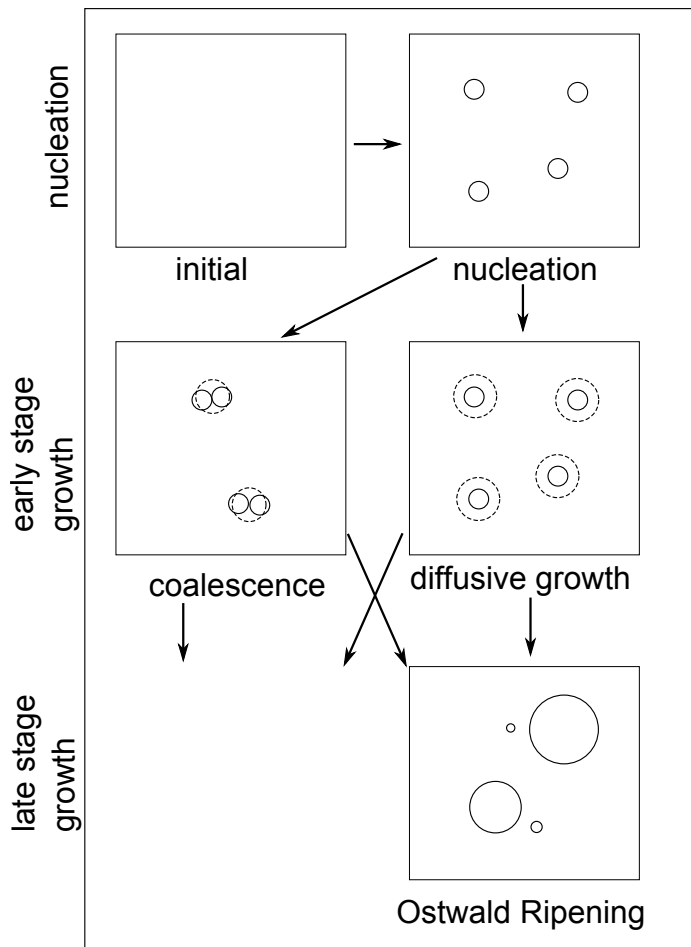


Figure 6.1: Schematic of the different stages of cluster evolution (Zinke-Allmang, Feldman and Grabow, 1992).

When the adatom supersaturation approaches its equilibrium value, a late stage growth phase is approached in which cluster evolution can continue via inter-cluster processes such as Ostwald ripening and coalescence. Ostwald

Ripening is characterized by the growth of larger clusters at the expense of smaller clusters (Zinke-Allmang, Feldman and Grabow, 1992; Lifshitz and Slyozov, 1961; Voorhees, 1985) reflecting the fact that atoms on the surface of a cluster are energetically less stable than those in the interior. The long-time behaviour of ripening systems has been studied by Lifshitz and Slyozov (1961) and Wagner (1961) who showed that the cluster size distribution approaches a time-independent dynamical attractor state which can be evaluated analytically. This universal distribution does not depend on the initial distribution or other initial values if the appropriate-scaled parameters are used (Venzl, 1985). Coalescence is a process whereby two droplets merge into a larger one when they contact each other. Again, this is driven by a minimisation of surface energy and can occur in both early and late stages of growth.

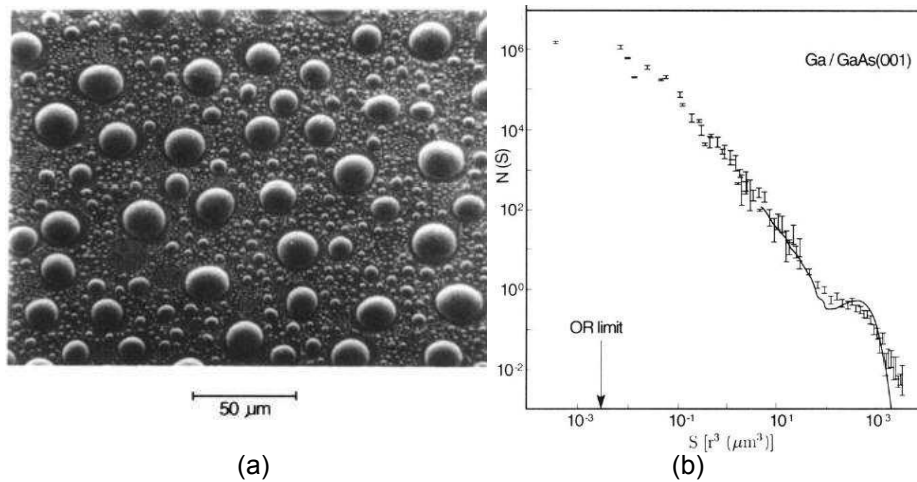


Figure 6.2: (a) Large-area scanning electron microscopy (SEM) image of Ga droplets on GaAs(001) after annealing the clean surface at  $660^\circ\text{C}$  for 5 min (Zinke-Allmang, Feldman and van Saarloos, 1992). (b) Double logarithmic representation of the corresponding droplet size distribution  $N(S)$  as a function of droplet size  $S \propto r^3$  where  $r$  is the droplet radius (Zinke-Allmang, Feldman and van Saarloos, 1992). The solid line is adapted from a computer simulation by Family and Meakin (Family and Meakin, 1988).

Our goal in this thesis is to understand the time-evolution of Ga droplet size distributions prepared by annealing a GaAs substrate above  $T_c$  (see Chapter 4 and 5). This is important for controlling quantum structure size distributions

following subsequent droplet recrystallisation under As flux. The starting point for this work is a previous study by Zinke-Allmang, Feldman and van Saarloos (1992) who measured a late stage Ga droplet size distribution over a large area using *ex situ* scanning electron microscopy (see Fig. 6.2(a)). The size distribution shows an initial power law decay, superimposed on a bell-shaped distribution peak. This was favourably compared with the vapour condensation model of Family and Meakin (1988) (see Fig. 6.2(b)). This is surprising given that the Family Meakin model considers the deposition of droplets of a fixed size, allowing the distribution to evolve via coalescence events. This would seem very different to the late stage processes governing the experimental droplet size distribution.

In Chapter 7 we therefore apply real-time surface electron microscopy to identify the key mechanisms governing the time evolution of the Ga droplet size distribution during Langmuir evaporation of GaAs (001). Surprisingly, new Ga droplets are seen to form in regions cleared by the coalescence of larger droplets. This is clearly different from the standard mechanisms governing cluster size distribution evolution discussed earlier. A simple Monte Carlo model incorporating daughter droplet generation by coalescence is able to reproduce and explain the major features of our experimental droplet size distributions. It is also consistent with the behaviour observed at higher annealing temperatures by Zinke-Allmang *et al.* (Zinke-Allmang, Feldman and van Saarloos, 1992).

---

# Time evolution of the Ga droplet size distribution during Langmuir evaporation of GaAs(001)

This chapter is an author generated post print of the article

Z. Y. Zhou, W. X. Tang, D. E. Jesson, and J. Tersoff, 'Time evolution of the Ga droplet size distribution during Langmuir evaporation of GaAs(001)', *Applied Physics Letters*, **97**, 191914(2010), available electronically at

[http://apl.aip.org/resource/1/applab/v97/i19/p191914\\_s1](http://apl.aip.org/resource/1/applab/v97/i19/p191914_s1)

or via doi:10.1063/1.3515925.

**Declaration for Thesis Chapter “Time evolution of the Ga droplet size distribution during Langmuir evaporation of GaAs(001)”**

Declaration by candidate

For this chapter, the nature and extent of my contribution to the work was the following:

Nature of contribution	Extent of contribution(%)
Developed the model used in the paper, performed the Monte Carlo simulation and analysis, co-wrote the paper.	70

The following co-authors contributed to the work. Co-authors who are students at Monash University must also indicate the extent of their contribution in percentage terms

Name	Extent of contribution(%)	Nature of contribution
Wen-XinTang		Provided experimental images and technical expertise.
David Jesson		Co-wrote the paper, helped develop the model and provided technical expertise.
Jerry Tersoff		Co-wrote the paper, helped develop the model.

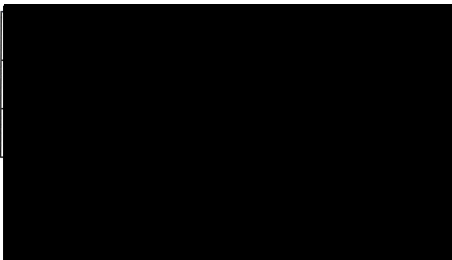
Candidate's signature		Date	17/08/2012
-----------------------	---	------	------------

**Declaration by co-authors**

The undersigned hereby certify that:

- (1) they meet the criteria for authorship in that they have participated in the conception, execution, or interpretation, of at least that part of the publication in their field of expertise;
- (2) they take public responsibility for their part of the publication, except for the responsible author who accepts overall responsibility for the publication;
- (3) there are no other authors of the publication according to these criteria;
- (4) potential conflicts of interest have been disclosed to (a) granting bodies, (b) the editor or publisher of journals or other publications, and (c) the head of the responsible academic unit; and
- (5) the original data are stored at the following location(s) and will be held for at least five years from the date indicated below:

Location(s)	School of Physics, Monash University, Clayton
-------------	---

Signature 1		Date	16-08-12
Signature 2			16-08-12
Signature 3			17/08/2012

# Time evolution of the Ga droplet size distribution during Langmuir evaporation of GaAs(001)

Z. Y. Zhou, W. X. Tang, D. E. Jesson\*

*School of Physics, Monash University, Victoria 3800, Australia*

J. Tersoff

*IBM Research Division, Thomas J. Watson Research Center,  
Yorktown, Heights, New York 10598, USA*

## Abstract

The time evolution of the Ga droplet size distribution is measured by *in situ* surface electron microscopy during Langmuir evaporation of GaAs. With a minimum of complexity, we are able to reproduce and explain the major features of the droplet size distribution by a simple Monte Carlo model. Guided by experiment, the model includes droplet formation in response to coalescence events.

PACS numbers: 02.70.Tt, 64.70.fm, 68.37.Nq, 68.47.Fg, 68.55.ag

---

\* 

During high temperature annealing of GaAs (001), As preferentially evaporates from the surface leaving behind Ga-rich liquid droplets[1–7]. There are both fundamental[3] and potential technological interest in the droplet size distributions since Ga droplets can be transformed into GaAs quantum structures of various types under As flux[8]. Until recently, however, the study of the droplet size distribution has been restricted to *ex situ* snapshots of quenched samples obtained at particular times[3, 4]. Here we apply *in situ* surface electron microscopy to study the in real-time evolution of the droplet size distribution. We find that the generation of new Ga droplets is highly non-uniform in space and time, with small daughter droplets forming in regions cleared by the coalescence of larger parent droplets[7]. These insights are used as a basis of a simple Monte Carlo (MC) model of droplet evolution. This is able to reproduce and explain the major features of our experimental droplet size distributions as well as the different behavior observed at higher annealing temperatures[3].

In Fig. 1(a) we display a photoemission electron microscopy (PEEM) image captured from a movie of GaAs(001) Langmuir decomposition at 630°C. The corresponding size distribution for 338 droplets was measured using particle counting software and is shown Fig. 1(b). The droplets number  $N(S)$  per  $\mu m^2$  is plotted as a function of scaled droplet size  $S = r^3$ , where  $r$  is the droplet radius in two-dimensional projection. Although the statistics are insufficient to fully quantify the size distributions, several qualitative features are clearly evident. In particular, the size-distribution curve can be partitioned into three distinct regimes; a build-up regime I, a fall-off regime II and a pile-up regime III. The reasons for the use of this nomenclature will become clear later. The evolution of the size distribution over time is shown in Fig. 2.

The size distribution in Fig. 1 (b) can be directly compared with the classic study of Zinke-Allmang *et al.*[3](ZA) who measured a late stage Ga

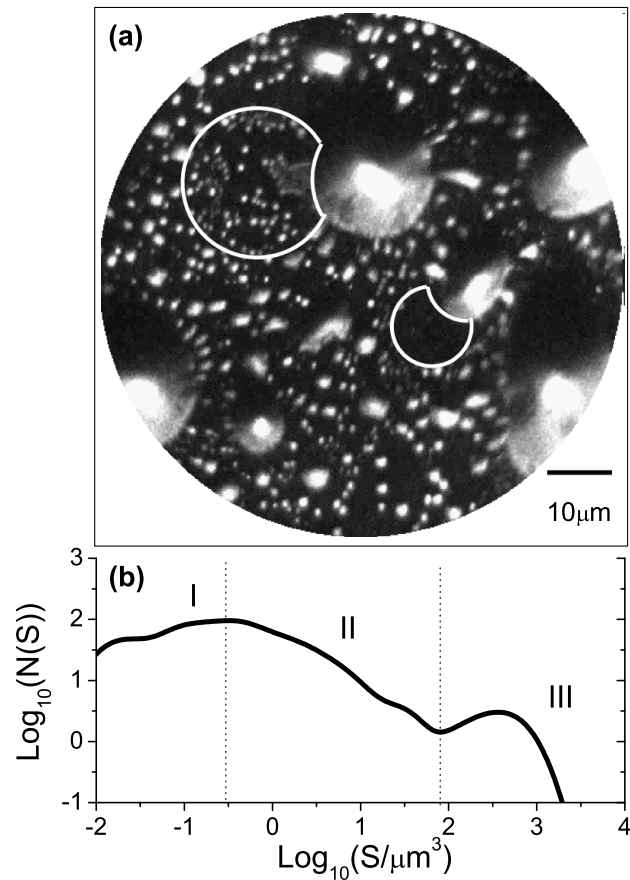


FIG. 1. (a) PEEM image captured from a movie of GaAs(001) Langmuir decomposition at 630°C. Due to relative work functions, liquid Ga appears bright against dark GaAs, providing excellent contrast. Areas recently vacated by droplets that have coalesced with neighbouring droplets are indicated by white borders. These are associated with bursts of daughter droplet nucleation. (b) Corresponding size distribution of the droplets. The droplet number  $N(S)$  per  $\mu\text{m}^2$  is plotted as a function of scaled droplet size  $S = r^3$ , where  $r$  is the plan-view droplet radius. Gaussian smoothing of  $N(\log_{10} S)$  with standard deviation  $8 \times 10^{-3}$  has been applied. A build-up regime I, fall-off regime II and a pile-up regime III are identified.

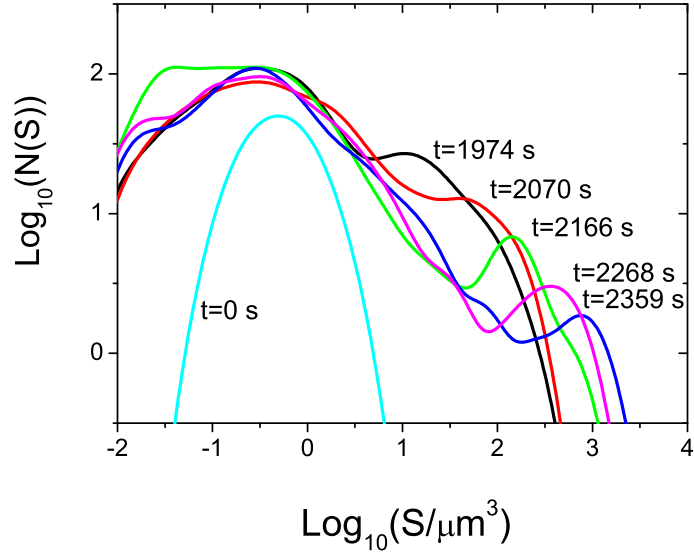


FIG. 2. (Color online) Time evolution of the droplet size distribution measured by PEEM. The initial  $t = 0$  distribution corresponds to a time before the onset of coalescence, when the size distribution is rather uniform and the width here is dominated by our Gaussian smoothing of  $N(\log_{10} S)$  with standard deviation  $8 \times 10^{-3}$ .

droplet size distribution over a large area using *ex situ* scanning electron microscopy. Regimes II and III are readily identified in both sets of data. The slope of regime II in our PEEM data is, however, much smaller than the value measured by ZA. Since this slope can be associated with the basic mechanisms governing the size distribution evolution[3], it is important to understand this difference.

Our *in situ* PEEM experiments reveal that droplet formation is highly non-uniform and linked to droplet coalescence. When two growing droplets touch, they coalesce by displacement of the smaller droplet, which exposes an etch pit[4]. Within less than a second, multiple Ga daughter droplets of

a similar size form within the pit[7]. Such vacated regions are outlined in Fig. 1(a) by white borders. These bursts of daughter droplet nucleation are attributed to the excess surface Ga generated by evaporation of steps associated with etch pits on exposure to vacuum[7]. This is the key mechanism controlling Ga droplet generation which we therefore incorporate directly in a simple MC model for the evolution of the droplet size distribution.

We begin with an initial array of droplets of fixed size  $r_I$  and density  $\rho_I$  which are randomly distributed across the surface. This is a good approximation to the experimentally observed initial distribution and the main features of the simulated distributions at later times were found to be insensitive to these initial conditions. The surface is assumed to supply Ga at a fixed volume rate of  $R_{Ga}$  per unit area as As evaporates. We take as our unit of time  $\beta(1\mu m)/R_{Ga}$  where  $\beta S$  is the droplet volume. Experimentally, to a good approximation, droplets are observed to grow by capturing this Ga with a rate proportional to their radius (see also ref. 9), so  $dS/dt = AR_{Ga}S^{1/3}/(\beta \sum_i S_i^{1/3})$  where the sum is over all droplets in area  $A$ . When two droplets touch we allow them to coalesce with the resulting centre of mass located at the projected centre of the larger of the two droplets. Daughter droplet generation is mimicked by randomly populating the area vacated by the coalescence event with droplets of a fixed radius  $r_D$  and density  $\rho_D$ . Periodic boundary conditions are assumed throughout. For simplicity, we ignore the motion of droplets[6] which we expect will not have a significant influence on the final size distribution. Simulation parameters are chosen to be consistent with our PEEM videos[10].

Three stages of the calculated droplet evolution are shown in panels (a)-(c) of Fig. 3. The evolution of the size distribution with time is shown in Fig. 4, which includes the times shown in Fig. 3(b) and (c). The simulation qualitatively reproduces all three regimes contained in the experimental data. With the aid of the MC simulations, we now consider the physical

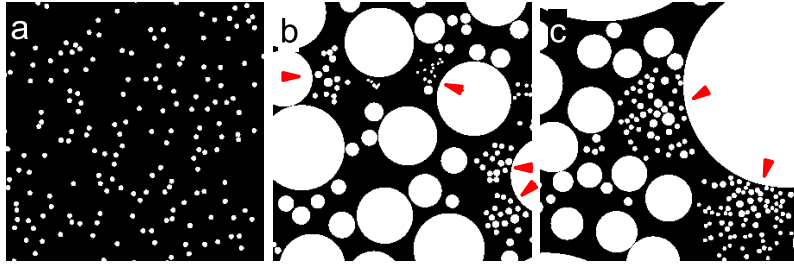


FIG. 3. (Color online) Snapshots of the evolving droplet distribution at three stages of our MC simulation. (a)  $t = 0$  (b)  $t = 200$  (c)  $t = 700$ . Solid arrows in (b) and (c) indicate areas recently vacated by coalescence events. Each panel is  $60\mu m$  across. Units of time are  $\beta(1\mu m)/R_{Ga}$ .

origin of these features.

Correlating the real-space simulations (Fig. 3) with the time evolution of size-distribution curves (Fig. 4) it is possible to associate build-up regime I with bursts of daughter droplet nucleation in areas recently vacated by coalescence events. These are indicated by solid arrows in Fig. 3(b) and (c). We specify the density at which daughter droplets nucleate, so the number is proportional to the area cleared by coalescence. The number of Ga droplets generated per unit time is therefore limited by the frequency of coalescence events involving relatively large 'parent' droplets. This explains the comparatively low number of very small sized droplets in the distribution curves. Once generated, these droplets rapidly increase in size by growth and coalescence, which is the origin of build-up regime I in the size distributions.

We next consider the peak associated with pile-up regime III. The surprising and important point that the distribution is bimodal due to the presence of this second peak has already been emphasized by ZA. To understand its origin we have recorded the age  $t_A$  of each droplet in the MC

simulation. When two droplets coalesce, the combination is assigned the age of the elder droplet. We plot droplet radius against age for two different times in Fig. 5. The ages range from young daughter droplets formed following recent coalescence events, to old droplets contained in the original starting distribution at  $t = 0$ . The distribution forms a smooth curve, except for pile-ups at the oldest age. The pile-ups become taller with increased evolution time, but the curves corresponding to the smaller droplets near the origin do not change much. This clearly demonstrates that the peak in regime III consists of the oldest droplets present before the onset of coalescence. We have confirmed this experimentally by monitoring the time evolution of specific droplets in the PEEM movie.

The size distribution fall-off with increasing droplet size (regime II) reflects the growth and coalescence of droplets with time for a given supply of daughter droplets. Fig. 5 indicates that all droplets in this regime evolve from daughter droplets. As discussed earlier, this regime has been studied in detail by ZA who were able to obtain sufficient statistics to establish a late stage scaling behaviour. Their power-law decay of  $N(S)$  was well-fitted by  $S^{-\theta}$  for  $\theta = 1.6 \pm 0.1$ , in good agreement with the value of  $5/3$  predicted by the geometrical deposition model of Family and Meakin[11]. Although our statistics are insufficient to address scaling, the slope of regime II in both Fig. 2 and 4 is clearly much smaller than the  $5/3$  of ZA.

To reconcile the difference in slope as well as the absence of regime I in the ZA data, we note that their experiments were conducted at substantially higher temperatures than ours ( $> 660^\circ\text{C}$ ). To plausibly account for the effects of temperature we imagine that Ga is released at a fixed rate on all bare regions of surface, and is then free to diffuse to nearby droplets, with some finite diffusivity. One would anticipate a larger activation energy for decomposition via As evaporation than for the subsequent Ga diffusion. The Ga release rate  $R$  should therefore increase much faster than

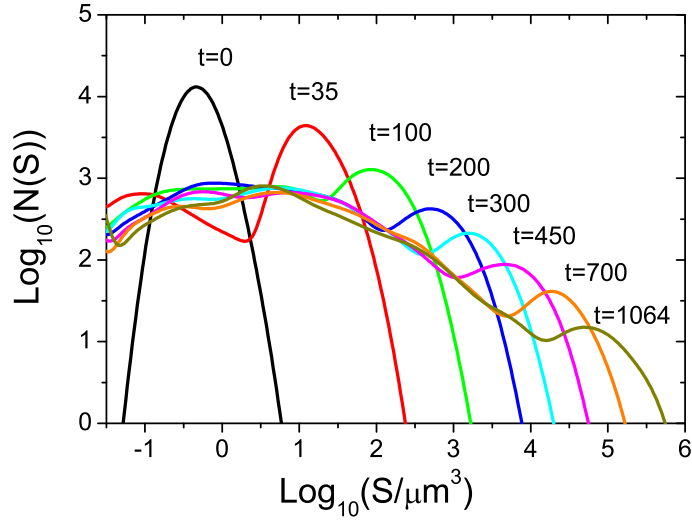


FIG. 4. (Color online) Ga droplet size distribution at various evolution times  $t$  of our MC simulation. Real space snapshots corresponding to distributions at  $t = 200$  and  $t = 700$  are shown in Fig. 3(b)-(c) respectively. Units of time are  $\beta(1\mu m)/R_{Ga}$ . The measurements are averaged over 10 simulations consisting of 1874 droplets randomly arranged in the starting distribution. Gaussian smoothing of  $N(\log_{10} S)$  with standard deviation  $4 \times 10^{-3}$  has been applied. Note that the initial  $t = 0$  distribution is really a delta function and gives a visual picture of the smoothing width.

the diffusivity with increasing  $T$ , decreasing the diffusion length  $l$ . Then in bare regions of size much greater than  $l$  there would be nucleation of new droplets. For low  $T$ ,  $l$  is larger than the distance between droplets, so there is no nucleation except in freshly exposed etch pits, where  $R$  is briefly much larger than elsewhere[7].

To explore this further in our MC calculations we have added an additional flux  $F$  of small droplets to bare regions of the surface to account

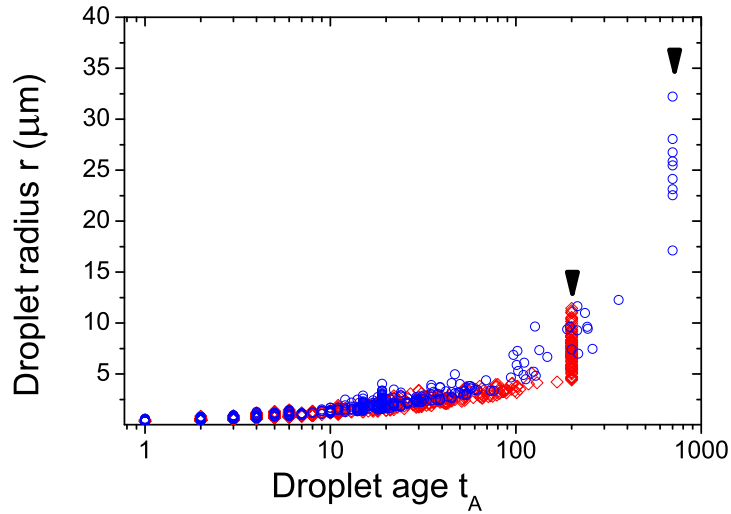


FIG. 5. (Color online) Droplet radius  $r$  plotted against age  $t_A$ . Open diamonds and circles correspond to evolution times  $t = 200$  and  $t = 700$  respectively. Vertical pileups occur for the oldest droplets as indicated by the solid arrows. Units of time are  $\beta(1\mu m)/R_{Ga}$ .

for nucleation. At high temperatures Ga is released too rapidly during evaporation to diffuse far because of increased nucleation. This is modelled by large  $F$ . The lower temperature limit is approximated by our existing simulations for zero  $F$ . MC calculations (not shown) indicate that continually increasing  $F$  increases the slope of region II to  $5/3$  and beyond. It also flattens regime I, compressing the range of droplet sizes over which the initial rise occurs that is consistent with the absence of a clear regime I in the ZA data. This can be attributed to a large  $F$  compared with growth rate of droplets by adatom capture, confining the build up to essentially the smallest droplets.

We are grateful to Rod Mackie for technical support. D.E.J and W.X.T.

acknowledge support from the ARC (Grant No. DP0985290).

- 
- [1] C. Foxon, J. A. Harvey, and B. A. Joyce, *J. Phys. Chem. Solids* **34**, 1693 (1973).
  - [2] J. Y. Tsao, *Materials Fundamentals of Molecular Beam Epitaxy* (Academic, San Diego 1993).
  - [3] M. Zinke-Allmang, L. C. Feldman, and W. van Saarloos, *Phys. Rev. Lett.* **68**, 2358 (1992).
  - [4] T. D. Lowes and M. Zinke-Allmang, *J. Appl. Phys.* **73**, 4937 (1993).
  - [5] C. Chatillon and D. Chatain, *J. Cryst. Growth* **151**, 91 (1995).
  - [6] J. Tersoff, D. E. Jesson, and W. X. Tang, *Science* **324**, 236 (2009).
  - [7] J. Tersoff, D. E. Jesson, and W. X. Tang, *Phys. Rev. Lett.* **105**, 035702 (2010).
  - [8] See for example: T. Mano and N. Koguchi, *J. Cryst Growth.* **278**, 108 (2005); T. Mano, T. Kuroda, S. Sanguinetti, T. Ochiai, T. Tateno, J. Kim, T. Noda, M. Kawabe, K. Sakoda, G. Kido, and N. Koguchi, *Nano Lett.* **5**, 425 (2005); C. Somaschini, S. Bietti, N. Koguchi, and S. Sanguinetti, *Nano Lett.* **9**, 3419 (2009)
  - [9] Z. Y. Zhou, C. X. Zheng, W. X. Tang, D. E. Jesson, and J. Tersoff, *Appl. Phys. Lett.* **97**, 121912 (2010).
  - [10] Simulation parameters:  $r_I = 0.6\mu m$ ,  $r_D = 0.2\mu m$ ,  $\rho_I = 4.69 \times 10^{-2}\mu m^{-2}$ ,  $\rho_D = 8\rho_I$  and  $\beta/R_{Ga} = 2.67 \times 10^{-2}\mu m^{-1}s$
  - [11] F. Family and P. Meakin, *Phys. Rev. Lett.* **61**, 428 (1988).

---

# Dynamic observation and modelling of nanoscale ring formation during droplet epitaxy

This chapter is an author generated pre print of the article

Z. Y. Zhou, C. X. Zheng, W. X. Tang and D. E. Jesson, 'Dynamic Observation and Modelling of Nanoscale Ring Formation during Droplet Epitaxy', which will be submitted to *Nano Letter*.

### Declaration for Thesis Chapter “Dynamic Observation and Modelling of Nanoscale Ring Formation during Droplet Epitaxy”

Declaration by candidate

For this chapter, the nature and extent of my contribution to the work was the following:

Nature of contribution	Extent of contribution(%)
Designed the experiments, co-performed the experiments, co-developed the model used in the paper, designed and ran the simulation, co-wrote the paper.	65

The following co-authors contributed to the work. Co-authors who are students at Monash University must also indicate the extent of their contribution in percentage terms

Name	Extent of contribution(%)	Nature of contribution
Changxi Zheng	15	Co-performed the experiments, provided the data for the pre-existing inner ring.
Wen-XinTang		Helped perform the experiments and provided technical expertise.
David Jesson		Co-wrote the paper, helped developed the model and provided technical expertise.

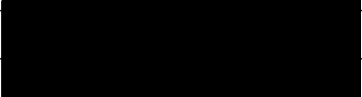
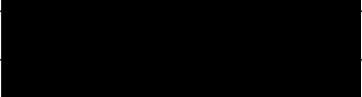
Candidate's signature		Date	17/08/2012
-----------------------	--	------	------------

**Declaration by co-authors**

The undersigned hereby certify that:

- (1) they meet the criteria for authorship in that they have participated in the conception, execution, or interpretation, of at least that part of the publication in their field of expertise;
- (2) they take public responsibility for their part of the publication, except for the responsible author who accepts overall responsibility for the publication;
- (3) there are no other authors of the publication according to these criteria;
- (4) potential conflicts of interest have been disclosed to (a) granting bodies, (b) the editor or publisher of journals or other publications, and (c) the head of the responsible academic unit; and
- (5) the original data are stored at the following location(s) and will be held for at least five years from the date indicated below:

Location(s)	School of Physics, Monash University, Clayton
-------------	---

Signature 1		Date	16-08-12
Signature 2			16-08-12
Signature 3			16-08-12

# Dynamic Observation and Modelling of Nanoscale Ring Formation during Droplet Epitaxy

Z. Y. Zhou, C. X. Zheng, W. X. Tang, and D. E. Jesson\*

*School of Physics, Monash University, Victoria 3800, Australia*

## Abstract

Droplet epitaxy of GaAs is studied in real-time using *in situ* surface electron microscopy which provides new insights into the dynamics of Ga droplet crystallisation under As flux. The resulting movies are used as the basis of a theoretical model for quantum ring formation which can qualitatively explain the origin of quantum features observed under a variety of experimental conditions. The model predicts that Ga adatom diffusion, under differing conditions of temperature and As flux, chiefly controls the quantum structure morphology.

---

\* 

Self-assembled semiconductor nanostructures are the subject of intense interest because of their potential use in quantum information technologies and nanoscale optoelectronics [1–4]. The goal is to create designer quantum structures such as dots, double-dots, rings, multi-rings or molecules where electronic and optical properties are controlled by their size, shape, strain and composition. Droplet epitaxy has recently emerged as a flexible technique for tailoring these parameters [3, 5–11]. This method of epitaxy consists of two main stages. First, liquid Ga or In droplets are deposited on the GaAs surface. This is followed by crystallisation and subsequent transformation into quantum structures under As flux. Droplet epitaxial formation of quantum-like structures including quantum double-dots [5], molecules [6], rings [7] and double-rings [8, 9] has now been demonstrated with potential applications including novel lasers, electron spin memory and quantum computing.

Until recently, however, the study of droplet epitaxy has been restricted to *ex situ* snapshots of quenched samples obtained at particular times using scanning electron microscopy (SEM) or atomic force microscopy (AFM). While providing valuable information, the time evolution of droplet crystallisation must be inferred. In this study we apply *in situ* surface electron microscopy to study the crystallisation of a model Ga droplet into GaAs in real-time under As flux. From the resulting movies, the key elements of droplet crystallisation are identified in space and time. These observations are used as the basis for a simple model for droplet epitaxy which can qualitatively describe a wide range of experimentally observed features including single, double, multi-ring and disk-like nanostructures.

Dynamic observations were performed in a low energy electron microscope (LEEM) specially designed for III-V epitaxy [12]. An undoped GaAs (001) $\pm 0.1^\circ$  epi-ready wafer was degassed at 300 °C at ultrahigh vacuum for 24 hours. This was followed by high temperature flashing up to 600

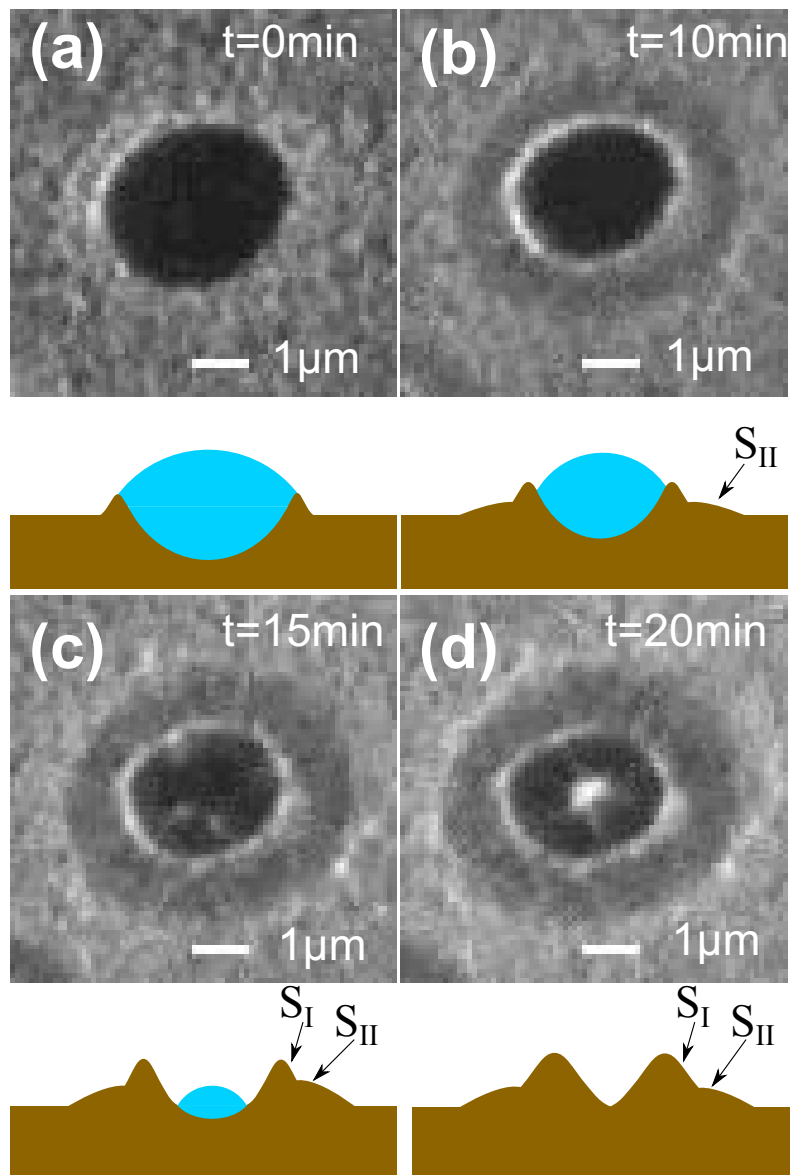


FIG. 1. (Colour online) Images taken from a MEM movie of Ga droplet crystallisation into GaAs during droplet epitaxy (see supplementary information II). A schematic of the droplet/ring morphology is shown beneath each image. (a) Ga droplet before adding As flux. (b) Under As flux a skirt, or disk-like structure,  $S_{II}$  forms outside the droplet periphery. (c) The Ga droplet shrinks, revealing an inner ring structure  $S_I$  at the original position of the droplet contact-line. (d) Final crystallised GaAs ring structure.

°C and annealing at 580 °C for 2 hours to remove the surface oxide. Model droplets for our crystallisation studies (radii  $\sim 1\mu\text{m}$ ) were prepared by annealing above the congruent evaporation temperature at 650 °C. The sample temperature was reduced to 460 °C and images were recorded in mirror electron microscopy (MEM) mode [13, 14], which is ideally suited to imaging real-time changes in surface morphology. Droplets appear in MEM as a uniform dark disc, somewhat larger than the actual droplet, surrounded by a concentric bright ring as in Figure 1a [14–17].

On opening the As shutter at  $t = 0$  min, the droplet was subjected to an  $\text{As}_4$  flux of beam equivalent pressure (BEP)  $1.45 \times 10^{-5}$  Torr. A skirt or disk-like structure ( $S_{II}$ ) is visible outside of the droplet perimeter after a few seconds and gradually increases in thickness (Figure 1b). The droplet gradually shrinks and a central ring structure ( $S_I$ ) begins to form at the original position of the droplet contact-line (Figure 1c). Finally, the droplet completely disappears leaving behind a central bright spot (Figure 1d) which corresponds to a central pit according to MEM imaging theory [14]. Schematics of the surface morphology are shown beneath each MEM image with the features derived from caustic imaging theory [14] (see also section 2.1.2). This general interpretation of the movie was confirmed by separately imaging various quenched droplet crystallisation morphologies using both MEM and AFM. The crystallised structure in Figure 1d can therefore be categorized as a double-ring morphology with  $S_{II}$  displaying disk-like character (see for example [3, 9])

The MEM movie in Figure 1 provides several important insights into the dynamics of Ga droplet crystallisation under As flux which can be used to evaluate existing theoretical description of droplet epitaxy. First, the movie directly confirms that the outer skirt structure  $S_{II}$  forms well outside the droplet perimeter over an extended region at the onset of  $\text{As}_4$  deposition. This rules out the possibility of localized nucleation as the

origin of the outer ring as proposed in the thermodynamic model of Li and Yang [18]. It is also inconsistent with a second growth kinetics model proposed by the same authors [19, 20] which predicts that outer rings should form discretely at the outer edge of the skirt. In fact, the skirt evolves continuously over an extended region with fixed outer radius. The possibility that quantum rings can arise from the morphological instability of droplets has also been considered by Blossey and Yorke [21] but our movie reveals that the outer skirt  $S_{II}$  is not directly linked to shape changes of the droplet during crystallisation. Rather, our observations suggest that  $S_{II}$  is linked to the reaction of Ga adatoms and As surface species over an extended reaction-diffusion zone.

A second key observation from the movie is that the inner structure  $S_I$  is associated with the original position of the droplet contact-line. To explore the geometry of the contact-line further, droplets were prepared by annealing at 650 °C in the LEEM and then quenched to room temperature and imaged *ex situ* by AFM in non-contact mode (Figure 2a). To characterise the morphology of the liquid-solid interface, the Ga droplets were selectively etched away using 10 mol/L NaOH solution at 50 °C which preserved the GaAs surface. The sample was then reimaged by AFM revealing the droplet etch pit (Figure 2b) which results from the etching of the GaAs surface by the droplet at 650 °C [22–25]. A line trace across the etch pit, shown in panel (c), clearly identifies a ridge which forms a rim around the etch pit. This appears similar in form to the ridge observed by Somaschini *et al.* [11] who identified that quantum structure inner-rings pre-exist before As deposition. The existence of such rings is consistent with mass transport at the liquid Ga/solid GaAs contact line to achieve exact balance of the surface tensions [22]. It is therefore clear that the role of pre-existing ridges must be considered in any model of quantum ring formation.

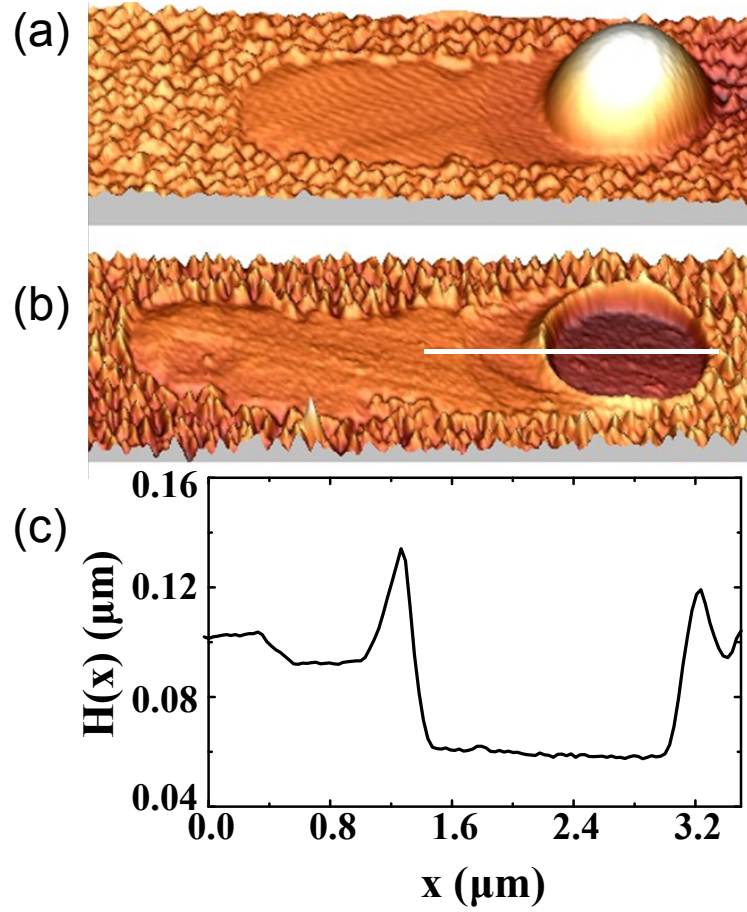


FIG. 2. (Colour online) AFM images of a Ga droplet morphology (a) before and (b) following selective etching of Ga [22] (a) A Ga droplet has left behind a smooth trail on the slightly rough epi-ready wafer surface. (b) An inner GaAs ring is revealed at the position of the original droplet contact-line. (c) Cross-sectional measurement of the height of the inner ring  $H(x)$  as a function of lateral distance  $x$  obtained from the scan-line in (b).

Based on the above experimental observations we seek the simplest model which encapsulates the major features of quantum structure formation. By analogy with skirt formation in the MEM movie we consider all outer quantum ring structures to be associated with the reaction of Ga adatoms and As surface species over an extended region. To model this, consider

a random array of droplets of radius  $r_D(t)$  at time  $t$  with typical nearest neighbour distance  $2L$ . We define As and Ga concentrations as  $C_{As}(r)$  and  $C_{Ga}(r)$  respectively and we assume Ga evaporation is negligible for the low temperatures associated with droplet epitaxy. Assuming radial symmetry we can then write the steady state diffusion equation for the Ga concentration outside the droplet as,

$$D_{Ga} \left( \frac{1}{r} \frac{dC_{Ga}}{dr} + \frac{d^2 C_{Ga}}{dr^2} \right) - k_r C_{Ga} C_{As} = 0, \quad (1)$$

where  $k_r$  is a reaction rate constant governing the reaction between As and Ga to form GaAs solid.  $D_{Ga}$  is the Ga diffusion coefficient. For As we also have an evaporation term  $C_{As}/\tau_{As}$  with evaporation lifetime  $\tau_{As}$  and a deposition flux  $F_{As}$ :

$$D_{As} \left( \frac{1}{r} \frac{dC_{As}}{dr} + \frac{d^2 C_{As}}{dr^2} \right) + F_{As} - \frac{C_{As}}{\tau_{As}} - k_r C_{Ga} C_{As} = 0. \quad (2)$$

We consider radial symmetry as a reasonable approximation by imposing the boundary condition:

$$\frac{dC_{Ga}}{dr} = \frac{dC_{As}}{dr} = 0 \quad \text{at} \quad r = L, \quad (3)$$

since the concentration is symmetric halfway between the droplets. In addition we assume that the Ga and As adatom concentrations at the droplet edge are in equilibrium with the liquid so that

$$C_{Ga} = C_{Ga}^0 \quad \text{at} \quad r = r_D(t), \quad (4)$$

$$C_{As} = C_{As}^0 \approx 0 \quad \text{at} \quad r = r_D(t). \quad (5)$$

This comes from assuming diffusion limited behaviour rather than attachment limited behaviour in the low temperature regime associated with droplet epitaxy.

Figure 3a contains typical Ga and As concentration profiles obtained by solving eqs (1) and (2) with boundary conditions (3) - (5) (see supplementary information I for details). It can be seen that the reaction of Ga and

As leads to a decreasing Ga concentration away from the droplet and a decreasing As concentration towards the droplet. Consequently, the crystallisation rate of GaAs ( $k_r C_{Ga} C_{As}$ ) has a maximum at a distance away from the droplet. This peak, in an extended reaction-diffusion zone, is therefore the basic physical origin of outer quantum rings.

To fully describe the outer ring structure, however, we note from the MEM movie that the droplet continually shrinks during the crystallisation process. The outer ring structure height profile  $h_0(r, t)$  is therefore the time-integration of the GaAs crystallisation rate from the initial droplet state at  $t = 0$ , when As deposition commences, until time  $t$ . We can then write,

$$h_0(r, t) \propto k_r \int_0^t C_{Ga}(r, r_D(t')) C_{As}(r, r_D(t')) dt', \quad (6)$$

where the rate of droplet shrinkage at time  $t'$  can be evaluated from the rate of loss of Ga atoms from the droplet,

$$J_D(t') = 2\pi r_D(t') D_{Ga} \left. \frac{dC_{Ga}}{dr} \right|_{r_D(t')}. \quad (7)$$

With  $r_D(t')$  from (7),  $h_0(r, t)$  can then be numerically evaluated from (6). If the droplet disappears at time  $t_0$ , when  $r_D(t_0) = 0$ , the final height profile is given by  $h_0(r, t_0)$ . However, to obtain the final quantum structure profile we must also incorporate the inner ring ridge. The simplest approximation is to add the ridge profile to  $h_0(r, t_0)$ , assuming that the quantum structure dynamical evolution is chiefly governed by reaction-diffusion. This is consistent with the observations of Somanchini *et al.* [11] who assign the origin of the inner ring solely to the pre-existing ridge which is present before deposition.

We now examine the time-evolution of a quantum structure height profile for a typical set of parameters (see supplementary information I). Figure 3b-e show calculated values of  $h_0(r, t)$  at various stages of evolution. The light (blue) shaded regions represent liquid Ga and the darker regions solid

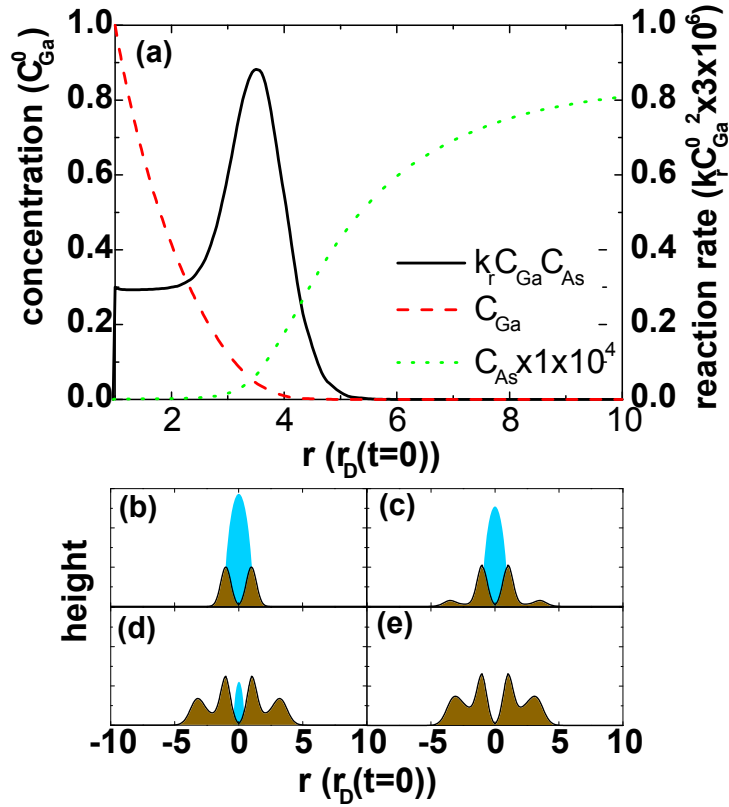


FIG. 3. (Colour online) Typical Ga and As concentration profiles and their resulting reaction rate which is peaked away from the droplet periphery. The time-evolution of the GaAs recrystallisation rate  $h_0(r, t)$  is evaluated in (b)-(e) using Eqs (6) and (7). Light (blue) and dark (brown) shaded regions represent the droplet and crystallised GaAs, respectively. The vertical scale is expanded to highlight ring formation. In (b), the initial inner ring is represented by a Gaussian peak (see text)) and this is added to the  $h_0(r, t)$  integration in (c)-(e). All heights are rescaled to show the qualitative shape. The As flux  $F_{\text{As}} = F_0$  (See supplementary information I).

GaAs. The vertical height scale is exaggerated to emphasise ring formation. In Figure 3b, the initial state consists of the droplet and inner ridge associated with the contact-line. The inner ridge is approximated by a

Gaussian profile with relative dimensions consistent with the observations of Somanchini *et al.* [11]. It can be seen that GaAs crystallisation, of the form shown in Figure 3a, gradually establishes an outer ring as the droplet shrinks in Figure 3b-e. When combined with the pre-existing inner ridge this can physically explain the origin of double-ring structures as evident in Figure 3e. Note that the outer ring structure does not expand during the time integration, consistent with the behaviour of the outer skirt in the MEM movie (Figure 1). This can be explained by the GaAs recrystallisation rate being much smaller than the droplet shrinking rate.

It is well appreciated that different types of quantum structures can be obtained by adjusting the growth temperature and/or As BEP (see for example, [3, 5–11]). A particularly elegant investigation of multi-ring structure geometry has been performed by Somanchini *et al.* [9] who carefully catalogued ring morphology while independently varying  $T$  and  $F_{As}$ . The left column of Figure 4 reproduces AFM line traces from this work and we now explore whether our simple model can qualitatively explain the main features of this data. Note that several parameters in the model are associated with an Arrhenius temperature dependence and so to rationalise the  $T$ -dependence we first seek to identify the dominant quantity which can act as a 'proxy' for  $T$ . In this manner, we might gain insight into the key factors controlling quantum ring formation.

Trial calculations using Eqs (3)-(7) show that the reaction constant  $k_r$  chiefly effects the sharpness of the outer ring but has little influence on its radius. Likewise, the equilibrium concentration  $C_{Ga}^0$  does not shift the ring position significantly for the relevant temperature range (275-350 °C). These parameters are therefore taken to be independent of  $T$  in our model. The As species lifetime  $\tau_{As}$  only influences the equilibrium  $C_{As}(r)$  far away from the droplet whereas, close to the droplet,  $C_{Ga}(r)$  is large and dominates the local form of  $C_{As}(r)$  via the reaction term. The effect of  $\tau_{As}$  is

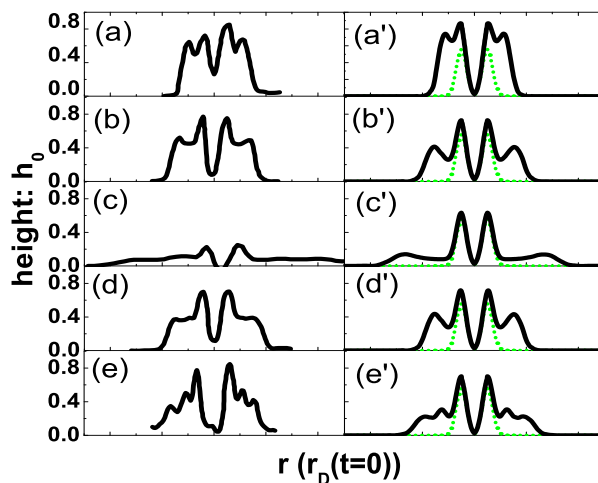


FIG. 4. (Colour online) Left panels; AFM measurements of quantum ring profiles: (a) double ring,  $T=275$  °C,  $\text{BEP} = 4 \times 10^{-7}$  Torr [9]; (b) double ring,  $T=300$  °C,  $\text{BEP} = 4 \times 10^{-7}$  Torr [9]; (c) skirt,  $T=350$  °C,  $\text{BEP} = 4 \times 10^{-7}$  Torr [9]; (d) double ring,  $T=350$  °C,  $\text{BEP} = 8 \times 10^{-6}$  Torr [9]; (e) triple ring, structure first annealed at  $T=250$  °C,  $\text{BEP} = 8 \times 10^{-7}$  Torr for 20 seconds then annealed at  $T=300$  °C,  $\text{BEP} = 8 \times 10^{-7}$  Torr for 2 minutes [11]. Right panels: Corresponding calculations of quantum structure height profiles : (a') double ring,  $T=275$  °C,  $F_{As} = F_0$ ; (b') double ring,  $T=300$  °C,  $F_{As} = F_0$ ; (c') skirt,  $T=350$  °C,  $F_{As} = F_0$ ; (d') double ring,  $T=350$  °C,  $F_{As} = 3F_0$ ; (e') triple ring, first annealed at  $T=270$  °C,  $F_{As} = F_0$  for  $r_D(t) > 0.9r_D(t=0)$  ; then annealed at  $T=320$  °C,  $F_{As} = F_0$  when  $r_D(t) < 0.9r_D(t=0)$  . The dotted line in (a')-(e') is a Gaussian representation of the initial inner ring (see text).

therefore negligible. The two remaining candidates for the proxy are then  $D_{Ga}$  and  $D_{As}$  . It is known that the activation barrier for As surface diffusion is much smaller than the barrier for Ga diffusion (see, for example, [26]). Consequently,  $D_{As}$  varies much more slowly with  $T$  than  $D_{Ga}$  and we assume this variation can also be neglected to first order. We therefore

assign  $D_{Ga}$  as the proxy to understand the  $T$ -dependence with all other  $T$ -dependent parameters held constant.

With this much simplified model, we can evaluate  $h_0(r, t_0)$  for various  $T$  and  $F_{As}$  as shown in the right column of Figure 4. The dashed lines show the position of the inner ridge which is added to  $h_0(r, t_0)$  to obtain the final quantum structure profile. The calculated profiles (Figure 4a'-e') compare favourably with the experimental profiles (Figure 4a-e). At relatively low  $T$ , a quantum double-ring is obtained with the outer ring of small radius (Figure 4a'). The radius of the outer ring becomes larger at intermediate  $T$  (Figure 4b'). At high  $T$  (Figure 4c'), the outer ring broadens into a skirt, in good agreement with experiment. Note that at high  $T$ , the morphology of the exposed inner ring may flatten with time driven by surface energy minimisation which is not included in our model and might explain the lower height profile of the inner ring observed experimentally. At the same  $T$  as Figure 4c', an increase in  $F_{As}$  results in a reduced outer ring radius (Figure 4d'). Finally, a triple-ring structure is produced by depositing As first at a lower  $T$ , then at a higher  $T$  (Figure 4e'), which is in good agreement with experiment (Figure 4e).

We can now use our model to qualitatively analyse the behaviour of the outer ring in terms of the Ga and As concentration profiles. Figure 5b shows that increasing  $T$  expands  $C_{Ga}$  away from the droplet so that more As atoms are consumed by reaction to form GaAs (Figure 5c) and the outer ring radius increases (Figure 5a). If the temperature is very high, the outer ring radius becomes large and the ring approaches a flat skirt structure (Figure 4c'). In the low  $T$  limit the model predicts the formation of quantum dots rather than rings because Ga diffusion away from the droplet will be negligible, restricting crystallisation to the Ga droplet. Increased  $F_{As}$  enhances  $C_{As}(r)$  (Figure 5f) which reduces  $C_{Ga}(r)$  (Figure 5e) leading to a reduction in outer ring radius (Figure 5d). In the

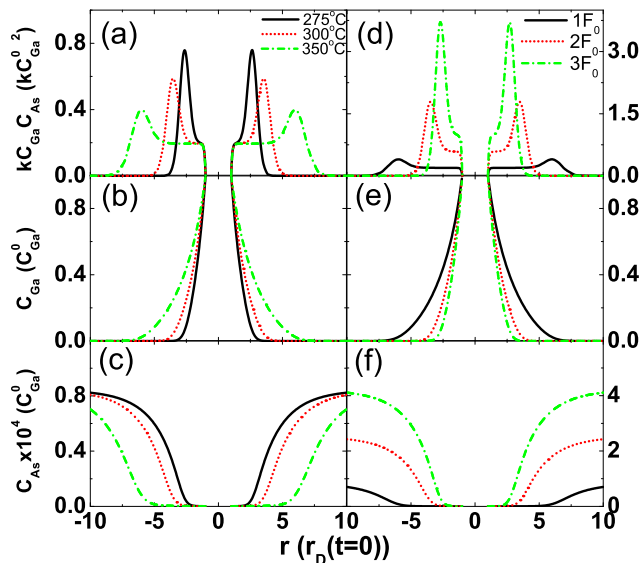


FIG. 5. (Colour online) Temperature variation of (a) reaction rate, (b) Ga concentration and (c) As concentration. As flux variation of (d) reaction rate, (e) Ga concentration and (f) As concentration.

high flux limit, the outer ring will converge with the inner ring, producing a single ring structure, in agreement with experiment [8].

The use of a simple reaction-diffusion model to explain quantum ring formation and general behaviour in terms of surface concentration profiles under different experimental conditions is an important qualitative advance. The model can however be readily extended to incorporate more detailed information. For example, it is thought that spatially variations in surface reconstruction may influence the dynamics of quantum structure formation by changing adatom diffusivities [9, 11]. Such effects can be directly incorporated by suitably modifying Eqs (1) and (2) with appropriate boundary conditions. As more detailed information on the various surface parameters becomes known, it might be hoped that a fully quantitative

reaction-diffusion approach can be developed to model quantum structure evolution and predict and design specific quantum features.

In summary, we have dynamically imaged Ga droplet re-crystallisation into GaAs under As flux using surface electron microscopy. The movies are used to formulate a theoretical model of droplet epitaxy which can qualitatively explain the origin of quantum rings in terms of reacting Ga and As surface species. The model predicts that Ga adatom diffusion, under differing conditions of temperature and As flux, chiefly controls the quantum ring structure.

#### ACKNOWLEDGMENTS

D.E.J. and W.X.T. acknowledge support from the ARC (Grant No. DP120101486).

- 
- [1] D. Bimberg, M. Grundmann, and N. N. Ledentsov, *Quantum Dot Heterostructures*, edited by Wiley (Chichester, 1998).
  - [2] P. Bhattacharya, S. Ghosh, and A. Stiff-Roberts, *Annu. Rev. Mater. Res.* **34**, 1 (2004).
  - [3] J. H. Lee, Z. M. Wang, Z. Y. AbuWaar, and G. J. Salamo, *Crystal Growth & Design* **9**, 715 (2009).
  - [4] B. A. Joyce and D. D. Vvedensky, *Materials Science and Engineering: R* **46**, 127 (2004).
  - [5] M. Yamagiwa, T. Mano, T. Kuroda, T. Tateno, K. Sakoda, G. Kido, N. Koguchi, and F. Minami, *Applied Physics Letters* **89**, 113115 (2006).
  - [6] S. Huang, Z. Niu, Z. Fang, H. Ni, Z. Gong, and J. Xia, *Appl. Phys. Lett.* **89**, 031921 (2006).

- [7] T. Mano and N. Koguchi, *J. Cryst. Growth* **278**, 108 (2005).
- [8] T. Mano, T. Kuroda, S. Sanguinetti, T. Ochiai, T. Tateno, J. Kim, T. Noda, M. Kawabe, K. Sakoda, G. Kido, and N. Koguchi, *Nano Letters* **5**, 425 (2005).
- [9] C. Somaschini, S. Bietti, N. Koguchi, and S. Sanguinetti, *Applied Physics Letters* **97**, 203109 (2010).
- [10] Z. Gong, Z. C. Niu, S. S. Huang, Z. D. Fang, B. Q. Sun, and J. B. Xia, *Applied Physics Letters* **87**, 093116 (2005).
- [11] C. Somaschini, S. Bietti, N. Koguchi, and S. Sanguinetti, *Nano Letters* **9**, 3419 (2009).
- [12] D. E. Jesson and W. X. Tang, in *Surface Electron Microscopy of Ga Droplet Dynamics on GaAs (001)*, edited by A. Méndez-Vilas and J. D. Álvarez (Formatex Research Center (Badajoz, Spain), 2010) Chap. 3, p. 1608.
- [13] S. A. Nepijko, N. N. Sedov, and G. Schönhense, *J. Microsc.* **203**, 269 (2001).
- [14] S. Kennedy, C. Zheng, W. Tang, D. Paganin, and D. Jesson, *Ultramicroscopy* **111**, 356 (2011).
- [15] J. Tersoff, D. E. Jesson, and W. X. Tang, *Science* **324**, 236 (2009).
- [16] J. Tersoff, D. E. Jesson, and W. X. Tang, *Phys. Rev. Lett.* **105**, 035702 (2010).
- [17] S. M. Kennedy, C. X. Zheng, W. X. Tang, D. M. Paganin, and D. E. Jesson, *Proc. Roy. Soc. A* **466**, 2857 (2010).
- [18] X. L. Li and G. W. Yang, *The Journal of Physical Chemistry C* **112**, 7693 (2008).
- [19] X. L. Li and G. W. Yang, *Journal of Applied Physics* **105**, 103507 (2009).
- [20] X. L. Li, *The Journal of Physical Chemistry C* **114**, 15343 (2010).
- [21] R. Blossey and A. Lorke, *Phys. Rev. E* **65**, 021603 (2002).
- [22] C. X. Zheng, W. X. Tang, and D. E. Jesson, *Applied Physics Letters* **100**, 071903 (2012).

- [23] Chatillon and C. Chatain, *J. Cryst. Growth* **151**, 91 (1995).
- [24] M. Zinke-Allmang, L. C. Feldman, and W. van Saarloos, *Phys. Rev. Lett.* **68**, 2358 (1992).
- [25] T. D. Lowes and M. Zinke-Allmang, *Journal of Applied Physics* **73**, 4937 (1993).
- [26] C. T. Foxon and B. A. Joyce, *Surface Science* **50**, 434 (1975).

## Supplementary Information:

### I. Rescaling of the differential equation set:

In cylindrical symmetry, the basic equation set can be written as,

$$D_{Ga} \left( \frac{1}{r} \frac{dC_{Ga}}{dr} + \frac{d^2 C_{Ga}}{dr^2} \right) - k_r C_{Ga} C_{As} = 0, \quad (S1)$$

$$D_{As} \left( \frac{1}{r} \frac{dC_{As}}{dr} + \frac{d^2 C_{As}}{dr^2} \right) + F_{As} - \frac{C_{As}}{\tau_{As}} - k_r C_{Ga} C_{As} = 0. \quad (S2)$$

Rescaling the units,

$$\tilde{r} = \frac{r}{r_0}, \quad \tilde{C}_{Ga} = \frac{C_{Ga}}{C_{Ga}^0}, \quad \tilde{C}_{As} = \frac{C_{As}}{C_{As}^0}, \quad (S3)$$

where  $r_0 = r_D(t=0)$

For convenience we set,

$$C_{Ga}^0 = C_{As}^0 \quad (S4)$$

The equations then become,

$$\frac{1}{\tilde{r}} \frac{d\tilde{C}_{Ga}}{d\tilde{r}} + \frac{d^2 \tilde{C}_{Ga}}{d\tilde{r}^2} - \beta_{Ga} \tilde{C}_{Ga} \tilde{C}_{As} = 0, \quad (S5)$$

$$\frac{1}{\tilde{r}} \frac{d\tilde{C}_{As}}{d\tilde{r}} + \frac{d^2 \tilde{C}_{As}}{d\tilde{r}^2} - \alpha_{As} \tilde{C}_{As} - \beta_{As} \tilde{C}_{Ga} \tilde{C}_{As} + \gamma = 0, \quad (S6)$$

With coefficients,

$$\alpha_{As} = \frac{r_0^2}{D_{As} \tau_{As}}, \quad \beta_{Ga} = \frac{k_r r_0^2 C_{Ga}^0}{D_{Ga}}, \quad \beta_{As} = \frac{k_r r_0^2 C_{As}^0}{D_{As}} \quad \text{and} \quad \gamma = \frac{F_{As} r_0^2}{D_{As} C_{Ga}^0}; \quad (S7)$$

Equations were numerically solved using the COMSOL package. Since  $D_{Ga}$  can be treated as ‘proxy’ for the temperature dependence of ring formation, all of the basic parameters are held constant with respect to  $T$ , except for  $D_{Ga}$ . The values of the parameters used in the numerical simulations are

$$\alpha_{As} = 0.18, \quad (S8)$$

$$\beta_{Ga} = 1 / \exp(-0.65eV / (kT)), \quad (S9)$$

$$\beta_{As} = 1.6 \times 10^2, \quad (S10)$$

$$\gamma = 5.1 \times 10^{-11} F_{As} . \quad (\text{S11})$$

Units of  $F_{As}$  are  $F_0 = 3 \times 10^5 \mu\text{m}^2 \text{s}^{-1}$

## II. Movie

Movie S1: A MEM movie of droplet crystallisation at  $T = 460$  °C under an  $\text{As}_4$  flux of beam equivalent pressure (BEP)  $1.45 \times 10^{-5}$  Torr. During MEM operation the primary electron energy was offset with respect to surface potential by  $-0.4$  eV. The duration of the movie corresponds to 20 minutes of real time. The abrupt image shift between frames 52 and 53 corresponds to specimen drift during a missing time interval of 231 s between two separate movie segments.

---

## Real-time imaging and modelling of local droplet etching

This chapter is an author generated pre print of the article

Z. Y. Zhou, C. X. Zheng, W. X. Tang and D. E. Jesson, 'Real-time Imaging and Modelling of Local Droplet Etching', which will be submitted to *Applied Physics Letter*.

### Declaration for Thesis Chapter “Real-time Imaging and Modelling of Local Droplet Etching”

Declaration by candidate

For this chapter, the nature and extent of my contribution to the work was the following:

Nature of contribution	Extent of contribution(%)
Designed the experiments, co-performed the experiments, co-developed the model used in the paper, designed and ran the simulation, co-wrote the paper.	65

The following co-authors contributed to the work. Co-authors who are students at Monash University must also indicate the extent of their contribution in percentage terms

Name	Extent of contribution(%)	Nature of contribution
Changxi Zheng	15	Co-performed the experiments, co-wrote the paper.
Wen-XinTang		Helped perform the experiments and provided technical expertise.
David Jesson		Co-wrote the paper, helped developed the model and provided technical expertise.

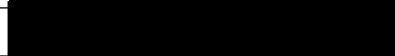
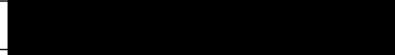
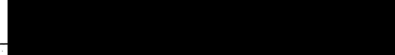
Candidate's signature		Date	17/08/2012
-----------------------	--	------	------------

#### Declaration by co-authors

The undersigned hereby certify that:

- (1) they meet the criteria for authorship in that they have participated in the conception, execution, or interpretation, of at least that part of the publication in their field of expertise;
- (2) they take public responsibility for their part of the publication, except for the responsible author who accepts overall responsibility for the publication;
- (3) there are no other authors of the publication according to these criteria;
- (4) potential conflicts of interest have been disclosed to (a) granting bodies, (b) the editor or publisher of journals or other publications, and (c) the head of the responsible academic unit; and
- (5) the original data are stored at the following location(s) and will be held for at least five years from the date indicated below:

Location(s)	School of Physics, Monash University, Clayton
-------------	---

Signature 1		Date	16-08-12
Signature 2			16-08-12
Signature 3			16-08-12

## Real-time Imaging and Modelling of Local Droplet Etching

Z. Y. Zhou, C. X. Zheng, W. X. Tang, D. E. Jesson<sup>a)</sup>

*School of Physics, Monash University, Victoria 3800, Australia*

a)

**Local droplet etching is studied in real-time using surface electron microscopy which provides new insights into the time-evolution of Ga droplet etching of GaAs under As flux. A theoretical model of the etching process is developed from the movies which requires a minimum number of assumptions and is simply based on the liquid droplet maintaining a composition close to its equilibrium liquidus value.**

Local droplet etching (LDE) has received significant attention over recent years as a means of fabricating nanoscale holes in semiconductor surfaces [1-7]. The technique offers the significant advantage that it avoids the need for lithographic processes and can be applied to a wide range of materials. LDE can be regarded as a variant of the droplet epitaxy technique in which group III metallic droplets are deposited on a substrate and annealed at high temperatures with or without a low As flux. This produces local nanoholes in the surface beneath the droplets surrounded by distinct walls. As the technique is entirely compatible with molecular beam epitaxy (MBE) it offers a new degree of freedom for fabricating low-dimensional structures. For example, nanoholes can be used as templates to create low density quantum dot arrays [3].

Despite the potential technological importance of LDE, the basic mechanism of etching remains controversial. For example, Wang *et al* [1]

qualitatively associate the nanohole formation with As evaporation from the droplet surface, but no quantitative model is provided. Conversely, Heyn [8] has proposed a model which neglects As evaporation and rests on detailed assumptions regarding the formation kinetics of a GaAs shell surrounding the droplet. The purpose of this letter is two-fold. We first use *in situ* surface electron microscopy to image LDE in real-time. Based on the resulting movies we then develop a model for the etching process which is driven by the simple assumption that the droplet remains close to liquidus composition.

Studies of LDE have largely been restricted to *ex situ* atomic force microscopy (AFM) images of quenched samples at specific times. While this has provided valuable details regarding nanohole morphology, the time evolution of the etching process must be inferred. In this study we apply *in situ* surface electron microscopy to study the etching of GaAs (001) by a model Ga droplet in real-time under As flux. Experiments were performed in a low energy electron microscope (LEEM) specially designed for III-V epitaxy [9]. An undoped GaAs (001)  $\pm 0.1^\circ$  epi-ready wafer was degassed at 300 °C at ultrahigh vacuum for 24 h. This was followed by high temperature flashing up to 600 °C and annealing at 580 °C for 2 h to remove the surface oxide. Model droplets for our etching studies (radius  $\sim 1 \mu\text{m}$ ) were prepared by annealing above the congruent evaporation temperature at 650 °C. The sample temperature was reduced to 525 °C and images were recorded in mirror electron microscopy (MEM) mode [10, 11], which is ideally suited to imaging real-time changes in surface morphology. Droplets appear in MEM as a uniform dark disc somewhat larger than the actual droplet, surrounded by a concentric bright ring as in Fig. 1(a) [11-14].

On opening the As shutter at  $t=0$  min, the droplet was subjected to an As<sub>4</sub> flux of beam equivalent pressure (BEP)  $4.3 \times 10^{-6}$  Torr which caused the droplet to shrink. On further shrinkage the etching droplet exposes a wall ( $S_1$ ) with an outer radius close to the original droplet contact-line at  $t=0$  (Fig. 1(b)(c)). Finally, the droplet completely disappears leaving behind a central

bright spot (Fig. 1(d)) which corresponds to a central pit according to MEM imaging theory [11]. Schematics of the surface morphology are shown beneath each MEM image with the features derived from caustic imaging theory [11].

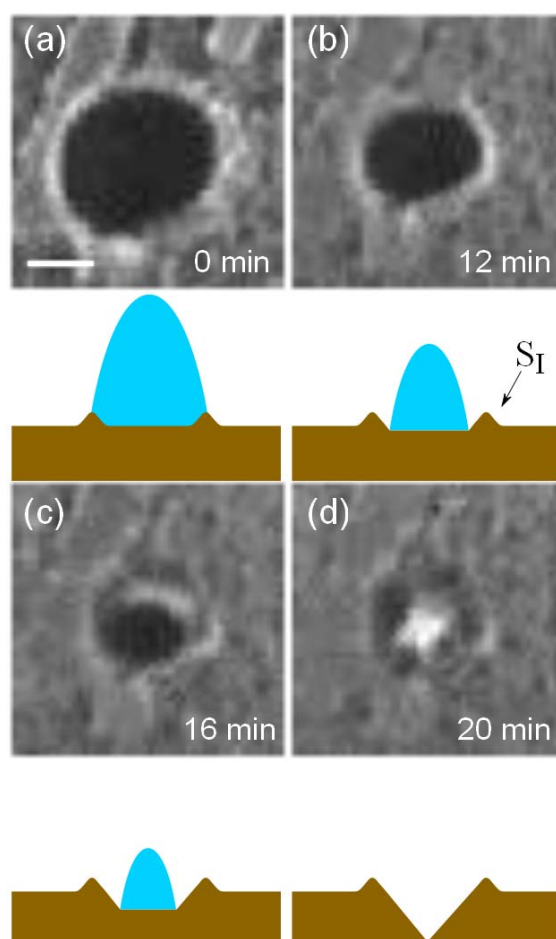


Fig. 1. Images taken from a MEM movie of Ga droplet etching into a GaAs substrate at 525 °C. A schematic of the droplet (light shading) and substrate (dark shading) morphology is shown beneath each image. The vertical scale is exaggerated to emphasise hole formation. (a) Ga droplet before adding As flux. (b) The droplet is shrinking under an As flux of  $4.3 \times 10^{-6}$  Torr. (c) A wall ( $S_I$ ) can be observed around the shrinking droplet. (d) Final hole surrounded by a wall. The length of the scale bar in (a) is 1  $\mu\text{m}$ .

The droplet radial shrinkage rate, as measured from the MEM movie in Fig. 1, is displayed in Fig. 2. It is interesting to note that the droplet ripening rate is very slow at 525 °C under zero As flux on the time-scale of the experiment. However, turning on the As<sub>4</sub> flux at  $t=0$  causes an immediate acceleration in the droplet shrinkage rate, which increases as the droplet becomes smaller. Eventually the droplet completely disappears.

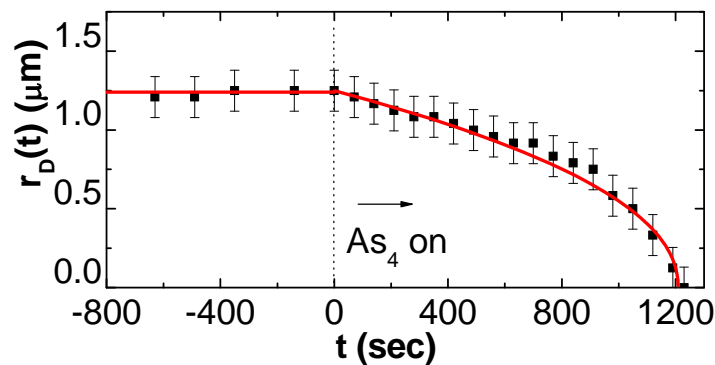


Fig. 2. Radial droplet shrinkage measured from the MEM movie in Fig. 1. The solid-line is a fit after the As<sub>4</sub> flux is turned on at  $t=0$  which is derived from the scaled form of  $r_D(t)$  in Fig. 4(a) (see text).

The MEM movie in Fig. 1 and the radial shrinkage rate in Fig. 2 provide important insights into the dynamics of Ga droplet etching under As flux. First, As deposition rapidly speeds up droplet shrinkage. Second, as the droplet shrinks, it reveals a wall, or ring, ( $S_1$ ) in a similar location to the original droplet contact-line position before As deposition commenced. Finally, the droplet is observed to shrink and etch continuously until it disappears. A theoretical description of LDE must therefore be consistent with these dynamic observations.

To construct a theory of LDE we first consider a simple model for a Ga droplet on the surface of a GaAs substrate as depicted in Fig. 3. We assume that the droplet and substrate are in equilibrium so that the droplet is at

liquidus composition. The droplet can however exchange Ga and As atoms with its environment in a number of ways including direct evaporation into the vacuum, surface diffusion and etching (or deposition) of GaAs. Under an As flux  $J_{As,F}$  we would expect the droplets to act as a source of Ga surface adatoms and a sink for As surface species as represented by  $J_{Ga,D}$  and  $J_{As,D}$  in Fig. 3. As is assumed to evaporate from the droplet with a flux  $J_{As,E}$  and Ga evaporation from the droplet surface is assumed negligible. The etching (or deposition) of GaAs beneath the droplet then gives rise to a flux of Ga (and As) atoms  $J_e$ .

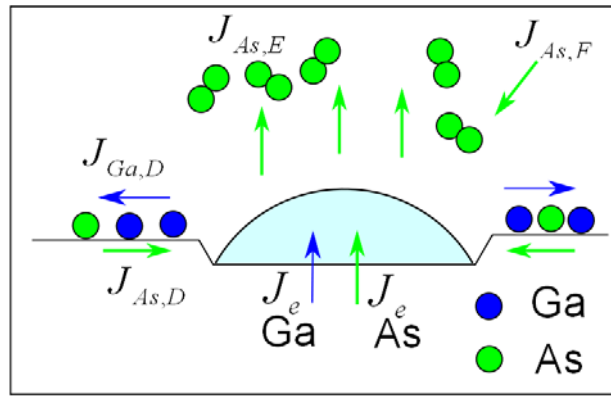


Fig. 3 Schematic of local droplet etching showing the various atomic fluxes incorporated in our model.

The physical basis of our etching model is quite simple. Let us define the liquidus mole fraction of As in the droplet as

$$\rho_{As}^e = \frac{N_{As}^e}{N_{Ga}^e + N_{As}^e}, \quad (1)$$

where  $N_{Ga}^e$  and  $N_{As}^e$  are the respective number of Ga and As atoms per unit volume at liquidus composition. To maintain liquidus composition at a given time  $t$ , the fluxes must be related by

$$\frac{J_{Ga,D} + J_e}{J_{As,F} - J_{As,E} + J_{As,D} + J_e} = \frac{1 - \rho_{As}^e}{\rho_{As}^e}. \quad (2)$$

Noting that the droplet etching rate  $\frac{dh}{dt}$  is proportional to  $J_e$ , then from (2)

we can write,

$$\frac{dh}{dt} = \frac{\Omega_V^{GaAs}}{\pi r_D(t)^2} \frac{(1 - \rho_{As}^e)(J_{As,E} - J_{As,F} - J_{As,D}) + \rho_{As}^e J_{Ga,D}}{(1 - 2\rho_{As}^e)}, \quad (3)$$

where  $\Omega_V^{GaAs}$  is the volume of a GaAs molecule in solid GaAs and  $r_D(t)$  is the time dependent droplet radius. At the relatively high temperatures associated with LDE ( $\sim 525$  °C), we assume the residence time of As surface species  $\tau_{As}$  is small so that the surface As concentration is uniform and given by  $C_{As} = F_{As} \tau_{As}$  where  $F_{As}$  is the incident As flux. For a small and uniform As concentration we assume  $J_{As,D} \approx 0$  and with  $\rho_{As}^e \approx 3 \times 10^{-4} \ll 1$  at 525 °C [15] we can neglect all but the net As evaporation flux,  $J_{As,E} - J_{As,F} = \eta(T) \pi r_D(t)^2$  in Eq (3)

$$\frac{dh}{dt} = \eta(T) \Omega_V^{GaAs}. \quad (4)$$

In this approximation, the etching rate is almost constant and the As flux gained by etching  $J_e$  roughly balances the net As evaporation flux

$$J_{As,E} - J_{As,F}.$$

As the droplet etches the substrate, its radius also decreases. Typically, the volume of etched GaAs comprising the nanohole is much smaller than the initial volume of the etching droplet [1, 5] so we assume that the droplet shrinks mainly due to the loss of Ga atoms to the surface via,

$$\frac{dr_D(t)}{dt} = \frac{\Omega_V^{Ga}}{\varphi r_D(t)^2} J_{Ga,D}, \quad (5)$$

where  $\Omega_V^{Ga}$  is the volume of a Ga atom in the droplet and  $\varphi$  is a geometric coefficient related to the volume of the droplet  $V_D = \varphi r_D(t)^3 / 3$ . To determine the droplet shrinkage rate we must therefore evaluate the diffusional flux  $J_{Ga,D}$ . To achieve this, consider a random array of droplets of radius  $r_D(t)$  at time  $t$  with typical nearest neighbour distance  $2L$ . Assuming radial symmetry, we can then write the steady state diffusion equation for the Ga concentration  $C_{Ga}(r)$  outside the droplet as,

$$D_{Ga} \left( \frac{1}{r} \frac{dC_{Ga}}{dr} + \frac{d^2 C_{Ga}}{dr^2} \right) - \frac{C_{Ga}}{\tau_{Ga}} - k_r C_{Ga} C_{As} = 0, \quad (6)$$

where  $k_r$  is a reaction rate constant governing the reaction between As and Ga to form GaAs solid.  $D_{Ga}$  is the diffusion coefficient and  $\tau_{Ga}$  the evaporation lifetime of surface Ga.

We impose the radially symmetric boundary conditions

$$\frac{dC_{Ga}}{dr} = 0 \text{ at } r = L, \quad (7)$$

since the concentration is symmetric halfway between the drops. The number of atoms attaching or detaching at the drop by diffusion is

$$J_{Ga,D} = 2\pi r_D D_{Ga} \left. \frac{dC_{Ga}(r)}{dr} \right|_{r=r_D}, \quad (8)$$

and must be equal to the number of atoms transferring to the droplet via interface transfer. Let us assume this only occurs at the collar giving,

$$J_{Ga,D} = 2\pi D_{Ga} \left. \frac{dC_{Ga}(r)}{dr} \right|_{r=r_D} = 2\pi\beta[C_{Ga}(r_D) - C_{Ga}^0], \quad (9)$$

where  $C_{Ga}(r_D)$  is the adatom density at the edge of the droplet,  $C_{Ga}^0$  is the adatom concentration in equilibrium with a droplet of radius  $r_D$  and  $\beta$  is a coefficient assumed to be a constant. Based on the boundary conditions (7) and (9), for  $r \ll L$  one finds the solution of Eq. (6) consists of a modified bessel function, which can be written as,

$$C_{Ga}(r) = EK_0(\sqrt{Br}), \quad (10)$$

where,

$$B = (1 + k_r F_{As} \tau_{As} \tau_{Ga}) / D_{Ga} \tau_{Ga}, \quad (11)$$

and

$$E = \frac{\beta C_{Ga}^0}{\sqrt{BD_{Ga}} K_1(\sqrt{Br_D}) + \beta K_0(\sqrt{Br_D})}. \quad (12)$$

We can then evaluate the diffusional Ga flux from (8) and (10) giving

$$J_{Ga,D} = -2\pi r_D D_{Ga} E \sqrt{B} K_1(\sqrt{Br_D}). \quad (13)$$

Eqs (4), (5) and (13) are the basic equations of our LDE model. The droplet shrinkage rate can be obtained by combining Eqs (5) and (13),

$$\frac{dr_D(t)}{dt} = -\frac{2\pi\Omega_v^{Ga} D_{Ga} C_{Ga}^0 \sqrt{B}}{\varphi} \frac{1}{r_D(t)} \left[ \frac{\sqrt{BD_{Ga}}}{\beta} + \frac{K_0(\sqrt{Br_D}(t))}{K_1(\sqrt{Br_D}(t))} \right]^{-1} \quad (14)$$

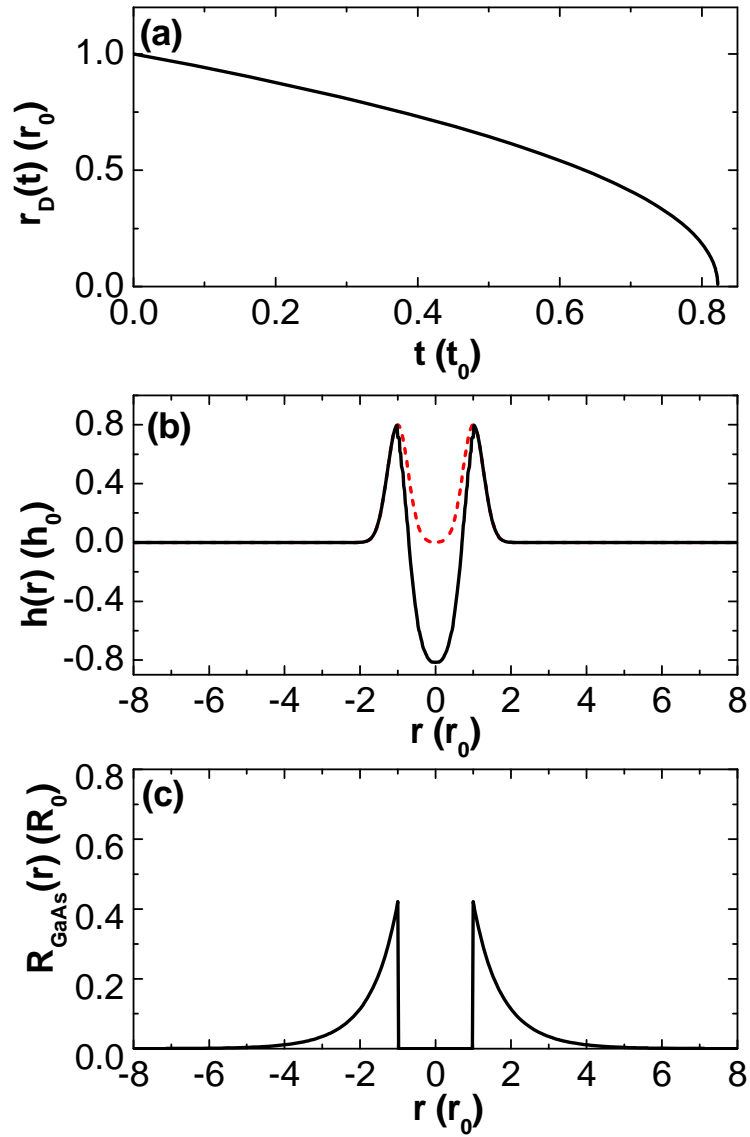


Fig. 4. (a) Radial droplet shrinking rate. (b) Etching profile. Dashed lines represent pre-existing inner ring structures which are approximated by Gaussian peaks and are superimposed in  $h(r)$  (see text). (c) Reaction term  $R_{GaAs}(r)$  showing the rate of GaAs crystallisation. The scaled units  $r_0, t_0, h_0$  and  $R_0$  are defined in the text.

The time dependence of the droplet radius  $r_D(t)$  is evaluated from Eq (14) and displayed in Fig. 4(a). The scaled units of distance and time are  $r_0 = 1/\sqrt{B}$  and  $t_0 = \varphi/[2\pi\Omega_V^{Ga} D_{Ga} C_{Ga}^0 B^{3/2}]$ , respectively. We find the parameter  $(\sqrt{B}D_{Ga})/\beta$  does not significantly influence the qualitative form of the shrinkage and this is set to unity. The scaled form of  $r_D(t)$  in Fig. 4(a) is superimposed on the measured radial shrinkage rate in Fig. 2 and is in good qualitative agreement. In addition, the shrinking rate in Fig. 4(a) can be seen to depend on  $F_{As}$  via the factor  $B$  (Eq. (11)) in the scaled units of time  $t_0$ . Increasing  $F_{As}$  is therefore expected to increase the droplet radial shrinkage rate in agreement with the dynamic observations of Fig. 2 where droplet shrinkage accelerated immediately on turning on the As<sub>4</sub> flux at  $t=0$ . Physically, this can be attributed to As reacting with surface Ga which increases the Ga concentration profile gradient at the droplet edge, increasing the Ga flux away from the droplet.

The final etching depth of a given point is the integral of the etching rate

$\frac{dh}{dt}$  with respect to the overall etching time. Combining Eqs. (4) and (14),

the final etching profile is,

$$h(r) = -\frac{\eta(T)\varphi\Omega_V^{GaAs}}{2\pi\Omega_V^{Ga} D_{Ga} C_{Ga}^0 \sqrt{B}} \int_{r_D(0)}^r \left[ \frac{\sqrt{B}D_{Ga}}{\beta} + \frac{K_0(\sqrt{B}r_D)}{K_1(\sqrt{B}r_D)} \right] r_D dr_D. \quad (15)$$

In plotting the etching profile from Eq. (15) we must also consider the origin of  $S_I$  in Fig. 1, which is associated with the original position of the droplet contact-line. Our model predicts that GaAs will be deposited during LDE at a rate given by,

$$R_{GaAs}(r) = k_r C_{Ga}(r) C_{As}(r) = \frac{k_r F_{As} \tau_{As} C_{Ga}^0}{(\sqrt{B}D_{Ga}/\beta)K_1(\sqrt{B}r_D) + K_0(\sqrt{B}r_D)} K_0(\sqrt{B}r). \quad (16)$$

which is plotted in Fig. 4(c) using scaled units  $R_0 = [k_r C_{Ga}^0 F_{As} \tau_{As}] / [(\sqrt{B} D_{Ga} / \beta) K_1(\sqrt{B} r_D) + K_0(\sqrt{B} r_D)]$ . Although this will contribute to the side wall material contained in  $S_I$ , it is also known from droplet epitaxy studies that quantum structure inner-rings pre-exist beneath droplets [16]. The existence of such rings is consistent with mass transport at the liquid Ga/solid GaAs contact line to achieve exact balance of the surface tensions [17]. Pre-existing ridges are therefore to be expected beneath droplets used for LDE and must be directly included in the model. In Fig. 4(b) such preexisting ridges are approximated as Gaussian shapes of dimensions consistent with those observed during droplet epitaxy [16] and, for simplicity, we ignore contributions from Eq. (16).  $h(r)$  is plotted in Fig. 4(b) in scaled units of height  $h_0 = [\varphi \eta(T) \Omega_v^{GaAs}] / [2\pi C_{Ga}^0 \Omega_v^{Ga} D_{Ga} B^{3/2}]$ . It can be seen that the etch profile qualitatively agrees with experimentally observed profiles [1, 5].

Our model is also consistent with the experimental observations that LDE occurs for zero As deposition flux [4,18]. Zero flux simply reduces the value of the parameter  $B$  in Eq (11). Finally, we also comment on the interesting model proposed by Heyn [8] which is based on the formation kinetics of a GaAs shell surrounding the droplet. In photo-emission electron microscopy (PEEM), GaAs appears dark on bright liquid Ga due to work function considerations [13]. In our PEEM imaging experiments during this work, we have not observed any conclusive evidence for the existence of such a shell.

In summary, we have observed LDE in real-time using *in situ* surface electron microscopy. A simple model of the etching process, consistent with these observations, is developed and is based on the liquid droplet maintaining a composition close to its equilibrium liquidus value. This can qualitatively explain experimentally observed etching profiles and the

dynamic observation of increased droplet shrinking rate with increasing As flux. It is worth noting that our model becomes analytical in certain limits, such as attachment limited growth. Such simplifications may be relevant to particular LDE experimental regimes. In the future, as particular surface parameters become known more accurately, it might be hoped that the model can be extended towards a fully quantitative treatment of LDE.

### ACKNOWLEDGMENTS

We are grateful to Rod Mackie for technical support. D.E.J. and W.X.T. acknowledge support from the ARC (Grant No. DP120101486).

- [1] Zh. M. Wang, B. L. Liang, K. A. Sablon and G. J. Salamo, *Appl. Phys. Lett.*, **90**, 113120 (2007).
- [2] A. Stemmann, Ch. Heyn, T. Köppen, T. Kipp, and W. Hansen, *Appl. Phys. Lett.*, **93**, 123108 (2008).
- [3] Ch. Heyn, A. Stemmann, T. Köppen, Ch. Strelow, T. Kipp, M. Grave, S. Mendach and W. Hansen, *Appl. Phys. Lett.*, **93**, 183113 (2009).
- [4] Ch. Heyn, A. Stemmann and W. Hansen, *Appl. Phys. Lett.*, **95**, 173110 (2009).
- [5] Ch. Heyn, A. Stemmann, R. Eiselt and W. Hansen, *J. Appl. Phys.*, **105**, 054316 (2009).
- [6] A. Stemmann, T. Köppen, M. Grave, S. Wildfang, S. Mendach, W. Hansen and Ch. Heyn, *J. Appl. Phys.*, **106**, 064315 (2009)
- [7] O. Boonpeng, W. Jevasuwan, S. Panyakeow and S. Ratanathamphan, *Jpn. J. Appl. Phys.*, **49**, 04DH09, (2010).
- [8] Ch. Heyn, *Phys. Rev. B*, **83**, 165302 (2011)
- [9] D. E. Jesson and W. X. Tang, Surface Electron Microscopy of Ga Droplet Dynamics on GaAs (001), in *Microscopy: Science, Technology, Applications and Education*, Edited by A. Méndez-Vilas and J. D. Álvarez, Formatex Research Center (Badajoz, Spain), **3**, 1608 (2010)

- [10] S. A. Nepijko, N. N. Sedov, and G. Schönhense, *J. Microsc.*, **203**, 269 (2001).
- [11] S. M. Kennedy, C. X. Zheng, W. X. Tang, D. M. Paganin and D. E. Jesson, *Ultramicroscopy*, **111**, 356 (2011).
- [12] J. Tersoff, D. E. Jesson and W. X. Tang, *Science*, **324**, 236 (2009).
- [13] J. Tersoff, D. E. Jesson and W. X. Tang, *Phys. Rev. Lett.*, **105**, 035702 (2010).
- [14] S. M. Kennedy, C. X. Zheng, W. X. Tang, D. M. Paganin and D. E. Jesson, *Proc. Roy. Soc. A*, **466**, 2857 (2010).
- [15] I. Ansara, C. Chatillon, H.L. Lukas, T. Nishizawa, H. Ohtani, K. Ishida, M. Hillert, B. Sundman, B.B. Argent, A. Watson, T.G. Chart and T. Anderson, *Calphad*, **18**, 177 (1994).
- [16] C. Somaschini, S. Bietti, N. Koguchi, and S. Sanguinetti, *Nano Lett.*, **9**, 3419 (2009).
- [17] C. X. Zheng, W. X. Tang and D. E. Jesson, *Appl. Phys. Lett.*, **100**, 071903 (2012).
- [18] Ch. Heyn, A. Stemmann, M. Klingbeil, Ch. Strelow, T. Köppen, S. Mendach, W. Hansen, *J. Cryst. Growth*, **323**,263 (2011)



---

## Conclusions and future work

The central aim of this thesis has been to develop a method capable of imaging III-V droplet epitaxy in real-time under high incident As flux. Further goals were to investigate the basic thermodynamics of the technique and establish models to understand the formation of quantum ring features.

We have designed and developed a III-V low energy electron microscope (LEEM) which combines a commercially available LEEM system with In, Ga and As molecular beam epitaxy (MBE) sources and a specially designed cooling shroud to minimise the build up in background As pressure. We have established the feasibility of studying droplet epitaxy using III-V LEEM by imaging droplet nucleation, evolution, motion and coalescence during Langmuir evaporation.

The congruent evaporation temperature  $T_c$  is a fundamental surface characteristic of GaAs and similar compounds. We have developed a sensitive approach to measure  $T_c$  based on Ga droplet stability, and have shown that external As flux directly controls  $T_c$ . The dependence of  $T_c$  on  $F$  is then measured and explained by a simple model for evaporation in the presence of external flux. Controlling  $T_c$  via changing  $F$  offers a means of manipulating congruent evaporation with relevance to MBE, surface preparation methods and droplet epitaxy.

Real-time movies of the Ga droplet size distribution have been obtained

by *in situ* surface electron microscopy during Langmuir evaporation of GaAs. Droplet formation in response to coalescence is identified as an important factor governing the time-evolution of droplets. This is incorporated into a simple Monte Carlo model which can reproduce and explain the major features of our experimental droplet size distributions. This provides important insight into this method of creating droplet arrays for use in droplet epitaxy.

We have studied droplet epitaxy of GaAs in real-time using surface electron microscopy under As flux. The main features of the movies are used as a guide to develop a theoretical model for quantum ring formation which can qualitatively explain the origin of quantum rings as a function of temperature and As flux. The model predicts that Ga adatom diffusion primarily controls the quantum structure morphology.

Finally, local droplet etching (LDE) is studied in the III-V LEEM under As flux. A theoretical model of the etching process is developed from the mirror electron microscopy (MEM) movies which is simply based on the liquid droplet maintaining a composition close to its equilibrium liquidus value.

The study of III-V droplet epitaxy in this thesis can be extended in a number of ways. The qualitative theory of ring formation presented in Chapter 8 uses a simple reaction-diffusion model to explain quantum ring formation in terms of surface concentration profiles under different experimental conditions. As more detailed information on the various surface parameters becomes known from experiment, it might be hoped that a fully quantitative approach can be developed to predict specific quantum features. More generally, the development of III-V LEEM now creates wide ranging possibilities for future work in the III-V system. This includes the study of droplet heteroepitaxy and the formation of quantum molecules. Additionally, movies of wetting layer formation and strain-induced quantum dot self-assembly during InAs growth on GaAs are important topics for future research.

---

## Bibliography

Altman M, Chung W, He Z, Poon H and Tong S (2001). Quantum size effect in low energy electron diffraction of thin films, *Applied Surface Science* **169-170**(0), 82–87.

**URL:** <http://www.sciencedirect.com/science/article/pii/S0169433200006449>

Altman M, Chung W and Liu C (1998). LEEM phase contrast, *Surface Review and Letters* **5**(6), 1129–1142.

**URL:** <http://www.worldscinet.com/srl/05/0506/S0218625X98001468.html>

Altman M S (2010). Trends in low energy electron microscopy, *Journal of Physics: Condensed Matter* **22**(8), 084017.

**URL:** <http://stacks.iop.org/0953-8984/22/i=8/a=084017>

Amar J G and Family F (1995). Critical Cluster Size: Island Morphology and Size Distribution in Submonolayer Epitaxial Growth, *Phys. Rev. Lett.* **74**, 2066–2069.

**URL:** <http://link.aps.org/doi/10.1103/PhysRevLett.74.2066>

Arthur J (1967). Vapor pressures and phase equilibria in the Ga-As system, *Journal of Physics and Chemistry of Solids* **28**(11), 2257 – 2267.

**URL:** <http://www.sciencedirect.com/science/article/pii/002236976790251X>

- Bauer E (1962). Low energy electron reflection microscopy, *Fifth international congress for electron microscopy*(S. S. Breese, Jr. editor) New York, Academic Press **1**, D11.
- Bauer E (1994). Low energy electron microscopy, *Reports on Progress in Physics* **57**(9), 895.  
**URL:** <http://stacks.iop.org/0034-4885/57/i=9/a=002>
- Bauer E, Mundschau M, Świąch W and Telięps W (1989). Surface studies by low-energy electron microscopy (LEEM) and conventional UV photoemission electron microscopy (PEEM), *Ultramicroscopy* **31**(1), 49–57.  
**URL:** <http://www.sciencedirect.com/science/article/pii/0304399189900338>
- Baumann G, Richter H, Baumgartner A, Ferling D, Heilig R, Hollmann D, Muller H, Nechansky H and Schlechtweg M (1995). 51 GHz frontend with flip chip and wire bond interconnections from GaAs MMICs to a planar patch antenna, in *Microwave Symposium Digest, 1995., IEEE MTT-S International*, pp. 1639–1642 vol.3.
- Becker R and Döring W (1935). Kinetische Behandlung der Keimbildung in übersättigten Dämpfen, *Annalen der Physik* **416**(8), 719–752.  
**URL:** <http://dx.doi.org/10.1002/andp.19354160806>
- Binder K and Stauffer D (1976). Statistical theory of nucleation, condensation and coagulation, *Advances in Physics* **25**(4), 343–396.  
**URL:** <http://www.tandfonline.com/doi/abs/10.1080/00018737600101402>
- Cao Y L, Yang T, Xu P F, Ji H M, Gu Y X, Wang X D, Wang Q, Ma W Q and Chen L H (2010). Delay of the excited state lasing of 1310 nm InAs/GaAs quantum dot lasers by facet coating, *Applied Physics Letters* **96**(17), 171101.  
**URL:** <http://link.aip.org/link/?APL/96/171101/1>

Chakrabarti S, Adhikary S, Halder N, Aytac Y and Perera A G U (2011). High-performance, long-wave ( $10.2\mu\text{m}$ ) InGaAs/GaAs quantum dot infrared photodetector with quaternary  $\text{In}_{0.21}\text{Al}_{0.21}\text{Ga}_{0.58}\text{As}$  capping, *Applied Physics Letters* **99**(18), 181102.

**URL:** <http://link.aip.org/link/?APL/99/181102/1>

Chang H Y, Liu Y C, Weng S H, Lin C H, Yeh Y L and Wang Y C (2011). Design and Analysis of a DC-43.5-GHz Fully Integrated Distributed Amplifier Using GaAs HEMT-HBT Cascode Gain Stage, *Microwave Theory and Techniques, IEEE Transactions on* **59**(2), 443–455.

**URL:** <http://ieeexplore.ieee.org/xpl/articleDetails.jsp?arnumber=5671514>

Chiu S Y, Tsai J H, Huang H W, Liang K C, Tsai T M, Hsu K Y and Lour W S (2009). Integrated Hydrogen-Sensing Amplifier With GaAs Schottky-Type Diode and InGaP-GaAs Heterojunction Bipolar Transistor, *Electron Device Letters, IEEE* **30**(9), 898–900.

**URL:** <http://ieeexplore.ieee.org/xpl/articleDetails.jsp?arnumber=5184885>

Chung W and Altman M (1998). Step contrast in low energy electron microscopy, *Ultramicroscopy* **74**(4), 237–246.

**URL:** <http://www.sciencedirect.com/science/article/pii/S0304399198000436>

Claudon J, Bleuse J, Malik N, Bazin M, Jaffrennou P, Gregersen N, Sauvan C, Lalanne P and Gérard J (2010). A highly efficient single-photon source based on a quantum dot in a photonic nanowire, *Nature Photonics* **4**(3), 174–177.

**URL:** <http://www.nature.com/nphoton/journal/v4/n3/full/nphoton.2009.287.html>

Davisson C and Germer L H (1927). Diffraction of Electrons by a Crystal of Nickel, *Phys. Rev.* **30**, 705–740.

**URL:** <http://link.aps.org/doi/10.1103/PhysRev.30.705>

Family F and Meakin P (1988). Scaling of the Droplet-Size Distribution in Vapor-Deposited Thin Films, *Phys. Rev. Lett.* **61**, 428–431.

**URL:** <http://link.aps.org/doi/10.1103/PhysRevLett.61.428>

Family F and Meakin P (1989). Kinetics of droplet growth processes: Simulations, theory, and experiments, *Phys. Rev. A* **40**, 3836–3854.

**URL:** <http://link.aps.org/doi/10.1103/PhysRevA.40.3836>

Fedorova K A, Cataluna M A, Krestnikov I, Livshits D and Rafailov E U (2010). Broadly tunable high-power InAs/GaAs quantum-dot external cavity diode lasers, *Opt. Express* **18**(18), 19438–19443.

**URL:** <http://www.opticsexpress.org/abstract.cfm?URI=oe-18-18-19438>

Foxon C, Harvey J and Joyce B (1973). The evaporation of GaAs under equilibrium and non-equilibrium conditions using a modulated beam technique, *Journal of Physics and Chemistry of Solids* **34**(10), 1693–1701.

**URL:** <http://www.sciencedirect.com/science/article/pii/S0022369773801350>

Frenkel J (1924). Theorie der Adsorption und verwandter Erscheinungen, *Zeitschrift für Physik A Hadrons and Nuclei* **26**, 117–138. 10.1007/BF01327320.

**URL:** <http://dx.doi.org/10.1007/BF01327320>

Goldstein B, Szostak D J and Ban V S (1976). Langmuir evaporation from the (100), (111A), and (111B) faces of GaAs, *Surface Science* **57**(2), 733–740.

**URL:** <http://www.sciencedirect.com/science/article/pii/0039602876903587>

Gong Z, Niu Z C, Huang S S, Fang Z D, Sun B Q and Xia J B (2005). Formation of GaAs/AlGaAs and InGaAs/GaAs nanorings by droplet molecular-beam epitaxy, *Applied Physics Letters* **87**(9), 093116.

**URL:** <http://link.aip.org/link/?APL/87/093116/1>

Griffith O H and Engel W (1991). Historical perspective and current trends in emission microscopy, mirror electron microscopy and low-energy electron microscopy: An introduction to the proceedings of the second international symposium and workshop on emission microscopy and related techniques, *Ultramicroscopy* **36**(1-3), 1–28.

**URL:** <http://www.sciencedirect.com/science/article/pii/030439919190135S>

Günther S, Kaulich B, Gregoratti L and Kiskinova M (2002). Photoelectron microscopy and applications in surface and materials science, *Progress in Surface Science* **70**(41C8), 187 – 260.

**URL:** <http://www.sciencedirect.com/science/article/pii/S0079681602000072>

Heiblum M, Thomas D C, Knoedler C M and Nathan M I (1985). Tunneling hot-electron transfer amplifier: A hot-electron GaAs device with current gain, *Applied Physics Letters* **47**(10), 1105–1107.

**URL:** <http://link.aip.org/link/?APL/47/1105/1>

Heyn C, Stemmann A and Hansen W (2010). Self-Assembly of Quantum Dots and Rings on Semiconductor Surfaces, in *Quantum Materials, Lateral Semiconductor Nanostructures, Hybrid Systems and Nanocrystals*, D Heitmann, ed., NanoScience and Technology, Springer Berlin Heidelberg, pp. 1–24. 10.1007/978-3-642-10553-1\_1.

**URL:** [http://dx.doi.org/10.1007/978-3-642-10553-1\\_1](http://dx.doi.org/10.1007/978-3-642-10553-1_1)

Hohenberg P C and Halperin B I (1977). Theory of dynamic critical phenomena, *Rev. Mod. Phys.* **49**, 435–479.

**URL:** <http://link.aps.org/doi/10.1103/RevModPhys.49.435>

Huang S, Niu Z, Fang Z, Ni H, Gong Z and Xia J (2006). Complex quantum ring structures formed by droplet epitaxy, *Applied Physics Letters* **89**(3), 031921.

**URL:** <http://link.aip.org/link/?APL/89/031921/1>

Huffaker D L, Park G, Zou Z, Shchekin O B and Deppe D G (1998). 1.3  $\mu\text{m}$  room-temperature GaAs-based quantum-dot laser, *Applied Physics Letters* **73**(18), 2564–2566.

**URL:** <http://link.aip.org/link/?APL/73/2564/1>

Ikezawa M, Sakuma Y, Zhang L, Sone Y, Mori T, Hamano T, Watanabe M, Sakoda K and Masumoto Y (2012). Single-photon generation from a nitrogen impurity center in GaAs, *Applied Physics Letters* **100**(4), 042106.

**URL:** <http://link.aip.org/link/?APL/100/042106/1>

Isomura N, Tsukamoto S, Iizuka K and Arakawa Y (2007). Investigation on GaAs(001) surface treated by As-free high temperature surface cleaning method, *Journal of Crystal Growth* **301-302**(0), 26 – 29. 14th International Conference on Molecular Beam Epitaxy MBE XIV.

**URL:** <http://www.sciencedirect.com/science/article/pii/S0022024806013868>

Jesson D E, Pavlov K M, Morgan M J and Usher B F (2007). Imaging Surface Topography using Lloyd's Mirror in Photoemission Electron Microscopy, *Phys. Rev. Lett.* **99**, 016103.

**URL:** <http://link.aps.org/doi/10.1103/PhysRevLett.99.016103>

Joyce B A and Vvedensky D D (2004). Self-organized growth on GaAs surfaces, *Materials Science and Engineering: R: Reports* **46**(6), 127 – 176.

**URL:** <http://www.sciencedirect.com/science/article/pii/S0927796X04001147>

Kelton K (2005). *Nucleation in Condensed Matter, Volume 15: Applications in Materials and Biology*, Pergamon.

Kennedy S M (2010), Image contrast in mirror and low energy electron microscopy, PhD thesis, Monash University, Australia.

Kennedy S, Schofield N, Paganin D and Jesson D (2009). Wave Optical Treatment of Surface Step Contrast in Low-Energy Electron Microscopy,

*Surface Review and Letters* **16**(6), 855.

**URL:** <http://www.worldscinet.com/srl/16/1606/S0218625X09013402.html>

Kennedy S, Zheng C, Tang W, Paganin D and Jesson D (2011). Caustic imaging of gallium droplets using mirror electron microscopy, *Ultramicroscopy* **111**(5), 356–363.

**URL:** <http://www.sciencedirect.com/science/article/pii/S0304399111000349>

Koguchi N and Ishige K (1993). Growth of GaAs Epitaxial Microcrystals on an S-Terminated GaAs Substrate by Successive Irradiation of Ga and As Molecular Beams, *Japanese Journal of Applied Physics* **32**(Part 1, No. 5A), 2052–2058.

**URL:** <http://jjap.jsap.jp/link?JJAP/32/2052/>

Koguchi N, Takahashi S and Chikyow T (1991). New MBE growth method for InSb quantum well boxes, *Journal of Crystal Growth* **111**(1-4), 688–692.

**URL:** <http://www.sciencedirect.com/science/article/pii/002202489191064H>

Lay G L and Kern R (1978). Physical methods used for the characterization of modes of epitaxial growth from the vapor phase, *Journal of Crystal Growth* **44**(2), 197 – 222.

**URL:** <http://www.sciencedirect.com/science/article/pii/0022024878901951>

Lee J H, Wang Z M, AbuWaar Z Y and Salamo G J (2009). Design of Nanostructure Complexes by Droplet Epitaxy, *Crystal Growth & Design* **9**(2), 715–721.

**URL:** <http://pubs.acs.org/doi/abs/10.1021/cg701142%2d>

Lifshitz I and Slyozov V (1961). The kinetics of precipitation from supersaturated solid solutions, *Journal of Physics and Chemistry of Solids* **19**(1-2), 35 – 50.

**URL:** <http://www.sciencedirect.com/science/article/pii/0022369761900543>

Lowes T D and Zinke-Allmang M (1993). Microscopic study of cluster formation in the Ga on GaAs(001) system, *Journal of Applied Physics* **73**(10), 4937–4941.

**URL:** <http://link.aip.org/link/?JAP/73/4937/1>

Mano T and Koguchi N (2005). Nanometer-scale GaAs ring structure grown by droplet epitaxy, *Journal of Crystal Growth* **278**(1-4), 108–112. 13th International Conference on Molecular Beam Epitaxy.

**URL:** <http://www.sciencedirect.com/science/article/pii/S0022024804020986>

Mano T, Kuroda T, Sanguinetti S, Ochiai T, Tateno T, Kim J, Noda T, Kawabe M, Sakoda K, Kido G and Koguchi N (2005). Self-Assembly of Concentric Quantum Double Rings, *Nano Letters* **5**(3), 425–428.

**URL:** <http://pubs.acs.org/doi/abs/10.1021/nl048192%2B>

Mano T, Watanabe K, Tsukamoto S, Fujioka H, Oshima M and Koguchi N (2000). Fabrication of InGaAs quantum dots on GaAs(001) by droplet epitaxy, *Journal of Crystal Growth* **209**(2-3), 504–508.

**URL:** <http://www.sciencedirect.com/science/article/pii/S0022024899006065>

Michler P, Kiraz A, Becher C, Schoenfeld W V, Petroff P M, Zhang L, Hu E and Imamoglu A (2000). A Quantum Dot Single-Photon Turnstile Device, *Science* **290**, 2282.

**URL:** <http://www.sciencemag.org/content/290/5500/2282.short>

Muller J E, Grave T, Siweris H, Karner M, Schafer A, Tischer H, Riechert H, Schleicher L, Verweyen L, Bangert A, Kellner W and Meier T (1997). A GaAs HEMT MMIC chip set for automotive radar systems fabricated by optical stepper lithography, *Solid-State Circuits, IEEE Journal of* **32**(9), 1342–1349.

**URL:** <http://ieeexplore.ieee.org/xpl/articleDetails.jsp?arnumber=628737>

- N.Koguchi, Ishige K and Takahashi S (1993). New selective molecular beam epitaxial growth method for direct formation of GaAs quantum dots, *Journal of Vacuum Science & Technology* **11**, 787.  
**URL:** <http://dx.doi.org/10.1116/1.586789>
- Pan D, Towe E and Kennerly S (1998). Normal-incidence intersubband (In, Ga)As/GaAs quantum dot infrared photodetectors, *Applied Physics Letters* **73**(14), 1937–1939.  
**URL:** <http://link.aip.org/link/?APL/73/1937/1>
- Rotermund H H (1997). Imaging of dynamic processes on surfaces by light, *Surface Science Reports* **29**(71C8), 265 – 364.  
**URL:** <http://www.sciencedirect.com/science/article/pii/S0167572997000125>
- Slezov V V (2009). *Kinetics of First Order Phase Transitions*, 1st edn, Wiley-VCH.
- Stasio G D, Capozzi M, Lorusso G F, Baudat P A, Droubay T C, Perfetti P, Margaritondo G and Tonner B P (1998). MEPHISTO: Performance tests of a novel synchrotron imaging photoelectron spectromicroscope, *Review of Scientific Instruments* **69**(5), 2062–2066.  
**URL:** <http://link.aip.org/link/?RSI/69/2062/1>
- Świąch W, Fecher G, Ziethen C, Schmidt O, Schönhense G, Grzelakowski K, Schneider C M, Frömter R, Oepen H and Kirschner J (1997). Recent progress in photoemission microscopy with emphasis on chemical and magnetic sensitivity, *Journal of Electron Spectroscopy and Related Phenomena* **84**(1-3), 171–188.  
**URL:** <http://www.sciencedirect.com/science/article/pii/S0368204897000224>
- Świąch W, Rausenberger B, Engel W, Bradshaw A M and Zeitler E (1993). In-situ studies of heterogeneous reactions using mirror electron microscopy,

*Surface Science* **294**, 297.

**URL:** <http://www.sciencedirect.com/science/article/pii/0039602893901162>

Tang W X, Zheng C X, Zhou Z Y, Jesson D E and Tersoff J (2011). Ga droplet surface dynamics during Langmuir evaporation of GaAs, *IBM Journal of Research and Development* **55**(4), 10:1–10:7.

Telieps W and Bauer E (1985). An analytical reflection and emission UHV surface electron microscope, *Ultramicroscopy* **17**(1), 57–65.

**URL:** <http://www.sciencedirect.com/science/article/pii/0304399185901779>

Tersoff J, Jesson D E and Tang W X (2009). Running Droplets of Gallium from Evaporation of Gallium Arsenide, *Science* **324**, 236.

**URL:** <http://www.sciencemag.org/content/324/5924/236.short>

Tromp R, Hannon J, Ellis A, Wan W, Berghaus A and Schaff O (2010). A new aberration-corrected, energy-filtered LEEM/PEEM instrument. I. Principles and design, *Ultramicroscopy* **110**(7), 852–861.

**URL:** <http://www.sciencedirect.com/science/article/pii/S0304399110000835>

Tromp R, Mankos M, Reuter M, Ellis A and Copel M (1998). A new low energy electron microscope, *Surface Review and Letters* **5**(6), 1189–1198.

**URL:** <http://www.worldscinet.com/srl/05/0506/S0218625X98001523.html>

Tromp R and Reuter M (1991). Design of a new photo-emission/low-energy electron microscope for surface studies, *Ultramicroscopy* **36**(1-3), 99–106.

**URL:** <http://www.sciencedirect.com/science/article/pii/030439919190141R>

Tsao J Y (1993). *Materials Fundamentals of Molecular Beam Epitaxy*, Academic Press Inc, San Diego, p. 733.

Turner G H and Bauer E (1966). An ultrahigh vacuum electron microscope and its application to work function studies, *Sixth International Congress for Electron Microscopy*(R. Ueda, editor), Kyoto, Maruzen, Tokyo **1**, 163.

- Venables J A, Spiller G D T and Hanbucken M (1984). Nucleation and growth of thin films, *Reports on Progress in Physics* **47**(4), 399.  
**URL:** <http://stacks.iop.org/0034-4885/47/i=4/a=002>
- Veneklasen L H (1991). Design of a spectroscopic low-energy electron microscope, *Ultramicroscopy* **36**(1-3), 76–90.  
**URL:** <http://www.sciencedirect.com/science/article/pii/030439919190139W>
- Venzl G (1985). Dynamics of first-order phase transitions: Theory of coarsening (Ostwald ripening) for open systems, *Phys. Rev. A* **31**, 3431–3440.  
**URL:** <http://link.aps.org/doi/10.1103/PhysRevA.31.3431>
- Vogel J, Kuch W, Bonfim M, Camarero J, Pennec Y, Offi F, Fukumoto K, Kirschner J, Fontaine A and Pizzini S (2003). Time-resolved magnetic domain imaging by x-ray photoemission electron microscopy, *Applied Physics Letters* **82**(14), 2299–2301.  
**URL:** <http://link.aip.org/link/?APL/82/2299/1>
- Voorhees P (1985). The theory of Ostwald ripening, *Journal of Statistical Physics* **38**(1), 231–252.  
**URL:** <http://www.springerlink.com/content/g336525005556215/>
- Wagner C (1961). Theorie der altering von neiderschlagen durch umlosen, *Z. Elektrochem* **65**, 581.
- Walton D (1962). Nucleation of Vapor Deposits, *The Journal of Chemical Physics* **37**(10), 2182–2188.  
**URL:** <http://link.aip.org/link/?JCP/37/2182/1>
- Wan W, Feng J, Padmore H and Robin D (2004). Simulation of a mirror corrector for PEEM3, *Nuclear Instruments and Methods in Physics Research Section A: Accelerators, Spectrometers, Detectors and Associated Equipment* **519**(1-2), 222–229. Proceedings of the Sixth International Conference

on Charged Particle Optics.

**URL:** <http://www.sciencedirect.com/science/article/pii/S0168900203030249>

Wang Z, Holmes K, Mazur Y, Ramsey K and Salamo G (2006). Self-organization of quantum-dot pairs by high-temperature droplet epitaxy, *Nanoscale Research Letters* **1**, 57–61. 10.1007/s11671-006-9002-z.

**URL:** <http://dx.doi.org/10.1007/s11671-006-9002-z>

Wang Z M, Liang B L, Sablon K A and Salamo G J (2007). Nanoholes fabricated by self-assembled gallium nanodroplet on GaAs(100), *Applied Physics Letters* **90**(11), 113120.

**URL:** <http://link.aip.org/link/?APL/90/113120/1>

Watanabe K, Koguchi N and Gotoh Y (2000). Fabrication of GaAs Quantum Dots by Modified Droplet Epitaxy, *Japanese Journal of Applied Physics* **39**(Part 2, No. 2A), L79–L81.

**URL:** <http://jjap.jsap.jp/link?JJAP/39/L79/>

Wu J, Shao D, Dorogan V G, Li A Z, Li S, DeCuir E A, Manasreh M O, Wang Z M, Mazur Y I and Salamo G J (2010). Intersublevel Infrared Photodetector with Strain-Free GaAs Quantum Dot Pairs Grown by High-Temperature Droplet Epitaxy, *Nano Letters* **10**(4), 1512–1516. PMID: 20356102.

**URL:** <http://pubs.acs.org/doi/abs/10.1021/nl100217k>

Yamagiwa M, Mano T, Kuroda T, Tateno T, Sakoda K, Kido G, Koguchi N and Minami F (2006). Self-assembly of laterally aligned GaAs quantum dot pairs, *Applied Physics Letters* **89**(11), 113115.

**URL:** <http://link.aip.org/link/?APL/89/113115/1>

Zhou Z Y, Zheng C X, Tang W X, Jesson D E and Tersoff J (2010). Congruent evaporation temperature of GaAs(001) controlled by As flux, *Applied Physics Letters* **97**(12), 121912.

**URL:** <http://link.aip.org/link/?APL/97/121912/1>

Zinke-Allmang M, Feldman L C and Grabow M H (1992). Clustering on surfaces, *Surface Science Reports* **16**(8), 377 – 463.

**URL:** <http://www.sciencedirect.com/science/article/pii/016757299290006W>

Zinke-Allmang M, Feldman L C and van Saarloos W (1992). Experimental study of self-similarity in the coalescence growth regime, *Phys. Rev. Lett.* **68**, 2358–2361.

**URL:** <http://link.aps.org/doi/10.1103/PhysRevLett.68.2358>

Zinsmeister G (1966). A contribution to Frenkel's theory of condensation, *Vacuum* **16**(10), 529–535. cited By (since 1996) 45.

**URL:** <http://www.sciencedirect.com/science/article/pii/0042207X66903496>

